NRL Report 6900

Integration of Metallurgical and Fracture Mechanics Concepts of Transition Temperature Factors Relating to Fracture-Safe Design for Structural Steels

W. S. Pellini and F. J. Loss

Metallurgy Division

April 22, 1969

NAVAL RESEARCH LABORATORY
Washington, D.C.

This document has been approved for public release and sale; its distribution is unlimited.

CONTENTS

Abstract	ii
Problem Status	iii
Authorization	iii
NOMENCLATURE	1
INTRODUCTION	2
MICROMECHANICAL ASPECTS OF CLEAVAGE FRACTURE	4
EFFECTS OF MICROFRACTURE DUCTILITY TRANSITION ON CRACK TIP PLASTIC ZONES	11
DEVELOPMENT OF FRACTURE PROPAGATION TESTS	16
DEVELOPMENT OF DYNAMIC TEAR (DT) TEST	17
EFFECT OF SECTION SIZE CONSTRAINT FOR DT TEST	25
CORRESPONDENCE OF DT TRANSITION TO THE TEMPERATURE DEPENDENCE OF K_{Ic} AND K_{Id}	32
INTERPRETATIONS TO NDT	37
INTERPRETATIONS TO THE FRACTURE ANALYSIS DIAGRAM (FAD)	41
THE SPECIAL CASE OF PRESSURE VESSELS INVOLVING GEOMETRIC INSTABILITIES	46
SUMMARY	50
REFERENCES	55
BIBLIOGRAPHY	57
APPENDIX A — Elementary Aspects of Fracture Mechanics	59
APPENDIX B — Fracture Mechanics terms and Equations	66

ABSTRACT

The brittle-to-ductile transition for cleavage fracture of steels has been examined with integrated considerations of micromechanical and macromechanical features. The evolution of transition-temperature approaches to fracture-safe design has been based on concepts that metal ductility factors should override mechanical constraint factors, in the higher temperature range of the transition. The transition temperature range, determined by dynamic fracture tests, has provided the necessary guidance for the development of improved steels. Fracture mechanics concepts emphasize that macroscopic fracture toughness is controlled by mechanical constraint and flaw severity factors. While true, within limits, there has been an unwarranted extension of these principles to signify that the transition temperature does not have a basic significance to fracture processes. Contrary to popular beliefs, these concepts are not in opposition — metallurgical factors determine the intrinsic metal ductility, and mechanical parameters serve to describe the response of the metal to specific stress states. Recent investigations of the effects of large section size have demonstrated that increased mechanical constraint results in shifts of the transition temperature, as predicted by fracture mechanics theory. However, these shifts are of relatively small magnitude and, more importantly, do not eliminate transition temperature characteristics.

The rapid changes in fracture toughness which develop over a narrow temperature range indicate that practical engineering use of fracture mechanics must be based on transition temperature tests of simple types. Conventional fracture mechanics tests are not practical for transition temperature definitions because of large size, prohibitive expense and the very steep-slope temperature dependence of K_{Ic} and K_{Id} defined fracture toughness. In effect, the analytical capabilities of fracture mechanics are best used by contributions to improved definition of the significance of dynamic fracture toughness tests. For such use, the tests must be indexable to K_{Ic} and K_{Id} parameters. The Dynamic Tear (DT) test represents the most advanced engineering test which provides accurate indexing of the true transition temperature range and the specific interval in this range for which fracture mechanics applies. The temperature interval of high fracture toughness which is outside the range of fracture mechanics capabilities is also defined. Size effect can be interpreted and related to expected transition temperature shifts.

All of these factors have been integrated into simple reference diagrams which index flaw size-stress relationships for fracture initiation in the transition range. The Fracture Analysis Diagram (FAD) procedure is now extended to cover the full range of thickness. Its validity is confirmed by these additional studies and is no longer based entirely on experience factors. Conversely, the experience factors serve to validate the predictions of fracture mechanics theory and continue to provide engineering assurance that the analytical methods can be relied on.

PROBLEM STATUS

This is a special summary and interpretive report covering the results of a wide spectrum of investigations within the Metallurgy Division of NRL, aimed at the general problem of metallurgical optimization and fracture-safe design. The major portions of the studies are continuing under the established problem.

AUTHORIZATION

NRL Problem M01-25
RR 007-01-46-5432

and

NRL Problem M01-14
RR 007-11-41-5409

Manuscript submitted February 24, 1969.

INTEGRATION OF METALLURGICAL AND FRACTURE MECHANICS CONCEPTS OF TRANSITION TEMPERATURE FACTORS RELATING TO FRACTURE-SAFE DESIGN FOR STRUCTURAL STEELS

NOMENCLATURE

a	depth, half length, or half diameter of crack (in.)
a_c	critical microcrack length (grain diameters)
$2c$	crack width (in.)
T_c	critical transition temperature
B	thickness of plate or specimen (in.)
E	Young's modulus (psi)
K, K_I	stress intensity factor; the subscript I denotes the opening mode of crack extension (ksi $\sqrt{\text{in.}}$)
K_{Ic}	slow load (static) plane strain fracture toughness (ksi $\sqrt{\text{in.}}$)
K_{Id}	dynamic load plane strain fracture toughness (ksi $\sqrt{\text{in.}}$)
K_c	plane stress condition at crack tip for initiation — also crack conditions in propagation as related to this fracture mode (ksi $\sqrt{\text{in.}}$)
K_c (mixed mode)	plane stress (surface) and plane strain (center) condition for crack tip initiation — also crack conditions in propagation as related to this fracture mode (ksi $\sqrt{\text{in.}}$)
PZS	Plastic Zone Size
r	plastic zone radius (in.)
ν	Poisson's ratio
σ or σ_N	applied stress (psi or ksi)
σ_{ys}	yield strength for static (slow) loading (psi or ksi)
σ_{yd}	yield strength for dynamic loading (psi or ksi)
Q	crack shape parameter for semielliptical surface cracks
ϵ_P	plastic strain
ϵ_c	critical instability value of ϵ_P

NDT	Nil Ductility Transition temperature obtained by Drop Weight Test or indexed by DT test
FTE	Fracture Transition Elastic
FTP	Fracture Transition Plastic
DWT	Drop Weight Test
DWTT	Drop Weight Tear Test (now DT)
DT	Dynamic Tear test — all sizes
CAT	Robertson Crack Arrest Temperature
C_v	Charpy-V test
COD	Crack Opening Displacement
ECST	Explosion Crack Starter Test
FAD	Fracture Analysis Diagram
NAD	NDT Analysis Diagram
LTTR	Limiting Transition Temperature Range as defined by dynamic fracture propagation tests; normally considered as the NDT to FTP temperature interval
Enclave	fracture propagation condition involving through-thickness yielding (plastic contraction) and dimpling of the region in advance of the crack
Ratio	signifies K_{Ic}/σ_{ys} or K_{Id}/σ_{yd}
Regime 1	transition temperature range of initial, gradual increase of microfracture and macrofracture ductility (fracture toughness)
Regime 2	transition temperature range of rapid increase of microfracture and macrofracture ductility
Regime 3	transition temperature range of completion of microfracture and macrofracture ductility transition

INTRODUCTION

Steels of low to intermediate strength levels develop transition from brittle to ductile fracture over relatively narrow temperature ranges. A classical engineering example is provided by the large number of World War II ship failures which only occurred at temperatures below 50 to 60°F and at alarming rates at temperatures of 30 to 40°F. Another fascinating aspect of the ship failures is that the fractures generally started from small defects, such as welding electrode arc strikes or very small cracks in weld or heat-affected zones, despite the fact that relatively large flaws existed in the same locations. Other structures, such as bridges and pressure vessels, have shown similar disposition to this "inverse flaw size effect," which is apparently in conflict with fracture mechanics theory. Actually there is no conflict; the small flaws can "fit" into small regions of weld

residual stresses and localized embrittlement. Instability of the crack tip involving a few grain diameters, can precipitate a process of dynamic fracture which propagates through the entire structure. The metallurgical conditions which apply to the tips of these small cracks are entirely different from those of the large cracks. Deductions of conflict arise from neglect of metallurgical factors and the dynamic aspects of fracture.

Metallurgical concepts of temperature-induced, dynamic fracture toughness transition have also been considered in apparent conflict with fracture mechanics theory. The metallurgical concepts predict the existence of a limiting (highest possible) temperature range for the transition. The limiting transition temperature range (LTTR) is defined as a change in the nature of fracture propagation from unstable to stable (ductile) modes. At the low end of the transition, the release of elastic strain in an increment of propagation is sufficient to provide the energy required for the next increment of propagation. The fracture, therefore, is unstable and will traverse elastic stress fields at high velocities, in the order of several thousand feet per second. In the course of the transition the microductility of the metal (ductility of grain aggregates) becomes too high to allow fracture extension by release of purely elastic strain energy. As the transition is completed, the ductile separation of the metal cannot be considered as fracture in the conventional sense but rather as a plastic tearing process.

By basic definition, linear elastic fracture mechanics applies only to conditions for which unstable fracture may be obtained. Increasing the level of mechanical constraint at crack tips suppresses the natural tendency of the metal to increase its ductility with increase in temperature. Thus, increasing section size, which increases mechanical constraint, would be expected to cause an elevation of the dynamic instability temperature limit. Accordingly, the temperature of transition from unstable to stable fracture would be elevated.

Fracture mechanics concepts, as applied to fracture propagability considerations, run into conflict with metallurgical theory only as these are taken to infer that the fracture propagation transition may be eliminated entirely by increase in section size. The metallurgical concepts include acceptance of an increase in the dynamic transition, but emphasize that the temperature increase should be of relatively small magnitude.

The apparent conflict between the two basic theories is of crucial engineering and basic research significance. Fracture mechanics experts have predicted that steels of very thick section would be mechanically brittle (plane strain), because the LTTR would be eliminated with increasing section size. Conversely stated, steels of thick section could not be made metallurgically ductile (plane stress). The engineering implications are, therefore, of utmost seriousness — as an example, the safety of thick-walled reactor pressure vessels could be questioned and was.

The scientific implications are also of utmost seriousness, because all physical metallurgy procedures for alloying, processing, and heat-treatment optimization are based on meticulously evolved principles of microfracture ductility. If the thickness constraint effect could eliminate the LTTR, the most basic aspects of metallurgical practices would be in question. On the other hand, if the thickness constraint effect only resulted in moderate elevation of the LTTR, this would be fully in keeping with metallurgical theory. It is emphasized that a finding that metallurgical theory is correct would not invalidate basic fracture mechanics theory but would serve to provide a "marriage" of the two theoretical bases. This is a most important point — the conflict is only apparent because it emerges from past interpretations of fracture mechanics theory, which do not consider metallurgical factors. Fracture mechanics is concerned with the measurement of specific characteristics of a metal. If the intrinsic properties of the metal change due to temperature, the fracture mechanics measurement will reflect the change.

The only route for clarification of thickness constraint effects on the LTTR obviously involves tests of steels ranging from small to large section, over a range of temperatures. These should include K_{Ic} (static)-K_{Id} (dynamic) fracture mechanics tests, in comparison to LTTR determinations obtained by fracture transition tests of the various types that have been used as the basis for metallurgical guidance. These also require investigation over a range of section sizes.

The concept of the LTTR has a very interesting history of successful metallurgical and mechanical studies conducted in integrated fashion. The volume of research text on combined aspects of the subject is equal to or exceeds that of the field of purely mechanical studies of fracture, which treat the metal as a continuum or featureless solid. The scientific base which underlies the LTTR concept goes far deeper than purely phenomenological studies of microfracture processes. In the last decade it has included rationalizations evolving from defect structure theory. Thus, assumptions that transition-temperature concepts represent the product of purely empirical studies of fracture processes are in error.

It should be noted that the term transition temperature actually signifies a specific range of temperature over which the brittle-to-ductile transition occurs. When a specific temperature is cited, it represents an index point for the transition, such as "ductility transition temperature."

This report presents interpretations of the relationships between micromechanical and macromechanical ductilities, a broad survey of the evolution of the various aspects of transition temperature concepts, and a summary of recent research which has clarified the constraint-effects issue. As an essential part of the background survey, the basic aspects of micromechanical fracture processes are described in an abridged form. An introduction to the elementary aspects of fracture mechanics theory, for purposes of this report, is provided in Appendix A. A more detailed introduction to fracture mechanics for engineers has been presented previously (1).

It is emphasized that all discussions relate to steels which feature a transition to high levels of fracture toughness. The "low-shelf," i.e., "low-energy-tear" types are specifically excluded — discussions of tnese steels are provided in Ref. 1.

The conclusions of this survey are that a significant unification of mechanical and metallurgical theory has been accomplished. The transition concepts have a proper place in fracture mechanics theory and vice versa. The "marriage" of concepts is of crucial importance to the structural design engineer and to the alloy development metallurgist. It provides a common basis for the use of the vast reservoir of knowledge developed in the two fields.

MICROMECHANICAL ASPECTS OF CLEAVAGE FRACTURE

This subject and related aspects are covered intensively by Tetelman and McEvily (2); other important publications of summary scope include Averbach, Felbeck, Hahn, and Thomas (3) and Cohen (4). The following review represents a highly simplified description of primary aspects.

Cleavage fracture in metals competes with processes of slip. The critical cleavage stress for a single crystal may be attained in the elastic range, if slip is prevented by defect structure locking mechanisms. In the absence of significant slip, the development of cleavage may be said to be stress induced. Increased temperature provides the activation energy for decreasing the degree of locking of the slip systems. Accordingly, increased temperature decreases the stress level required to develop slip. The stress

levels for yielding and for subsequent plastic flow are markedly influenced by temperature and fall off relatively rapidly with increasing temperature. The critical stress level for cleavage is not strongly affected by temperature. The interrelationships of these effects are the basis for the development of increased micromechanical ductility with increased temperature. To understand the processes which determine the development of a ductility transition for different stress states it is necessary to consider these interrelationships for the case of single crystals, aggregates of crystals, and different degrees of mechanical constraint to plastic flow.

It should be noted that much divergence of opinion exists among investigators as to the fine details of the microfracture processes. However, these differences largely involve the scale of events that are considered, whether of grain size or atomistic levels. These then extend to questions as whether a stress, strain, or energy criterion provides the most fundamental answers. The differences of opinion lead to a full circle debate which culminates to an impasse, since fracture stress is a function of plastic flow. Moreover, the point of incipience of plastic flow is itself a question of definition and of the scale level being considered. There is no intent by the authors to arbitrate these questions, but rather to present a description of the salient features which apply to the grain size scale. The exact form and relative slopes of the temperature dependence of the cleavage stress and yield stress curves, which are presented as sketches in figures to follow, may be debated. This is true particularly in relation to the specific slope of the cleavage fracture stress. These are details of minor consequence; the important aspects lie in the concept of a crossover between these curves which has experimental justification and major physical significance.

Figure 1 illustrates the effects of temperature for a single crystal. The crossover point of the stress curves for cleavage and yielding is noted to occur at a critical temperature T_c. At temperatures below T_c the cleavage stress is reached before the stress for activation of sufficient slip to induce yielding. For these conditions, cleavage instability (fracture) for the single crystal is said to be stress induced, i.e., brittle. At temperatures above T_c yielding of the crystal occurs first, and plastic strain (ϵ_p) is

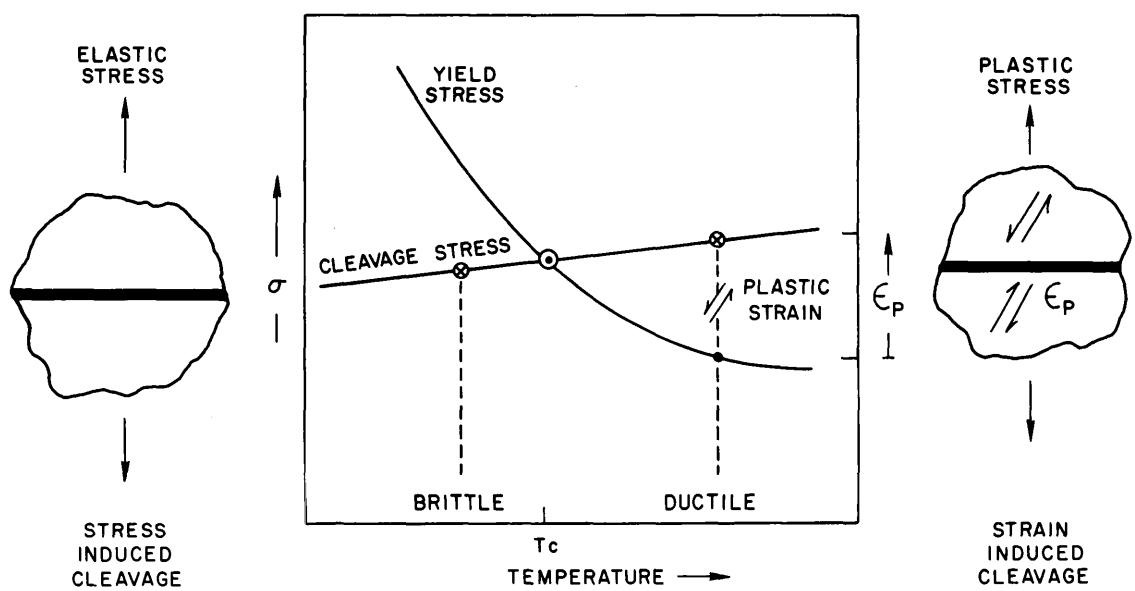

Fig. 1 - Transition from stress-induced to strain-induced cleavage fracture for a single crystal

developed to the extent required for elevating the flow stress (by work hardening) to the level of the cleavage stress. The term "strain-induced cleavage" defines ductile behavior, in that a critical level of plastic strain is required to reach the critical cleavage stress level. The T_c temperature marks a transition from brittle to ductile cleavage fracture. It is important to note that the differences in ductility are not involved in the actual splitting of the crystal (cleavage) but in the slip that occurred prior to attaining the stress required for cleavage. While it is not correct to speak of brittle cleavage or ductile cleavage (cleavage separation is always brittle), it is correct to speak of stress-induced and strain-induced cleavage. This point is of considerable importance, because the appearance of cleavage on a fracture surface is often mistaken as indicating brittleness. The appearance of cleavage does not necessarily indicate brittleness; it may relate to very high ductility, insofar as the total fracture process is concerned.

The ductility transition developed at low temperatures for the tensile state of stress provides a clear example of this fact, Fig. 2. The figure is a simplified replot of typical data presented in Ref. 4 due to Cohen and associates — the paper is highly recommended reading because of the exceptionally clear exposition of the micromechanisms of fracture in relation to microstructural factors. The tensile data illustrate sharp increases in

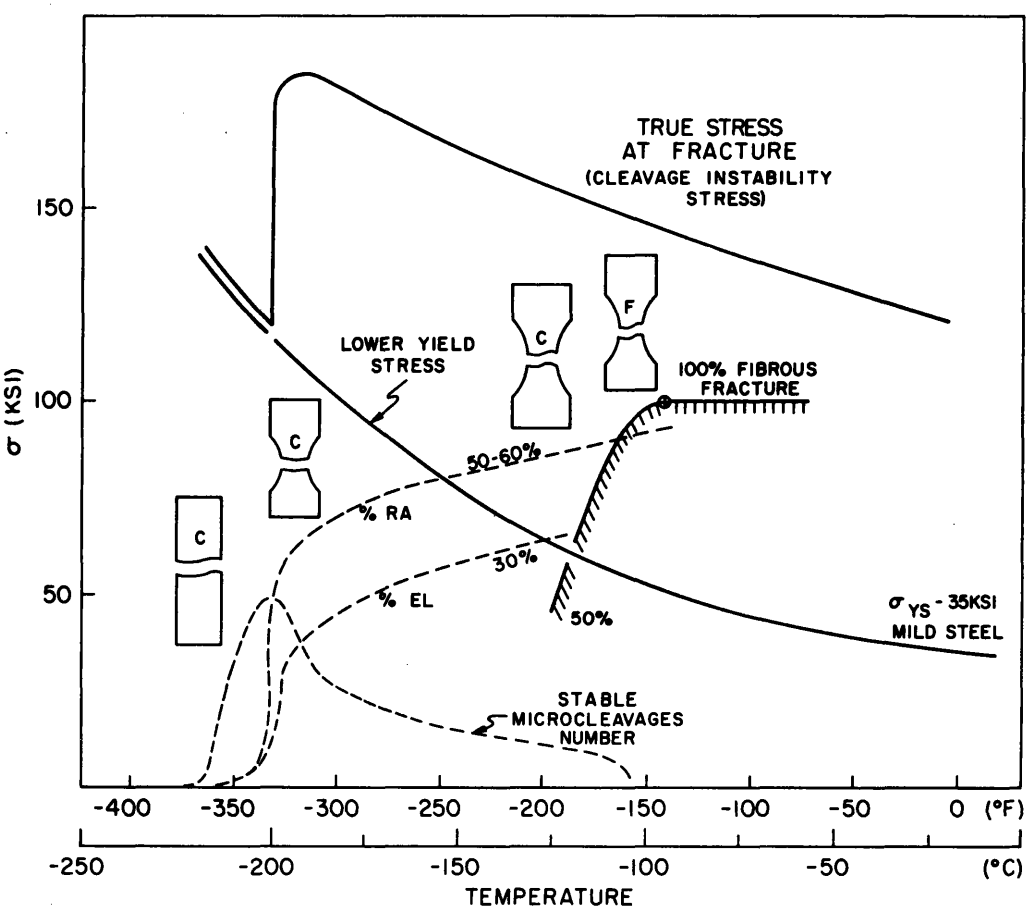

Fig. 2 - Typical transition features for tensile specimens (4). The three regimes of transition are indicated by the elongation and reduction of area curves, i.e., the toe region, the region of sharp rise, and the region of gradual completion of the transition.

ductility and fracture stress in a narrow range of temperature. It is important to note that high elongation and reduction of area values are associated with full cleavage fracture at intermediate and high levels of the tensile transition. Fibrous fracture is developed only after completion of the cleavage fracture transition. This is in accordance with the generalization that the appearance of fibrous fracture always marks the end point of temperature transitions.

The development of cleavage for an aggregate of crystal grains must be considered in terms of the critical stress required for instability, i.e., for the unstable propagation of cleavage. For this event to occur a critical microcrack length a_c must be attained as well as a critical stress. Cleavage will be stable (restricted to specific grains) until the required combination of critical stress and critical microcrack length is attained.

Figure 3 illustrates the conditions required for stress-induced and strain-induced cleavage instabilities for crystal aggregates. At this point it should be noted that the specific T_c for the individual grains may vary, due to the orientation of the cleavage planes with respect to the stress vector. Some grains will be in a favorable orientation for stress-induced cleavage while others may require strain for cleavage. As temperature is increased, all crystals will require strain. Due to the orientation of the crystals, some will require more strain than others. As the average ductility of the grains increases, fewer individual cleavages will occur, and it will become more difficult to connect the necessary numbers of stable microcleavages to evolve the critical microcrack length a_c.

Figure 3 illustrates a condition of brittleness at low temperatures, where grain C_1 of favored orientation for stress induced cleavage has split. Because of generally low ductility for all other grains at this temperature, there is an immediate instability, involving fast cleavage propagation through the entire matrix. At this temperature the

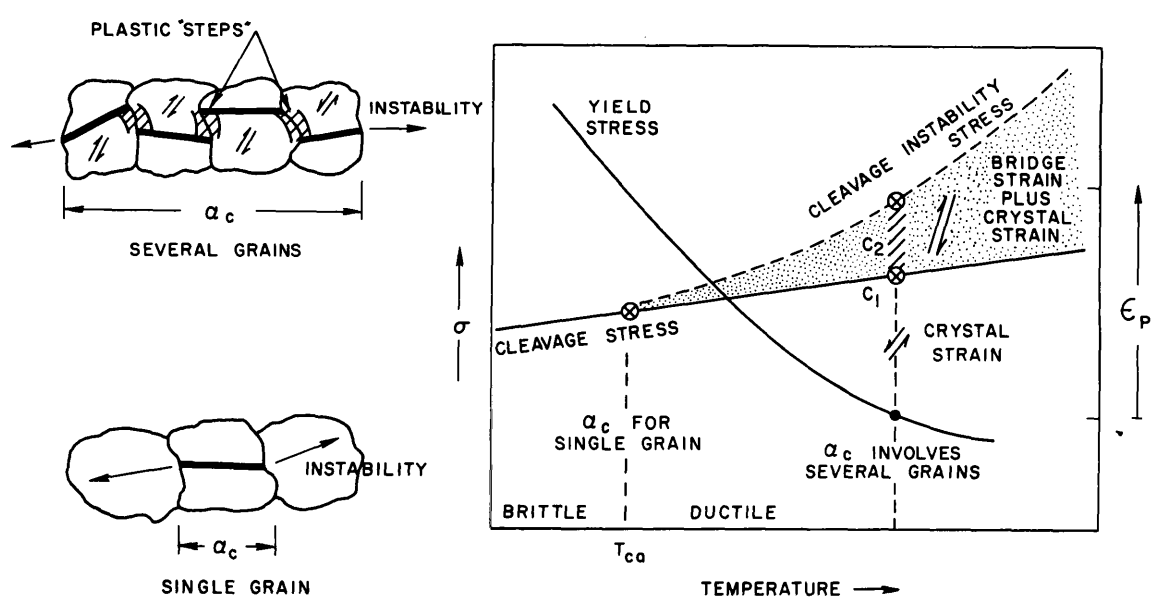

Fig. 3 - Features of the brittle-to-ductile transition for grain aggregates. The effect of increasing temperature on the ductility of individual grains is amplified by the plastic strain required for the joining of individual microcleavages to critical microcrack size. The cleavage instability stress, critical strain level, and critical microcrack size increase gradually with increasing temperature in the first stage (regime 1) of the transition.

critical microcrack length a_c is equal to one grain diameter. At a higher temperature of general strain-induced cleavage for most, or all, grains, significant number of microcleavages do not appear until both the C_1 and C_2 cleavage stress levels are reached. The C_2 level is meant to represent grains (other than C_1) that are not favorably oriented and, therefore, require higher levels of strain hardening prior to cleavage. At this point the aggregate features separated microcleavages which must be joined by breaking "plastic steps," i.e., connections at grain boundaries which represent regions of step mismatch of the cleavages for individual grains. We shall define this as "bridge strain," and it represents an additional increment of strain required for growing the microcracks to a_c size. Instability then will be determined by the dashed curve noted as "cleavage instability stress," which lies above and has a steeper temperature dependence than the cleavage stress curve for the individual grains. It is also noted that the temperature of ductility transition from stress-induced to strain-induced cleavage instability for the aggregate (T_{ca}) is somewhat lower than that of single crystals. The aggregate behaves in a more ductile fashion than a single grain because of the intergrain cooperation that is required for attaining instability.

Figure 4 repeats Fig. 3, with a somewhat enlarged temperature scale, to illustrate a point of sharp rise in the cleavage instability stress with increased temperature. The instability stress slope is gradual at first, but then rises sharply in a critical temperature interval. The illustration (top) explains the cause for this event. The microcleavages curve indicates that the number of stable microcleavages first increases and then decreases rapidly with temperature because of general increase in ductility for all grains. The critical microcrack length a_c increases continuously and at an increasing rate with increased temperature because of increased general ductility of all grains. Experimental proof of the bell-shaped microcleavage number curve is provided in Fig. 2.

The illustration is representative of many such determinations presented in the literature of tensile tests conducted at low temperatures. The counts are made by cross sectioning and metallographic polishing, followed by microscope examinations near the fracture surface. Since the microcleavages noted after the fracture represent stable cleavages of individual crystals, the shape of the curve is of particular importance. At the start of the transition, the critical a_c size is equivalent to one grain diameter — the first cleavage which develops results in instability. This marks the point at which the cleavage count is near zero. The transition from a gradual to a sharp rise in ductility is related to the large increase in stable cleavages which could not be connected to the required a_c size of several grain diameters. Other supporting evidence for the sharp rise in ductility is provided by Ref. 3, particularly the chapter by J. Low which shows photographs of highly deformed grains between stable cleavages which could not be connected to a_c size, and also the blunting of microcracks.

Following the sharp rise, the ductility increase continues as the number of microcleavages falls to very low levels and can never be joined to critical a_c size, even as small patches. Full fibrous microfracture is developed at this point.

The increase in plastic strain (microfracture ductility) is illustrated by the three regimes of the ϵ_p curve of Fig. 4, as follows:

Regime 1 — transition from stress-induced to strain-induced cleavage instability — features a gradual rise in strain level as the critical a_c size increases.

Regime 2 — transition to large a_c size and bridge-strain control — features an exponential rise in the strain level required for cleavage instability. Severe deformation of grains and blunting of microcracks are developed.

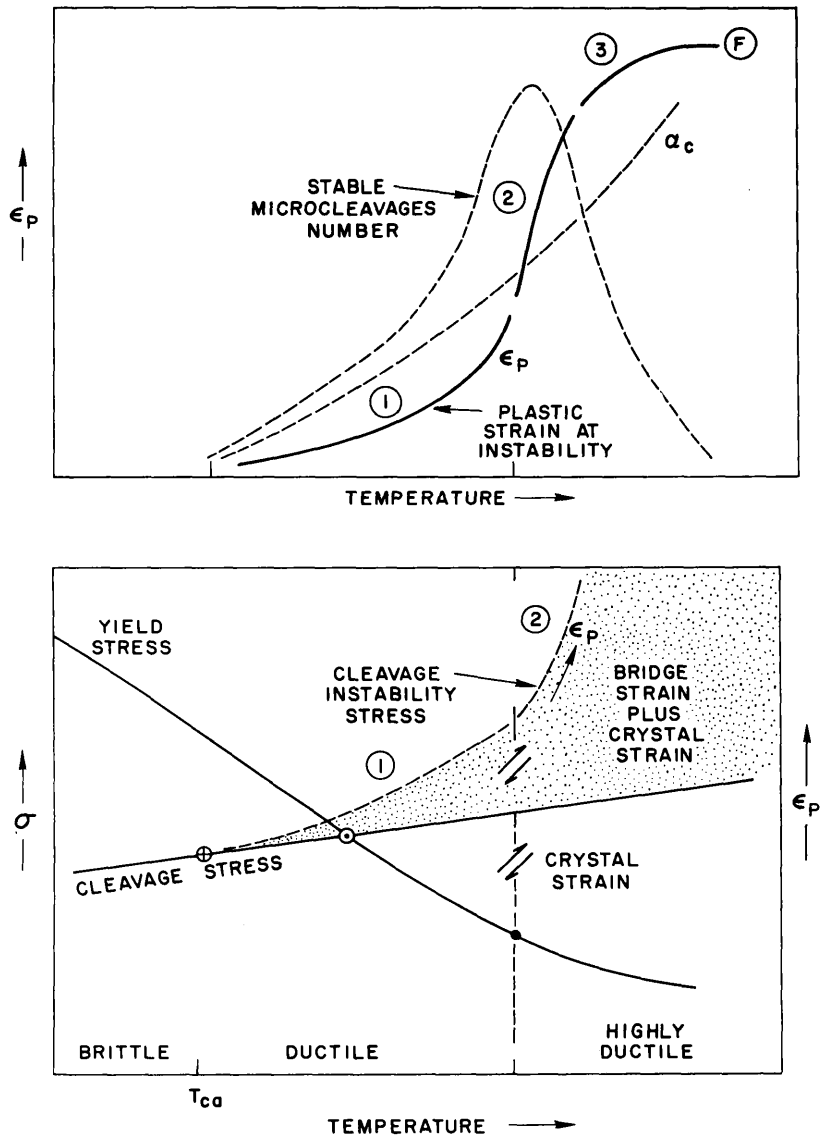

Fig. 4 - Features of exponential change in critical cleavage instability stress and plastic strain levels for grain aggregates. These ductility parameters increase sharply (regime 2) because the ductility of individual grains becomes sufficiently high to inhibit the joining of microcleavages to critical microcrack size. Additional increases in the ductility of individual grains then inhibit the formation of single-grain microcleavages and result in the completion (regime 3) of the transition to fibrous fracture.

Regime 3 — saturation of processes required for development of cleavage instability and transition to full fibrous fracture.

The temperature range of transition through these three microfracture regimes is characteristically narrow for any stress state. After the temperature of strain-induced cleavage for individual grains is reached, the interaction of the events described above leads to a cataclysmic rise in ductility at slightly higher temperatures. It is this chain of events which causes all temperature transitions to be sharp and irrepressible once started. The three regimes of the transition are evident from the course of tensile ductility shown in Fig. 2. The toe region of the transition features a gradual rise in ductility associated with regime 1; this is followed by the exponential rise of regime 2 and then by gradual completion of the regime 3 transition with the development of fibrous fracture.

Microcleavage count curves obtained for tensile tests of pure iron as well as for pearlitic steels show the same sequence of events as Refs. 3 and 4. However, the presence of brittle carbide phases (pearlitic, etc.) serves as microcrack incubation sites and also promotes joining of microcleavages to higher temperature. The tensile ductility curve is thereby shifted to the higher temperature. Fine grain sizes displace the transitions to lower temperature, while coarse grain sizes have the opposite effect. Fine and coarse distribution of ferrite-pearlite aggregates have corresponding effects. All of these factors influence the transition temperature, because they affect the stress and strain conditions required for attaining microfracture instability. In general, reduction in the "unit cell" size of stable cleavage, and decrease in the number of sites involving brittle phases as well as their relative size, results in lowering the temperature range of transition. Extensive studies of these interrelationships have been reported in the metallurgical literature and serve as the basic fund of knowledge regarding microstructural effects.

Before we discuss the effects of stress state (notches) on the transition, it should be noted that the effects of increased microfracture ductility are amplified by the presence of a notch as compared to a tensile specimen. As the ductility transition develops at a tip of notch, it eventually leads to blunting of the notch and thereby reduces its constraint effect. In brief, unstable macroscopic fracture cannot develop above the temperature range of regime 2, because the large increase in microfracture ductility blunts the notch and thereby stimulates the development of gross yielding of the metal in advance of the notch. The macroscopic fracture process then becomes of ductile (stable) nature. Macroscopic instabilities are controlled by microscopic instabilities involving relatively few grains.

The effects of stress state on the specific temperature range of the microfracture transition are illustrated in Fig. 5. The average cleavage stress for single grains remains a main point of reference. The yield stress (flow stress) temperature-dependence curves are shown schematically for the tensile stress state, for a very sharp crack loaded statically and for the same crack loaded dynamically. The elevation of the flow stress at a crack tip results from the associated triaxial state of stress. The additional elevation of flow stress resulting from dynamic loading is due to the fact that slip is a time-dependent (viscoplastic) process. Higher stresses are required to activate slip in short times.

The elevations of the flow stress curves result in increasing the temperatures at which these curves fall below the cleavage stress curve, as indicated. Three critical temperatures for transition from stress-induced to strain-induced cleavage instability are indexed by the crossover points of the curves. For each stress state cited, a sharp microfracture ductility transition will develop in a narrow temperature range above this critical temperature. More exactly, the start will be at a somewhat lower temperature related to the rise of the cleavage instability stress. For simplicity, the instability

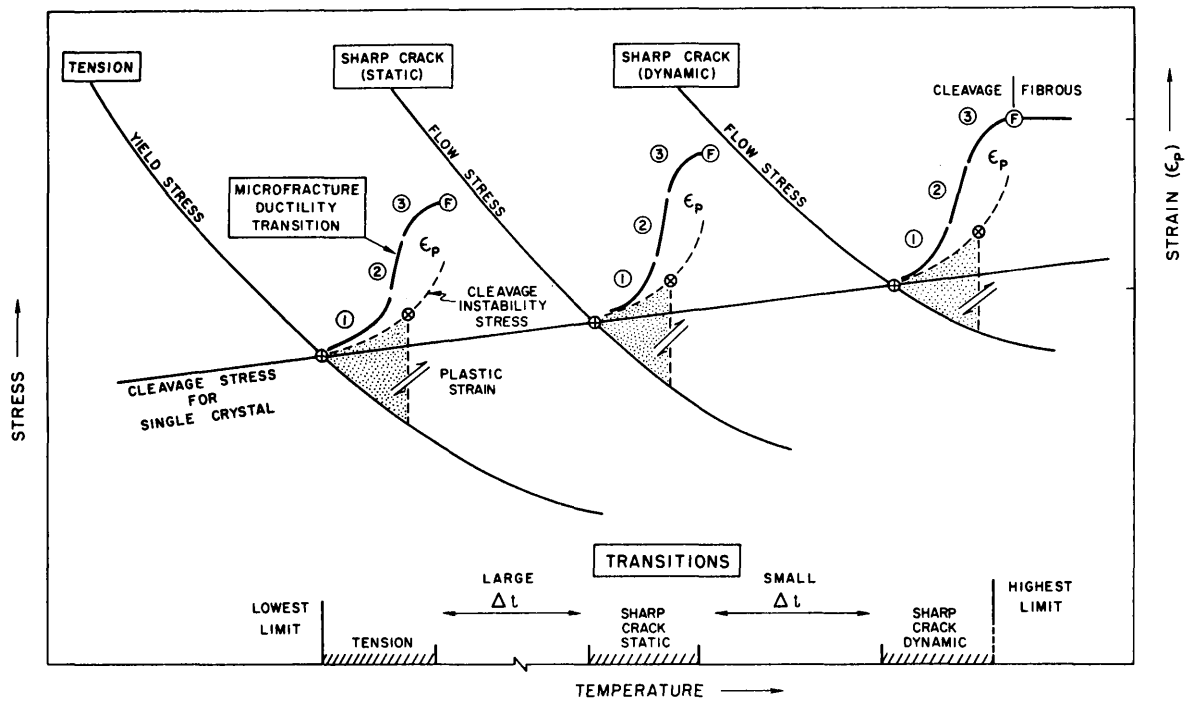

Fig. 5 - Effects of sharp cracks and dynamic loading. These factors increase the stress required for plastic flow and thereby shift the intersections of the cleavage and flow stresses to higher temperatures. The three characteristic regimes of the microfracture ductility transition evolve at related higher temperatures.

stress noted by the dashed curves is shown to start at the crossover points. Each of the microfracture ductility transitions will feature regimes 1, 2, and 3 in close sequence, as described previously. A change from cleavage to fibrous fracture (F) will occur as each ductility transition is completed. The temperature intervals between the transitions are not in proper scale, since the schematic illustration would be complicated. The notch transitions are relatively close together, while the tensile transition is developed at much lower temperatures.

EFFECTS OF MICROFRACTURE DUCTILITY TRANSITION ON CRACK TIP PLASTIC ZONES

Transition from stress-induced to strain-induced cleavage causes an increase in the plane strain plastic zone size, as illustrated in Fig. 6. The stress and strain fields normal to the crack are shown schematically to illustrate that maximum stress is attained at a point near the edge of the plastic zone, while maximum strain is attained near the crack tip. Maximum stress is developed at the location of maximum triaxial constraint, which must necessarily be in advance of the crack tip. The top part of Fig. 6 illustrates microfracture by stress-induced cleavage instability requiring a small a_c microcrack size. The growth of the crack tip plastic zone is terminated at an early stage as the elastic stress field attains the required stress value for cleavage instability. The fracture initiation point is located in advance of the elastic-plastic interface of the plastic zone. The stress field intensity K_{Ic} and, therefore, the K_{Ic}/σ_{ys} ratio are of low value, indicating low plane strain fracture toughness. The bottom part of Fig. 6 illustrates microfracture by strain-induced cleavage instability involving a large a_c microcrack

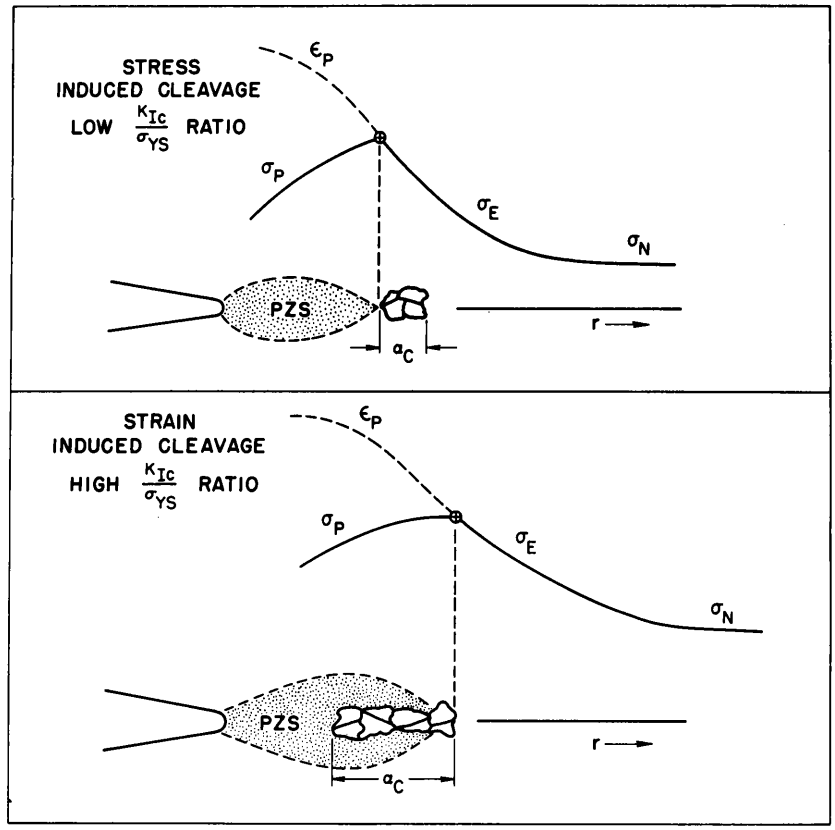

Fig. 6 - Transition from stress-induced (top) to strain-induced (bottom) microfracture processes which requires enlargement of the crack tip plastic zone size (PZS). The critical elastic field intensity K_{Ic} and the parameter K_{Ic}/σ_{ys}, must increase to enlarge the PZS, and therefore result in macrofracture transition from low to high values of plane strain fracture toughness.

size. The plastic zone must now grow to a larger size to develop high plastic stress values required for cleavage instability. The fracture initiation point is then located inside the plastic zone. The stress field intensity K_{Ic} and, therefore, the K_{Ic}/σ_{ys} ratio attain higher values for the case of strain-induced cleavage, indicating increased plane strain fracture toughness.

The increase in plane strain fracture toughness, which results from the increased microfracture ductility in regime 1, requires increased mechanical constraint for retention of the plane strain state. Increase in section size provides the increased mechanical constraint. However, there must be a limit to which the added constraint can keep pace with the increase in microfracture ductility. This limit is reached when the high ductility of microfracture regime 2 can no longer be suppressed by added mechanical constraint, irrespective of section size. The added constraint can only serve the purpose of expanding the temperature interval over which microfracture regime 1 conditions are retained. It is not possible to prevent the regime 1-to-regime 2 transition in microfracture ductility.

Once the plane strain constraint barrier is breached, the rapid increase in metallurgical ductility with increased temperature has a dramatic effect on macroscopic fracture toughness. The first effect involves a gross enlargement of the plastic zone consequent to rapid loss of triaxial stress field constraint. In effect, the elastic stress fields are replaced by plastic strain fields as the crack tip region becomes "plastic." This transition cannot be described quantitatively by fracture mechanics parameters, because the definitions relate to elastic stress fields which are no longer applicable. A qualitative description is provided by reference to the loss of constraint aspects and represents the equivalent of K_{Ic} to K_c transition (to plane stress). The subsequent (second) effect involves pronounced yielding in advance of the crack tip accompanied by general blunting of the crack. This process results in through-thickness contraction, similar to the development of the neck region in tensile specimens. The neck is evidenced by dimpling of the surface in advance of the crack, such as is generally associated with ductile tearing fracture. The volume of metal which undergoes through-thickness contraction will be defined as a plastic enclave. All future references to plastic enclave conditions will thus signify fracture processes involving relatively large volumes of plastic deformation prior to rupture.

Figure 7 illustrates the sequence of macrofracture transition events which are predicted from considerations of increased microfracture ductility as a function of increasing temperature. Two macrofracture transitions are indicated, one for static and the other for dynamic loading. We shall discuss the static K_{Ic} transition first. The temperature point marked L denotes the end of the K_{Ic} plane strain condition and K_c transition to the plane stress state, followed by transition to the plastic enclave condition. The L temperature corresponds to a sufficiently large specimen thickness, which provides maximum possible constraint. The dashed curve labeled "small B" indicates a similar transition at lower temperatures for a K_{Ic} specimen of small section size.

We shall now discuss the parallel set of transition events for the case of dynamic loading. The dynamic regime 1 transition starts sharply at the temperature noted as T_{c1}. Dynamically loaded K_{Ic} specimens of increasing B dimension are required to follow the course of the K_{Id} transition. If specimens of small size are used, the transition will follow the course of the dashed curve, indicated as "small B." The L point of the dynamic transition marks the highest temperature for the dynamic plane strain condition for specimens of large size. Above this point, plane strain relaxation again occurs with the development of plane stress conditions, followed rapidly by notch blunting and enclave formation. The macromechanical transition from plane strain to enclave conditions should develop over a narrow range of temperatures and require a change in definitions of fracture toughness level from fracture mechanics stress intensity indexing to plastic enclave energy indexing.

The dynamic transition may be referenced to five critical temperatures marking the start of the plane strain transition (T_{c1}), the end of this transition (T_{c2}), the end of the K_c transition (T_{c3}), the early development of the enclave state (T_{c4}), and the completion of enclave growth to full ductility (T_{c5}). The T_{c2}, T_{c3}, and T_{c4} transition points are grouped closely together, because these are developed as a consequence of "unleashing" microfracture regime 2, which features a large increase in ductility for a small increase in temperature. The ductility features of the three microfracture regimes are reproduced in the macrofracture ductility events. Thus, the regime definitions are interrelated and serve as common reference. The relationships to NDT, FTE, and FTP will be discussed later.

The main point of the metallurgical thesis on which the above postulates are based is that if large additions of constraint are required to define the true K_{Ic} or K_{Id} temperature dependence in regime 1, this is a certain sign that significant increases in microfracture ductility are evolving. Once regime 1 is entered, microfracture regime 2

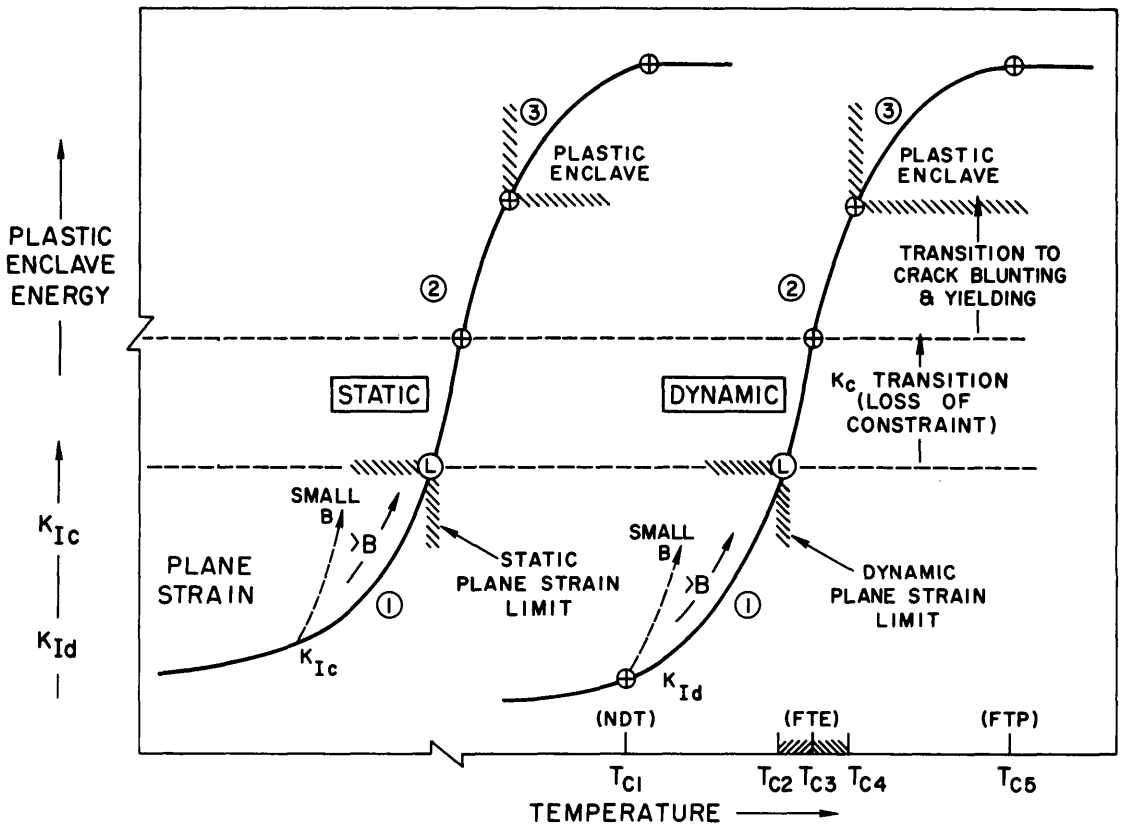

Fig. 7 - Metallurgical concepts illustrating that transitions through the three regimes of microfracture ductility should result in parallel macrofracture transitions. The degree of plastic constraint and the strain rate at crack tips determine the temperature for starting the regime 1 microfracture transition and therefore the starting of the macroscopic transition. Once started, the respective transitions run their full course and cannot be forced (mechanically) to remain in regime 1 state.

can be suppressed only for a modest temperature range, at the price of large increases in mechanical constraint. At some point the additional constraint will be defeated by rapidly increasing microfracture ductility and then plane stress and enclave conditions will evolve.

Until recently the described course of events could only be inferred from the results of dynamic fracture toughness tests which followed the "small B" curve route of Fig. 7, because these involved tests of small section size. The location of points L for the static and dynamic transition could not be defined explicitly, because large-section-size data were not available. We shall now explain the course of development of fracture propagation tests which have provided the index points referred to as T_{c1}, T_{c3}, and T_{c5}.

Figure 8 serves as an introduction to the discussions of propagation tests — it presents a generalized view of the significance of fracture energy transition curves, as defined by dynamic fracture propagation tests. These tests (to be explained) defined the course of the "small B" curve. Since we are discussing a generalized concept of the LTTR at this point, the notations of NDT, FTE, CAT, and DT of the figure should be ignored. The NDT to FTP, Δt range should be considered to be the T_{c1} to T_{c5} range of Fig. 7. The important point is that the fracture propagation tests indexed the change from regime 1 (constrained plastic zones of K_{Id} type) through regimes 2 and 3. The

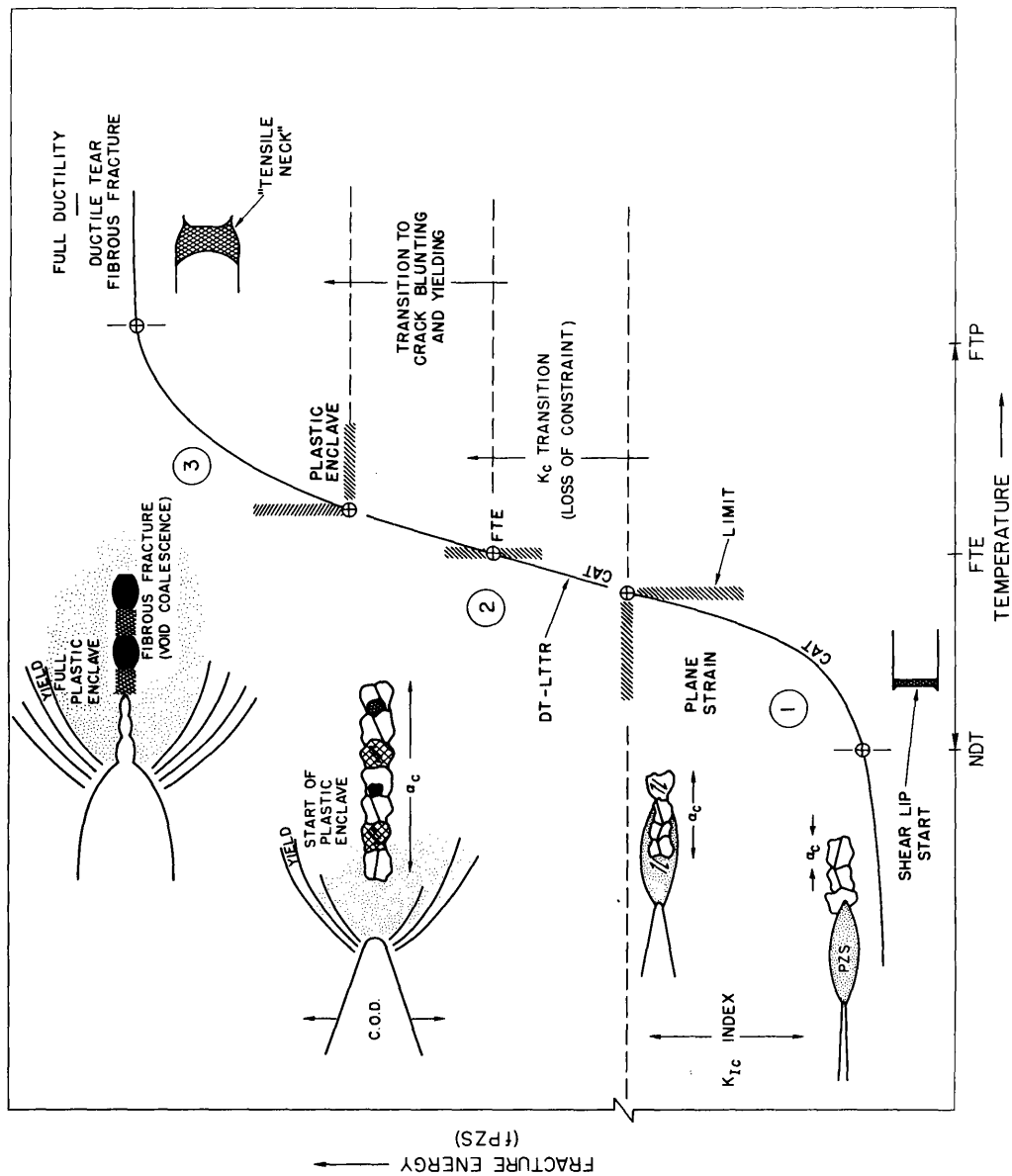

Fig. 8 - Typical energy transition curve for dynamic fracture propagation tests. The course of the fracture toughness transition defined by these tests is related to microfracture processes and plastic zone conditions by the sketches.

microfracture aspects are related schematically to the crack tip plastic zone condition. The microfracture and PZS aspects of regime 1 represent a repeat of Fig. 6. The microfracture aspects for the higher temperature ranges of regime 2 are related to crack opening displacement (COD) and yielding of the notch region. The end of regime 3 is indicated by the development of fibrous fracture; this is a void coalescence process involving the tensile necking of patches of grains located between open voids originating from inclusions, stable cleavages, cracking of carbide phases, etc.

The physical significance of increasing plane strain fracture toughness in regime 1 is indicated by the brittle fracture featuring small shear lips. The development of shear lips denotes that plane stress conditions are developed at the surface regions due to the increase in ductility. Shear lips come into evidence sharply (in a 10°F interval) and then grow rapidly with additional increase in temperature.

DEVELOPMENT OF FRACTURE PROPAGATION TESTS

The interacting effects of temperature and mechanical factors result in an infinity of transitions. Some of these can be classified as strictly mechanical, i.e., changes in flaw size and stress for a fixed temperature. Others could be ascribed strictly to changes in temperature and can be classified as due to metallurgical factors. Early interest in procedures for determining the LTTR was based on the concept that the transition which related to dynamic fracture propagation represented a singular transition of metallurgical nature, which could not be moved to higher temperatures. As such, it provided an index of the lowest, "floor" level of fracture toughness which could be developed at specific temperatures, as follows:

1. Start of transition — the "floor" is plane strain fracture; however, higher-order levels of fracture toughness can be developed by flaw size and loading rate factors.

2. Middle of transition — the "floor" is the elimination of unstable fracture propagation.

3. End of transition — the "floor" is full ductility; no other mechanical state can exist.

The simplicity of such definitions is immediately apparent — the infinities of metallurgical-mechanical transitions could only exist below the LTTR. The major questions involved the procedures for identification of the true LTTR and especially by means of relatively simple laboratory tests. The chronology of these events is now described.

The wide variety of small, notched laboratory tests investigated during the 1940's and 1950's represented attempts to determine a valid LTTR and its index temperature "points" by correlation and validation to service fracture experience. The complications of correlative methods for validating the LTTR indicated by these various tests forced some hard thinking as to methods for simulating the fracture propagation features of service failures. The basis for reference to propagation aspects was quite simple and remains valid today. The premise was that temperatures above which fractures could not be made to propagate dynamically in unstable mode likewise would not permit initiation of such fractures. The "if it cannot run unstably, it cannot start unstably" principle led to extensive investigations of wide-plate fracture tests representing prototypes of plate structures.

Gradually, it became evident that wide widths were not a necessary requirement for such tests. If "artificial" means for starting the fracture were used, the propagability

could be investigated using specimens of relatively small dimensions. The artificial means used by Robertson involved cooling the region of crack starting to low temperatures and plastic stressing of a notch located in this region by impact. The fracture was then made to propagate through a test region of uniform stress and controlled higher temperatures. The now famous Robertson Crack Arrest Temperature (CAT) transition curve became the primary reference for the lower half of the true LTTR.

Simultaneously, Pellini and associates developed an equivalent method for establishing the LTTR. This method was based on the use of a brittle weld for the artificial start of fracture and propagation through a bulge region developed by explosion loading. This was the Explosion Crack Starter Test (ECST) method. The extreme conditions of explosion loading rates did not affect the propagability features of fractures in the range of temperatures that unstable fractures were possible. This should not be surprising, since the propagation rates for unstable fracture exceed explosion loading rates. Exact correspondence was obtained with the CAT curve in that a transition from flat break, shattering fractures to arrested fractures near the edge of the bulge region were obtained in the CAT-curve-rise temperature region. The ECST was not inherently limited to fracture propagation studies for the temperature region of increased resistance to unstable fracture propagation. The test series could be carried to full ductility, involving the development of short ductile tears. Figure 9 illustrates a 1952 ECST series for a World War II ship plate of 1-in. thickness. This series is particularly significant because of the visual evidence of the LTTR that it presents — it speaks for itself. At the time it also served to illustrate why ship failures never occurred above 50 to 60°F.

A large number of such tests defined that the full course of the LTTR for fracture propagation (plane strain brittleness to full ductility) covered a temperature span of approximately 120 to 140°F. The investigations mostly involved plates of 1-in. thickness, for both the ECST and Robertson tests. The Robertson CAT transition terminated at approximately the midspan temperature of this range. The following "floor" transition temperature points (see Fig. 8) were defined as the result of these extensive investigations:

1. Nil Ductility Temperature (NDT) — this temperature marks the start of the cleavage-fracture ductility transition. It is evidenced by a change from flat break to bulging before fracture for the ECST and by a rise of the CAT curve from its toe region. Evidence of surface shear lips develop sharply at this temperature for both tests.

2. Fracture Transition Elastic (FTE) — this temperature is located approximately at NDT + 60°F and marks the end of the Robertson CAT curve, as extrapolated to yield stress levels. It also marks the temperature above which fracture propagation through the low-stress, hold-down regions of the bulge tests are prevented. It indicates the temperature limit for unstable (elastic stress) fracture.

3. Fracture Transition Plastic (FTP) — this temperature is reached at NDT + 120 to 140°F. It represents attainment of full plastic fracture ductility and fibrous fracture.

The clear evidence of a LTTR provided by the fracture propagation tests could now be used for indexing the significance of various types of laboratory notch impact tests. By the mid 1950's the propagation tests became the primary reference standards for the LTTR and for "calibrating" small tests, such as the Charpy V.

DEVELOPMENT OF DYNAMIC TEAR (DT) TEST

The DT test was evolved over the period of 1962 to date. The original concept of the test was that of a simplified, inexpensive equivalent of the Robertson test and the ECST.

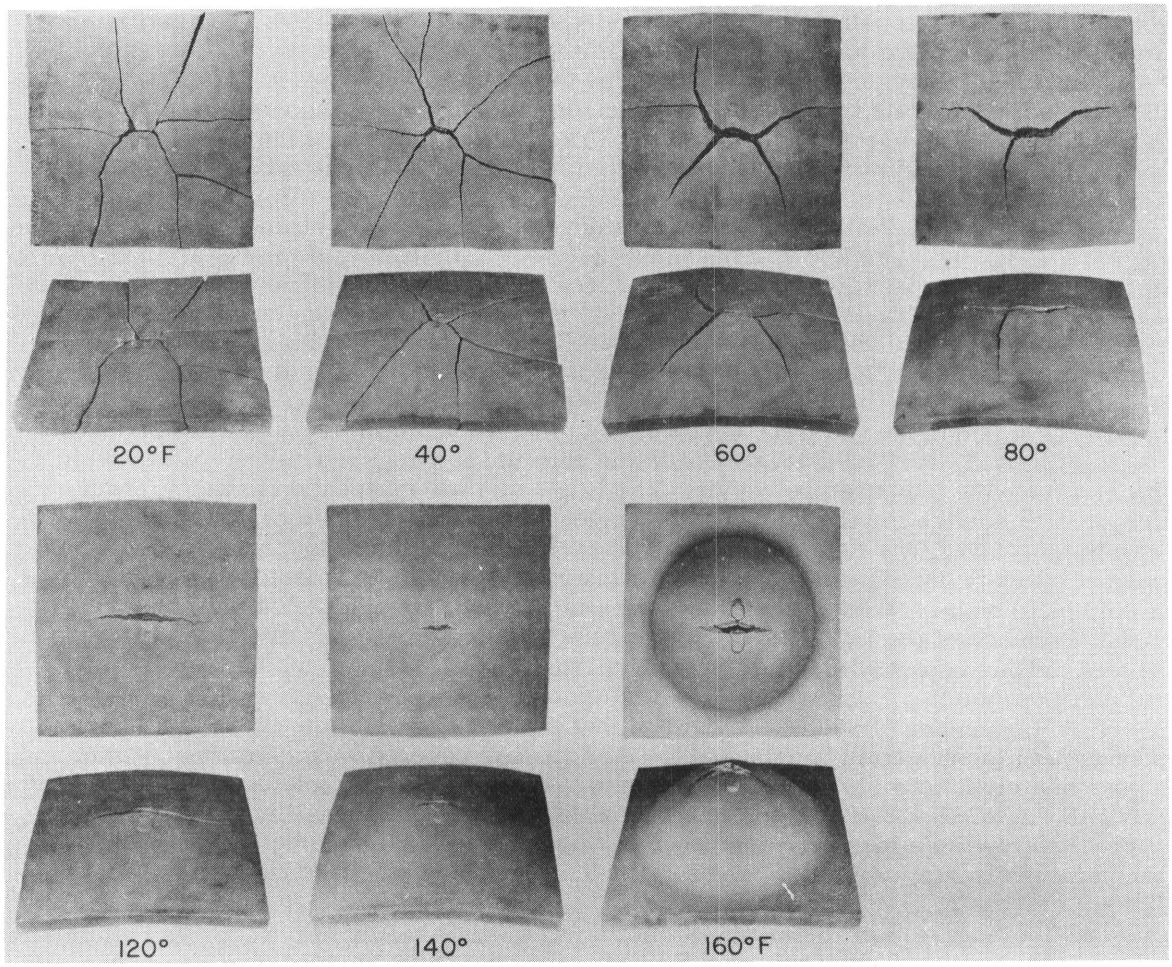

Fig. 9 - Physical significance of the LTTR as illustrated by Explosion Crack Starter Tests (ECST) of 1-in.-thick ship plate steel representative of ship failure material (7). Note the dramatic effect of temperature in 20°F increments. Nonarrestable fractures are evidenced below 60°F (FTE). The NDT temperature is 20°F, and the FTP temperature is 140 to 160°F.

The artificial crack starting feature was provided by a metallurgically brittle region. This was accomplished first by the welding of a notched, brittle steel bar to the test section. The specimen was fractured by a dropping weight, using the standard DWT machine. The fracture energy was determined by bracketing of break and no-break energies, resulting from changing the height of the fall of the weight. For this reason, it was first named the NRL Drop Weight Tear Test (DWTT). Later developments involved replacing the brittle bar with a brittle electron beam weld, which served the same purpose. For small specimen sizes pendulum-type machines were developed which provided for reading the fracture energy directly in a Charpy machine mode. For specimens of large size, drop weight machines are used which feature instrumented tups to provide for direct energy measurement, thus avoiding the bracketing technique. Figures 10, 11, and 12 illustrate the features of the test and the test equipment. Figure 13 illustrates the range of specimen sizes that have been investigated. Table 1 lists dimensions and weights.

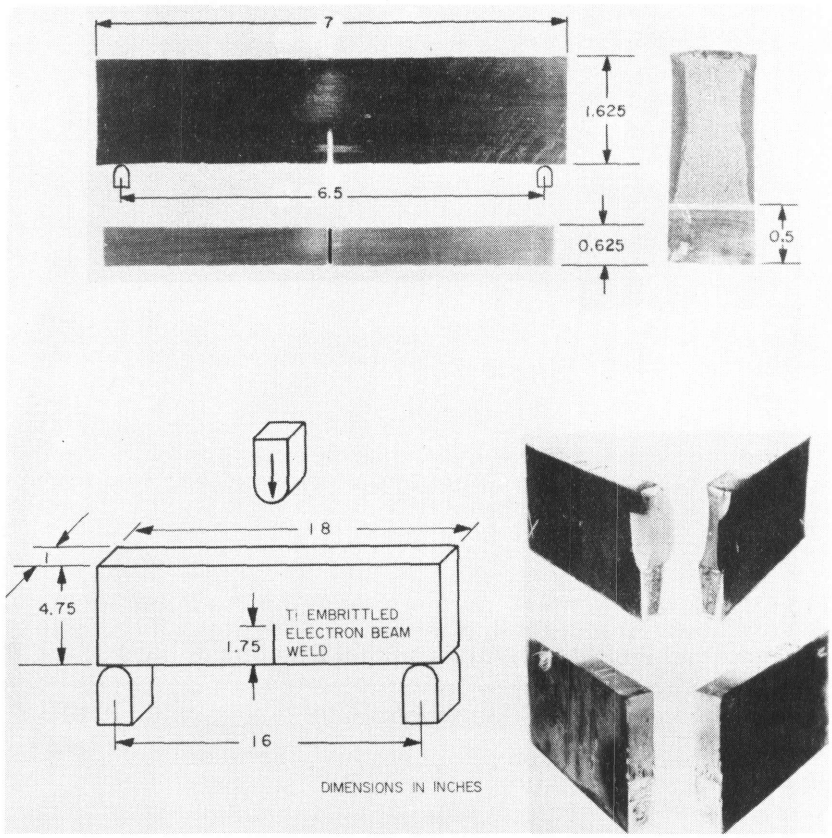

Fig. 10 - Features of 5/8-in. and 1-in. DT specimens. The 5/8-in. DT (top) is shown featuring the machine slit, with a knife-edge-sharpened notch tip. The 1-in. DT (bottom) features the brittle electron beam weld, which is also used for the 5/8-in. DT, as desired. The broken halves of the 1-in. DT specimens illustrates brittle and ductile type fractures.

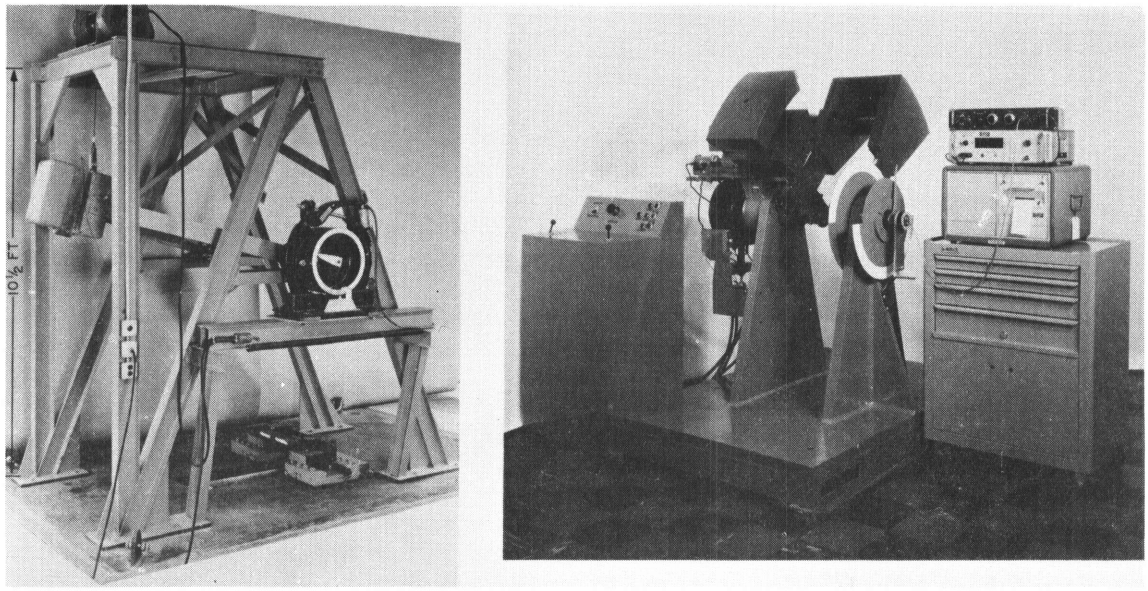

Fig. 11 - DT test pendulum machines, illustrating the single-pendulum type (5000 and 10,000 ft-lb capacity) on the left. The instrumented, double-pendulum type (right) provides for shockless testing of 5/8-in. DT specimens (2000 ft-lb capacity)

Table 1
Dimensions and Weights of Various Steel Specimens Used in the DT Test

Specimen Designation	Thickness, B		Depth, W		Length, L		Span between Supports, S		Brittle Weld or Notch Depth, a		Weight	
	In.	Cm	In.	Cm	In.	Cm	In.	Cm	In.	Cm	Lb	Kg
5/8 in. DT*	0.625	1.6	1.62	4.1	7	18	6.5	16.5	0.5	1.3	2	0.9
1 in.	1	2.5	4.75	12.0	18	46	16	40.6	1.75	4.4	24	10
2 in.	2	5.0	8	20.3	28	71	26	66.0	3	7.6	127	57
3 in.	3	7.6	8	20.3	28	71	26	66.0	3	7.6	190	86
6 in.	6	15.2	12	30.5	62	158	58	147.3	3	7.6	1220	554
12 in.	12	30.5	15	38.1	90	228	84	213.3	3	7.6	4580	2080

*Also deep machined notch having tip sharpened by pressed knife edge.

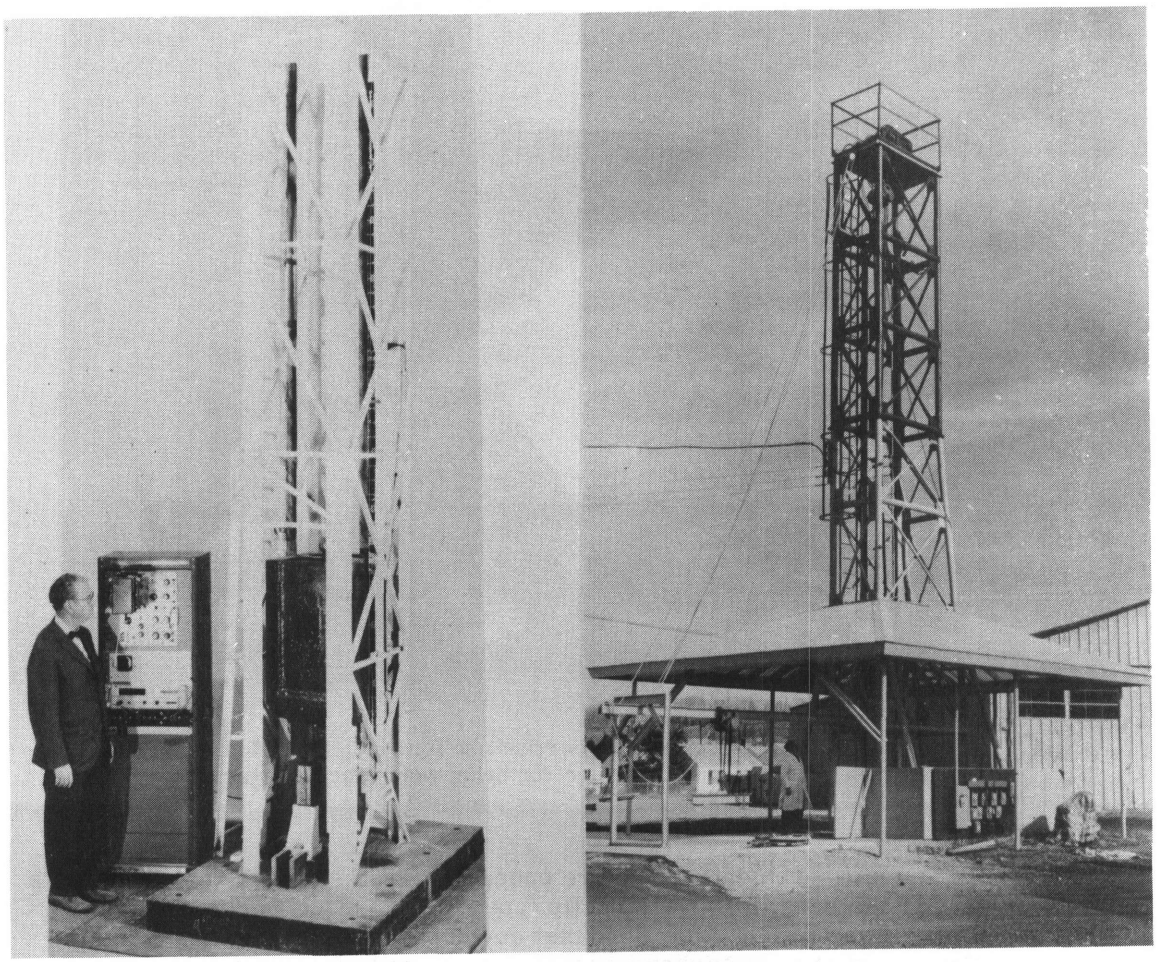

Fig. 12 - Drop weight type DT machines of 66,000 and 750,000 ft-lb capacity (9150 and 104,000 Kg/m)

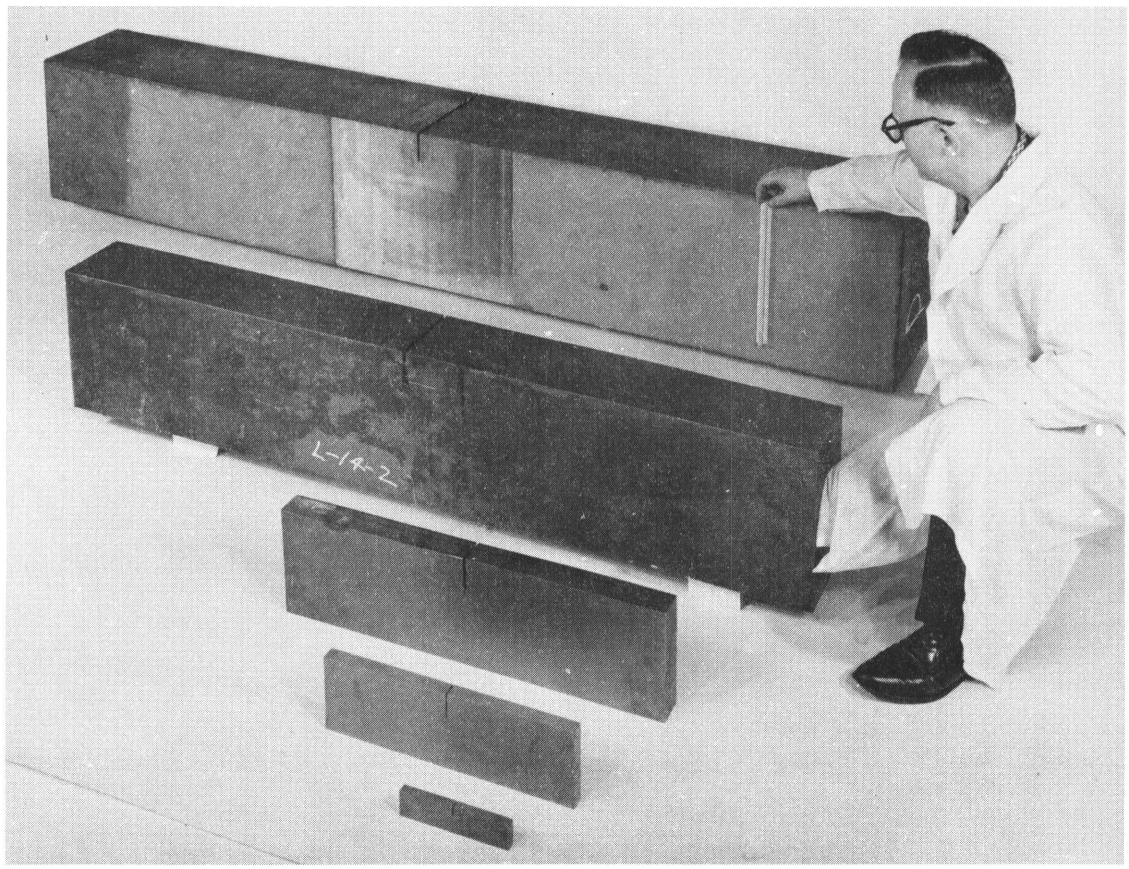

Fig. 13 - Range of DT specimens in current use for size effect studies. All of these feature the brittle electron beam weld crack starter.

The emphasis on measurement of fracture energy separates the DT test from tests of apparently similar features, i.e., the Battelle type (BDWTT), the Belgian National Metallurgical Center Drop Weight-Side Bend test developed by P. E. LaGasse, and the Technological University of Delft Nibbering test. These are basically fracture appearance transition tests and as such cannot be extended to analysis of the shelf level fracture toughness or to fracture toughness conditions involving nontransition metals. The Nibbering test also involves measurement of notch tip strains for brittle fractures.

The basis for the universal application of the DT test to all metals is that the energy measurement can be related to the plastic zone size, ranging from conditions of plane strain to those of plastic enclave ductility. Correlations with K_{Ic} fracture toughness (1,5,6) for the nontransition aspects of fracture have been developed for steels, titanium, and aluminum alloys. The DT test, therefore, serves as an "indirect" fracture mechanics test. This achievement should not be surprising because the fracture mechanics $(K_{Ic}/\sigma_{ys})^2$ parameter is the fracture toughness index which defines the energy required to enlarge the plastic zone to the point of instability (Appendix A). All fracture toughness tests must relate to energy, directly or indirectly.

The DT test is configured to provide a sufficient run of fracture for establishing the characteristic fracture mode — plane strain, plane stress, or plastic enclave. The use of

a deep sharp notch (or brittle weld) and dynamic loading provides for initiation conditions which do not contribute a significant amount of energy absorption, in comparison to that required for propagation. In effect, the energy measurement relates to the energy absorbed in sweeping the characteristic plastic zones through a fixed distance.

The fracture propagation indexing features of the DT test are ideal for determining the LTTR. Returning to Fig. 8, we may now describe the generalized transition curve as relating to a characteristic DT test energy transition curve. The following critical reference points for the DT test transition (for any size of DT test) may be recognized:

1. Transition Through DT Regime 1 — Entry into regime 1 is indicated by the distinct rise in fracture energy from a lower toe region. The DT specimens first begin to show visible shear lips as the energy rise is developed. The point of initial increasing rate of energy absorption is equivalent to and correlates invariantly with the NDT temperature.

2. Transition Through DT Regime 2 — Regime 2 is indicated by the features of the DT curve as well as by the fracture appearance. The increase in fracture energy evolves to a very steep slope which becomes almost "vertical" with increases in temperature. Arrest markings on the fracture surfaces appear sharply as the rapid energy rise is developed. Plastic enclave conditions become easily visible (dimpling) as the DT energy curve begins to decrease in slope. A conservative index of the FTE is the midpoint of DT regime 2.

3. Transition Through Regime 3 to Full Ductility — Regime 3 is indicated by the decrease in slope of the energy-rise curve and a "shelving-out" to fibrous fracture. In this temperature region the thickness reductions become very large, as the growth of the plastic enclave attains final dimensions. The point at which the shelf is reached indexes the FTP temperature.

The sketches of microfracture and plastic zone interrelationships may now be indexed to the course of DT curves, irrespective of thickness. While the DT energy curves may cover a small range of energy values for small specimens and a very large range for large specimens, the interpretations of the significance of the full curve remain the same. The toe rise region defines regime 1, and the decreasing slope region near the shelf defines regime 3. The transition through regime 2 is clearly indicated by the steep slope of the energy curve and the rapid change in fracture appearance.

Sufficient experience has now been obtained in such definitions that a more specific procedure for indexing the three DT regimes and the FTE point may be made. This procedure simply involves separating the total curve into three equal sections each representing one third of the toe to shelf energy range, as shown in Fig. 8. This procedure is sufficiently accurate for most engineering purposes, because the full range of the DT-LTTR covers a relatively narrow span of temperatures. As such, the temperature range for each regime is relatively narrow, and any uncertainty in the point of change between regimes resolves to questions of ±15°F temperature differences, which are within the range of reproducibility. The FTE point is indexed to the center of regime 2, i.e., the midpoint of the DT energy curve.

Figure 14 illustrates a check on the predictions of such indexing procedures based on data provided in Refs. 1 and 7. The 5/8-in. DT energy transitions for two pressure vessel steels (2.25% Cr - 1.00% Mo, Q and T) are indexed to define the FTE and NDT temperatures. In the absence of DWT data, the NDT can be established directly from the DT test — as the shear lip start point or the temperature of FTE — 60°F. The course of the CAT curve is then approximated from these two reference temperatures. The DT predictions of the Robertson CAT curves temperature locations for the two steels are

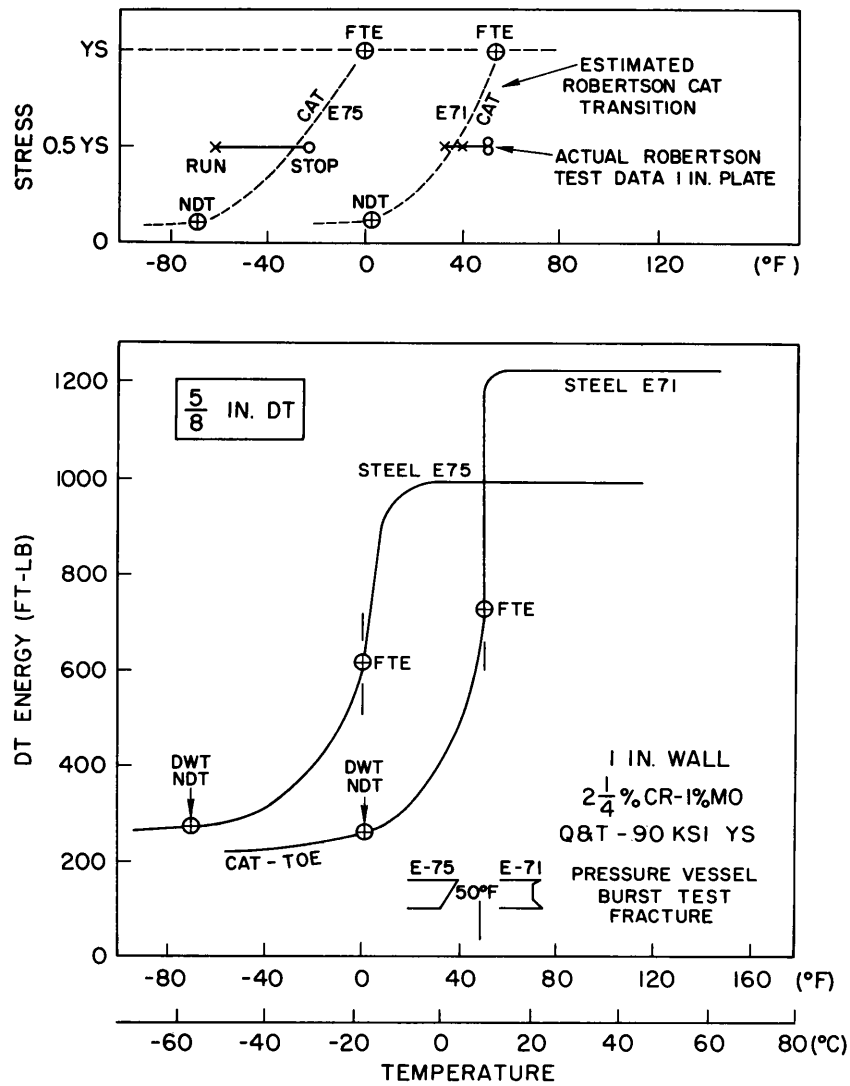

Fig. 14 - DT test indexing procedures for estimating the temperature scale position of the CAT curve (bottom). The DT energy midpoint indexes the FTE temperature which is equivalent to the CAT curve arrest temperature for yield stress loading. The CAT toe region (rise from lower shelf) is indexed to the NDT temperature, obtained directly by DWT or indirectly from the small-size DT test by the relationship NDT = FTE - 60°F. The estimated CAT curves (top) for the two steels are indicated to be located correctly by actual Robertson tests conducted at the 0.5 yield stress level.

presented at the top of the figure. Robertson test CAT determinations for the 1-in.-thick material were conducted previously for the two steels at 0.5 yield stress levels by the UK Reactor Materials Laboratory at Culcheth, England. The CAT "run" and "stop" temperature data points are plotted at the appropriate stress level of the DT predicted CAT curve. It is apparent that the 5/8-in. DT test predictions are almost in exact agreement with the Robertson CAT test data. The sketches at the bottom of the figure illustrate the

failure mode of the burst vessels at 50°F. These are exactly predicted by the DT test. Flask E-75 ruptured with a full slant fracture, while Flask E-71 ruptured with flat fracture and heavy shear lips.

EFFECT OF SECTION SIZE CONSTRAINT FOR DT TEST

Since the DT test can be scaled to any thickness of interest (Fig. 10), it provides a simple and unique method for investigating constraint effects. If plane strain conditions are retained to high temperatures by large section sizes, this fact should be evidenced by large DT tests. Evidence that the three regimes of the LTTR are not eliminated would indicate control by microfracture ductility.

The conflict of fracture mechanics and metallurgical predictions is illustrated in Fig. 15. These predictions relate to reactor pressure vessel quality A533-B steel used for the large DT tests to be described. Fracture mechanics K_{Ic} data for this steel were available only at relatively low temperatures because of the small specimens used (approximately 1-in. B thickness). These specimens had a K_{Ic}/σ_{ys} ratio measurement capacity in the order of 0.7. To measure K_{Ic} values at higher temperatures, specimens of greater B thickness would be needed. The extrapolated K_{Ic} values, compared to yield strength trends, indicated plane strain conditions of a K_{Ic}/σ_{ys} ratio 2.0 value at approximately 350 to 400°F. For the ratio 2.0, the B section size requirements are in the order of 10 to 12 in. The following fracture mechanics relationship of required section size to plane strain ratio, recommended by ASTM Committee E-24, is used for such determinations:

$$B \geqq 2.5(K_{Ic}/\sigma_{ys})^2$$

$$B \geqq 2.25(4) \geqq 10\,\text{in.}$$

Accordingly, the fracture mechanics extrapolations from low temperatures to the 300 to 400°F range indicated that brittle (plane strain) fracture could be obtained for plates of 10 or more in. in thickness. In effect, these extrapolations indicated that the LTTR would be eliminated due to thickness constraint effects, at least to 400°F.

The 5/8-in. DT transition curves for this steel characteristically locate the LTTR in the 0° to 140°F temperature range — the thick section DT transition was expected to be moved only moderately (less than 100°F). The DT curve plotted in Fig. 15 may be considered to represent an estimate of the location of a thick-section DT energy curve for this steel; the exact location is not important at this point. The metallurgical inferences derived from the estimated DT-LTTR suggested an upsweep in the K_{Ic}/σ_{ys} or K_{Id}/σ_{yd} ratios in the temperature range shown by the dashed bands. The infinity (∞) notation at the tip of the bands indicates plane strain saturation, i.e., loss of constraint due to increasing metal ductility.

The temperature range of the regime 3 conditions of the DT curve may be considered as a "plastic enclave wall" that could not be breached by increasing constraint due to section size. The bold arrow indicates that the dynamic plane strain (∞) limit should lie at somewhat lower temperatures. The static plane strain transition limit (∞) would thus be forced to temperatures lower than that of the dynamic transition limit.

The two "hypothetical" diagrams indicate the interesting state of events which essentially involved a head-on conflict of the two worlds of basic theory. Thus, the large DT test and large K_{Ic} tests which were conducted for this steel represented a most unique and interesting experiment. Metallurgical theory, which is based on events of microscale (grain-size) dimensions, was to be tested by the use of specimens of meter

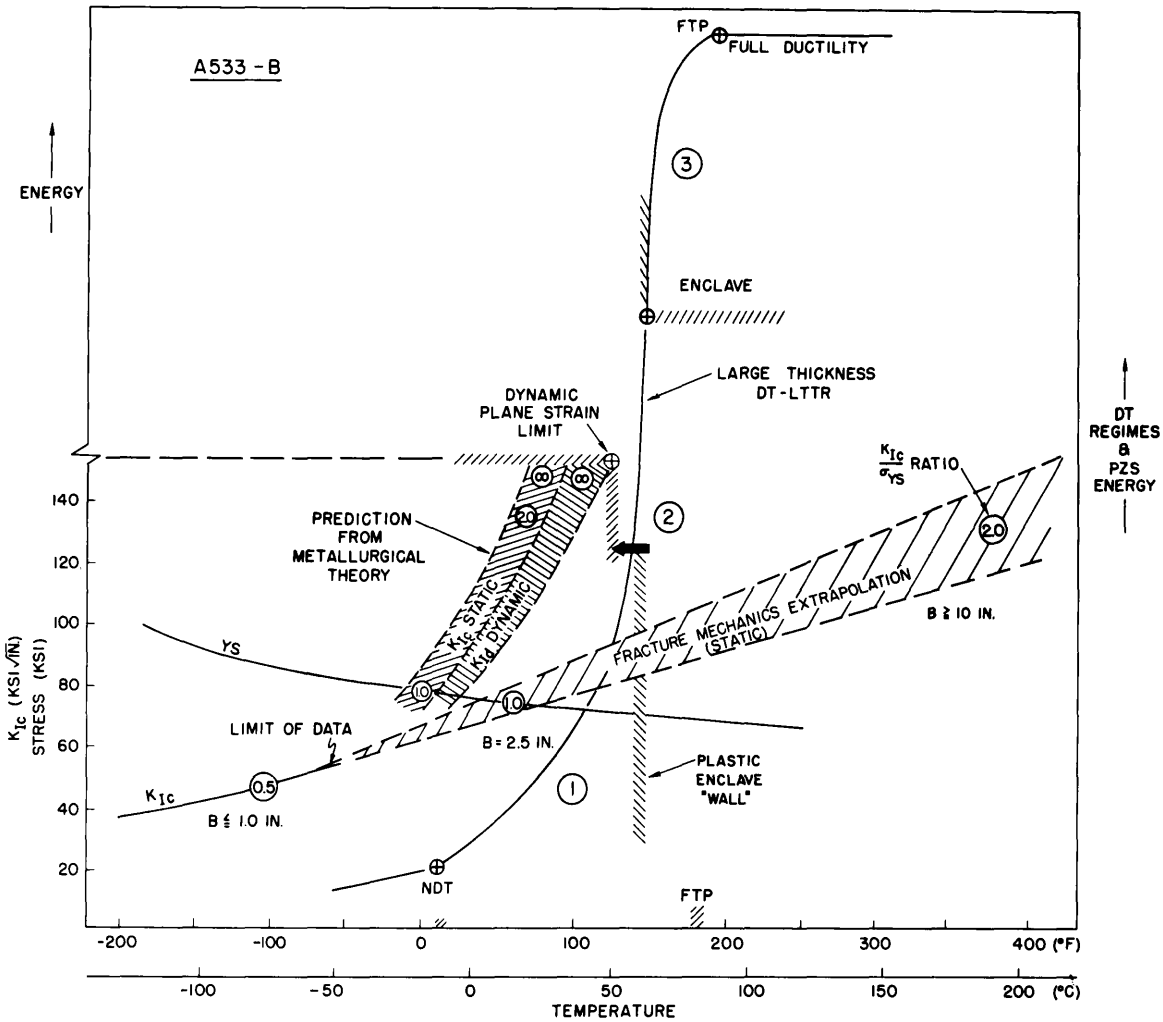

Fig. 15 - Nature of conflict between predictions based on metallurgical and fracture mechanics concepts as to the effects of large thickness on plane strain fracture toughness. Fracture mechanics extrapolations from low temperatures predicted retention of plane strain (brittle fracture) to high temperatures. Metallurgical considerations predicted a sharp rise of K_{Ic} and K_{Id} values at temperatures above NDT. The bold arrow signifies that the transition to plastic fracture (enclave) serves as a temperature "wall" barrier to the development of plane strain fracture.

dimensions and weights over 2 tons. The year 1968, during which these tests were conducted, provided intense excitement from points of view of both basic theory and engineering practicality.

The results of tests for a 6-in.-thick plate of A533-B steel are presented in Figs. 16 and 17. The chemical analysis, tensile properties, and Charpy-V data are presented in Table 2. Figure 16 presents data for 5/8-in. DT specimens involving through-thickness surveys for uniformity; the band includes over 100 test points. Representative fracture surfaces of the specimen are presented in the figure. Conventional DWT determination of the NDT at 1/4, 1/2, and 3/4 T positions indicated a range from 0 to 20°F. The indexing procedures for determining the temperature position of the three regimes defined the limits of plane strain from the 5/8-in. DT results as approximately 50°F, the FTE as

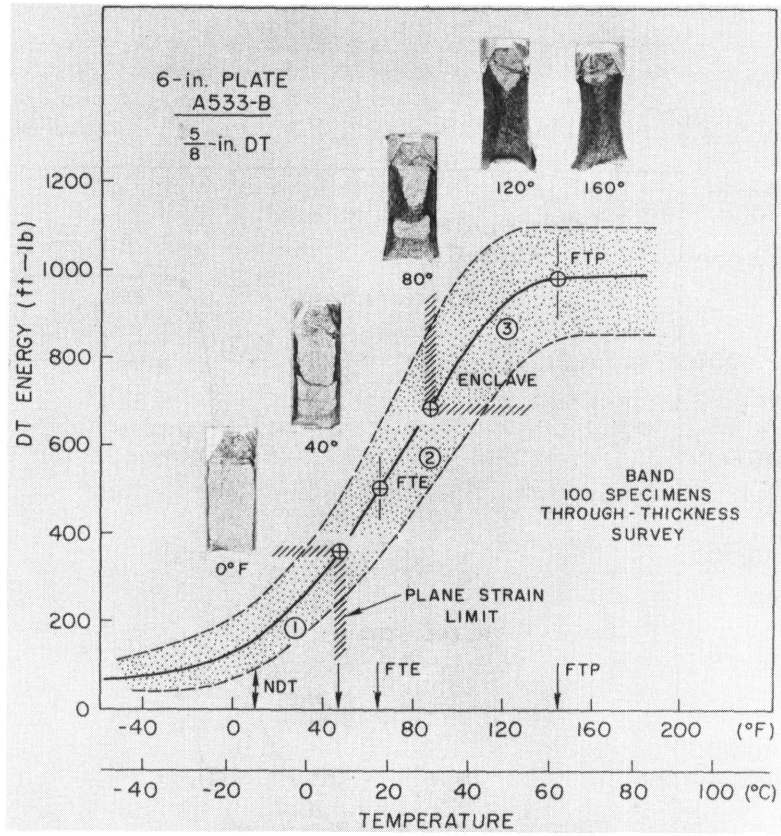

Fig. 16 - Procedure for indexing the 5/8-in. DT energy transition curve to the three characteristic regimes of fracture toughness transition. Data band for the RW direction relate to through-thickness surveys for the 6-in.-thick A533-B steel.

60°F, and the FTP as 140 to 150°F. Figure 17 presents similar data for 3-in. and 6-in. DT tests of this steel. The indexing procedures for these larger specimens define the limit of plane strain as approximately 120 to 130°F, the FTE as 140 to 150°F, and the FTP as 170 to 180°F.

Figure 18 presents a composite of fracture surfaces for the 5/8-, 3-, and 6-in. DT specimens. The lines separate the fractures into the three regimes defined previously. The changes in fracture appearance are clearly evident and show transition from flat fracture with small shear lips (regime 1) to fractures featuring slight and then strong arrest markings (regime 2) and finally to fractures featuring large lateral contraction and fibrous microfracture features. The change in fracture appearance through DT regimes 2 and 3 occurs dramatically in a narrow temperature range. The development of arrests is shifted to higher temperatures for the thick specimens (development of regime 2 is delayed).

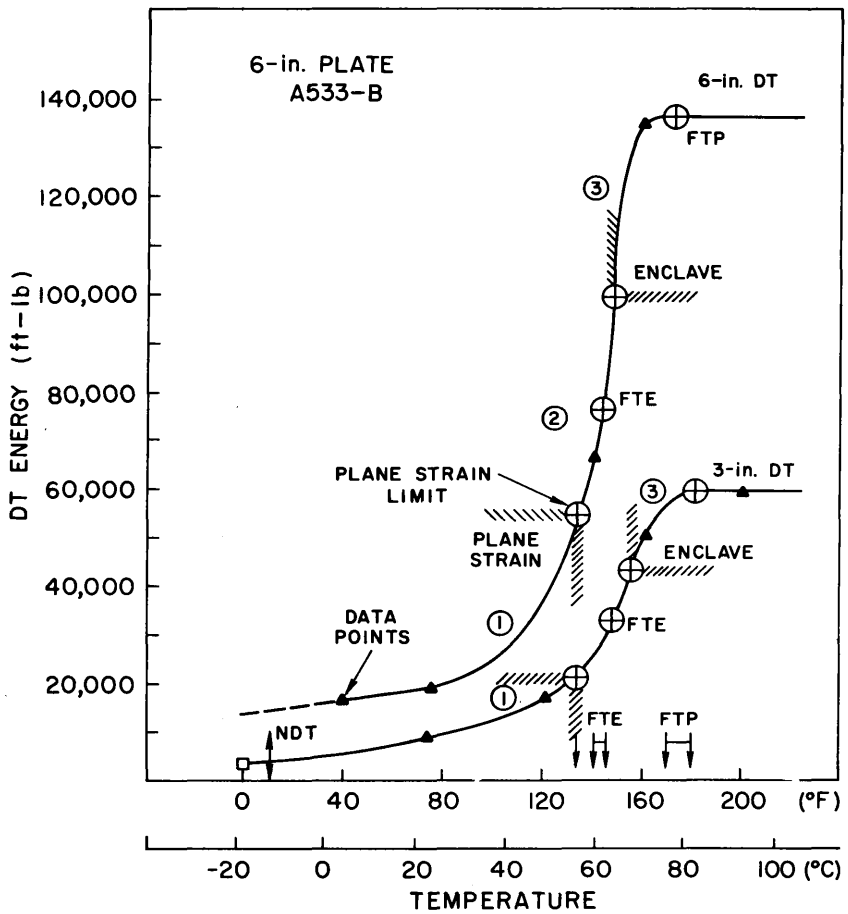

Fig. 17 - Results of 3-in. (RW direction) and 6-in. DT test series (WR direction) for the 6-in. A533-B steel. The energy transition curves are indexed to the three characteristic regimes of fracture toughness transition. The shifts in the temperature limit of plane strain, the FTE temperature, and the FTP temperature due to increased thickness may be deduced by comparison with the 5/8-in. DT data of Fig. 16.

Table 2
Chemical Analysis and Mechanical Properties
for 6-In. A533-B Class 2 Steel

(a)
Chemical Analysis Percentage

C	Mn	P	S	Si	Ni	Mo
0.23	1.18	0.007	0.014	0.20	0.57	0.46

(b)
Tensile Properties

Location	YS (ksi)	UTS (ksi)	Elongation (%)	RA (%)
Longitudinal				
Surface	79.3	99.2	23.8	66.6
1/2 T	74.1	93.2	25.2	64.5
Transverse				
Surface	83.8	108.8	21.7	60.1
1/2 T	78.9	97.4	23.7	59.6

(c)
Charpy-V Data

Temperature (°C)	Charpy-V Values* (ft-lb)	
	Longitudinal (RW)	Transverse (WR)
-120	13	10
-80	25	18
-40	43	28
0	68	40
40	94	55
80	108	70
120	112	78
160	112	78

Note: Charpy-V energy at NDT (+10°F)*: RW = 75 ft-lb and WR = 43 ft-lb. 50% FATT†: RW = -15°F and WR = 0°F.

*Average for 1/4 T and 1/2 T locations.
†Fracture appearance transition temperature (50% shear).

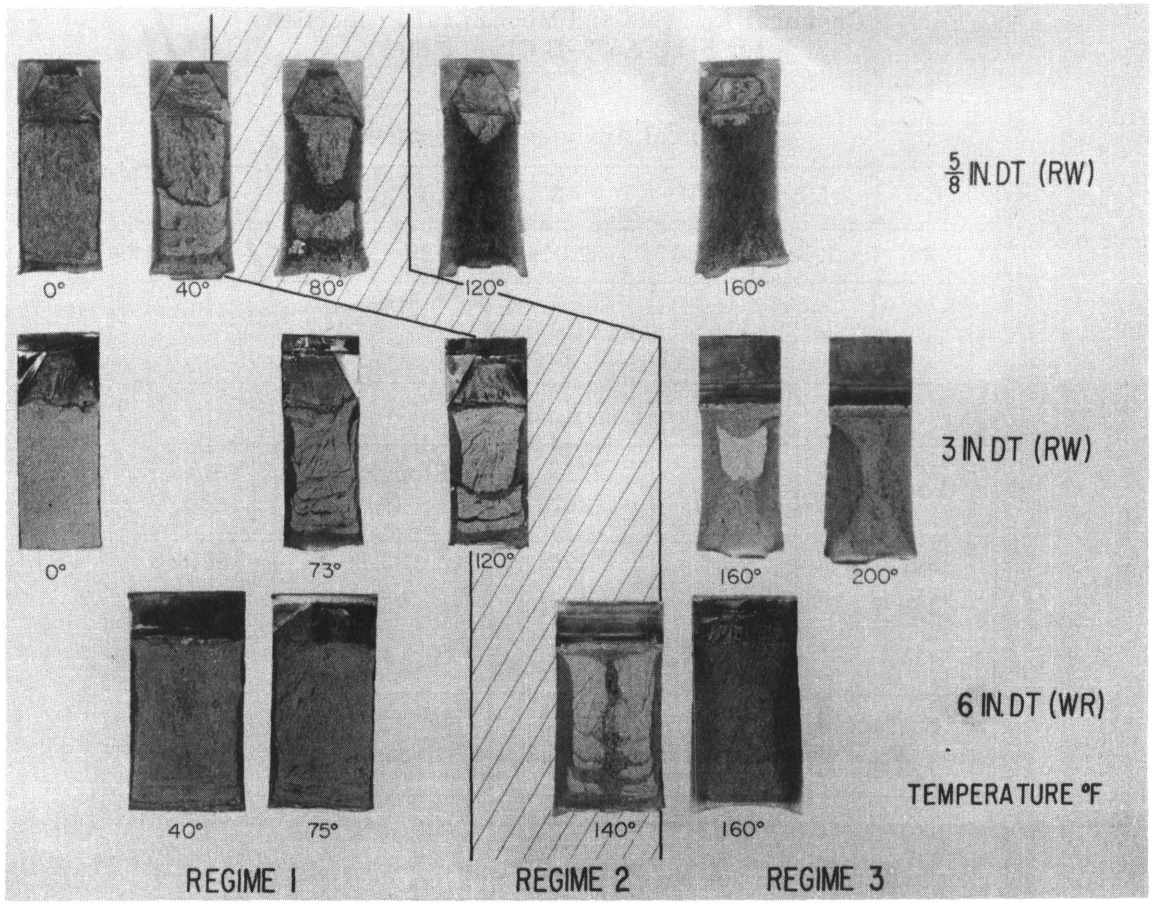

Fig. 18 - Correspondence of the fracture appearance transition of the DT test series to the three regimes defined by the energy transition curves. Featureless, flat fractures of regime 1 are extended to higher temperatures by increased thickness. The arrest markings indicate transition through regime 2. Fibrous fracture and lateral contraction features indicate completion of regime 3 transition. The transition temperature shift is fully developed in regime 1 by retention of the plane strain condition to higher temperatures. Regimes 2 and 3 are "compressed" for the thick sections, because there is little change in the total span of the transition from NDT to FTP.

The fracture surfaces and energy curves clearly indicate that the temperature range of regime 2 for the thick section was shifted in the order to 60 to 70°F. The shift occurs by the extension of regime 1, as anticipated. When regime 2 is entered by the thick specimens, an extremely sharp rise in fracture toughness occurs — the range of transition from plane strain to full ductility (FTP) is narrowed to approximately a 50°F span. When the high constraint imposed by the thick section is relaxed at the higher temperatures, a "surge" of microfracture ductility follows. The suppressed microfracture ductility comes into effect dramatically, in keeping with its expected characteristics for the higher temperature.

The high fracture toughness of this steel at 170°F is illustrated by Fig. 19. The 6-in. DT specimen was not fractured completely, because the energy delivered was slightly below the required level for full fracture. The illustration indicates ductile

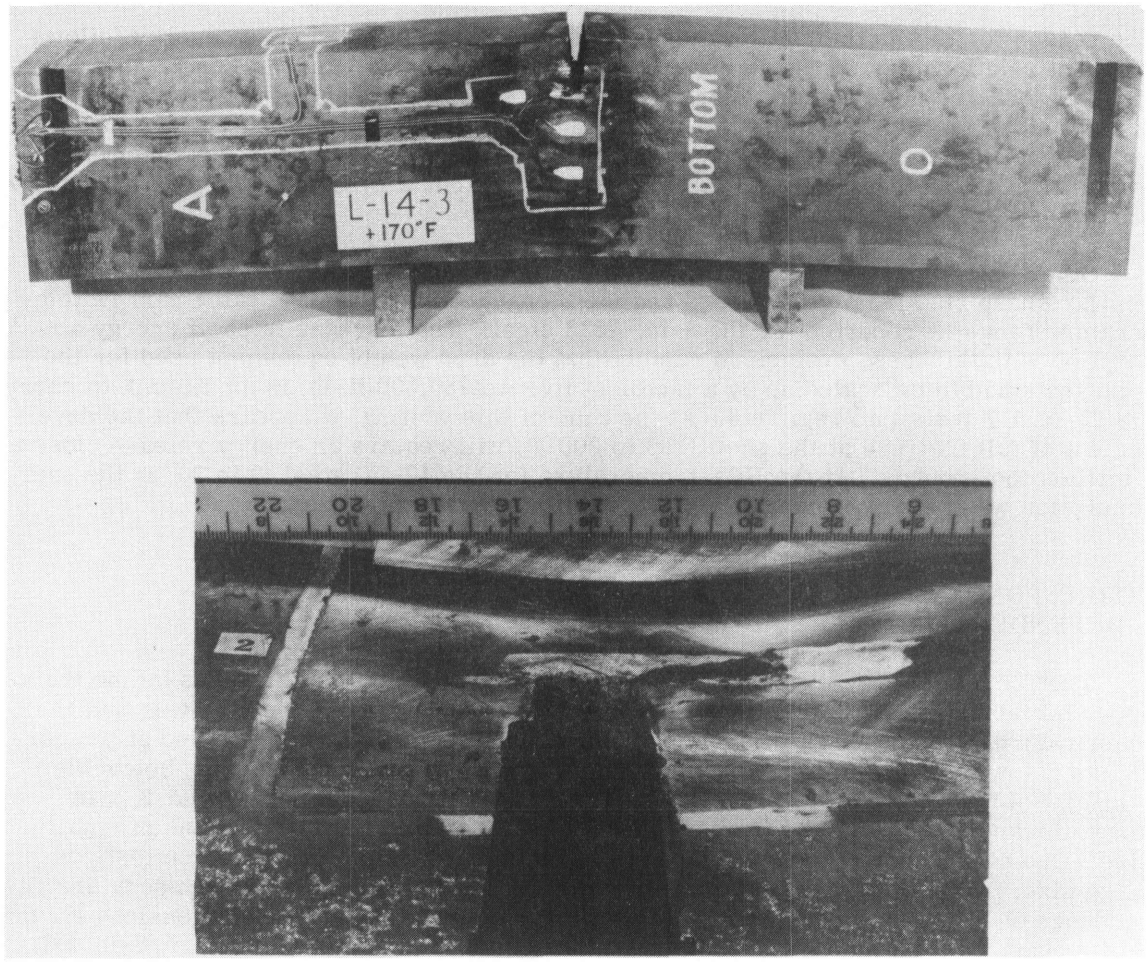

Fig. 19 - High fracture toughness of 6-in.-thick A533-B steel plate (full thickness DT) tested at 170°F in the RW direction. The energy delivered was inadequate to develop full fracture. Notch blunting and dimpling (enclave) is evident from the lower photograph.

fracture of enclave type. Another important aspect of these tests is the large increase in upper shelf fracture energy. In the RW orientation ("strong" — fracture across the primary rolling direction), this value ranges from 900 ft-lb for the 5/8-in. DT specimen to 61,000 ft-lb for the 3-in. DT. The 6-in. DT specimen was tested in the WR ("weak" — fracture in the primary rolling direction) because of machine limitations at the time — the shelf energy absorption was 135,000 ft-lb. In the RW direction (specimen of Fig. 19), the shelf energy for the 6-in. DT specimen is in excess of 160,000 ft-lb (machine limit). While an increase in shelf energy absorption is expected with specimens of increased dimensions, the magnitude of the increase cannot be calculated directly. Normalizing the energy in relation to the fracture area shows that this value is not constant but increases with thickness, because the absorbed energy is a function of the volume of the plastically deformed metal (enclave). This volume does not increase in geometric proportion to the specimen size, as a small specimen is scaled up.

None of the methods which could be used to normalize the energy absorbed by different size specimens are fully satisfactory for coverage of the total transition range.

The reason for this is the fact that the effects of increased thickness on energy follows different relationships for regime 1 as compared to regimes 2 and 3. For regime 1 constrained PZS are involved, and increased B is "embrittling," until the required B value is reached. For regimes 2 (upper half) and 3, plastic fracture is involved, and increasing B results in increasing enclave size which increases the energy requirement for fracture. The differences in the B effect are consistent with elastic and plastic fracture processes.

Other tests which are presently underway for 12-in.-thick A533-B steel indicate similar sharp rise from regime 1 to regime 3 characteristics in the same narrow temperature range as reported for the 6-in. A533 steel. The increase in shelf energy absorption with thickness evolves so rapidly that the drop weight equipment used for the 6-in. tests had to be scaled up by a factor of five (to 750,000 ft-lb) in an attempt to carry the 12-in. DT tests into regime 3. At the time of this writing, it appears that the development of full fracture at the shelf (180 to 200°F) will require an energy release close to 1 million foot-pounds. At the NDT temperature for the 12-in. steel (0 to 20°F) the energy absorption was only approximately 60,000 ft-lb.

CORRESPONDENCE OF DT TRANSITION TO THE TEMPERATURE DEPENDENCE OF K_{Ic} AND K_{Id}

The DT test energy transition curves for specimens of large thickness define the upper bound limit for dynamic plane strain fracture toughness. This signifies that the temperature-dependence relationships of K_{Ic} and K_{Id} must be fully evolved at temperatures below the subject DT energy curve and specifically at temperatures below the midpoint of this curve. The practical utility of these relationships (K_{Ic} and K_{Id} to large-thickness DT) must be derived ultimately from tests of DT specimens of small size. One cannot expect to routinely conduct materials evaluations based on tests of large size. Accordingly, we shall now consider the relationships of the temperature dependence of K_{Ic} and K_{Id} (which would require specimens of large B dimensions for determination) to temperature index points based on the course of the small, 5/8-in. DT specimens. There are two practical points of reference:

1. The FTE index point for the 5/8-in. DT specimen, which marks the temperature which is 40 to 60°F below the dynamic plane strain state limit for large specimens, as described in the previous section.

2. The familiar NDT temperature index, which marks the temperature of rapid increase in dynamic plane strain fracture toughness for small or large specimens. This temperature is approximately 100°F below the plane strain limit for large specimens.

Thus, by using these practical index points it is possible to define the plane strain limit temperature based on the Δt increment, i.e., either FTE + 40 to 60°F or NDT + 100°F. While knowledge of this ultimate limit is important, it is equally important to evolve information as to the temperature dependence of K_{Ic} and K_{Id} in the temperature range between the NDT and the limit temperature. This information would make it possible to use fracture mechanics procedures indirectly by reference to easily indexed temperatures. The following discussions will evolve the case for such procedures.

Figure 20 illustrates that the temperature range of plastic enclave fracture toughness for the 6-in. A533-B steels starts at NDT + 120 to 140°F. A vertical dashed band is used to emphasize this fact in the figure. The notation of infinity plane strain (∞) for dynamic fracture is then located conservatively at NDT + 100°F. It is possible that the limit is actually at somewhat lower temperatures but certainly not at higher temperatures, because this would then enter the plastic enclave fracture toughness temperature

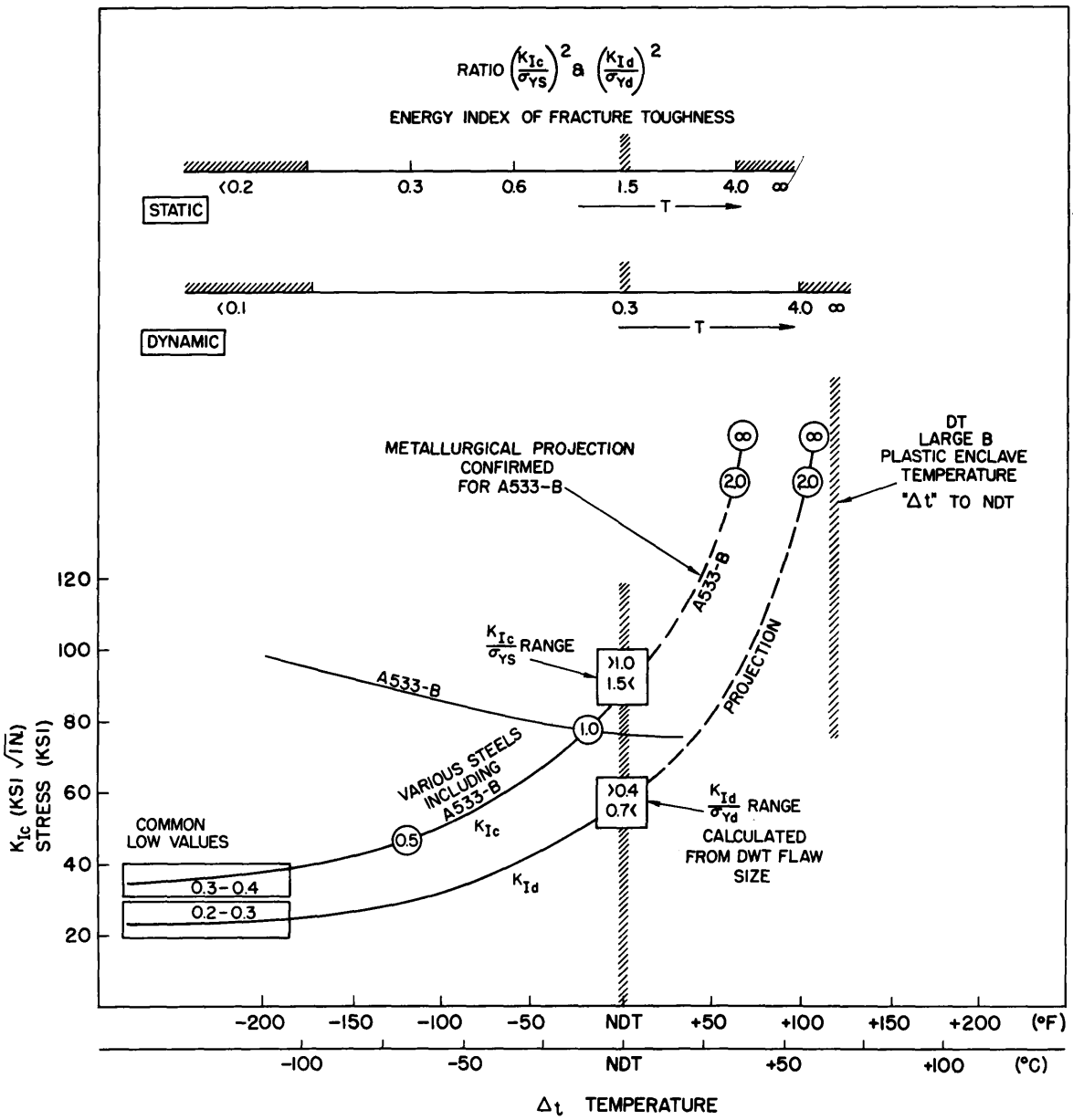

Fig. 20 - Indexing of the NDT temperature to the temperature-dependence features of K_{Ic} and K_{Id}. The expected range of K_{Ic}/σ_{YS} and K_{Id}/σ_{YD} ratio values are shown in the "boxes." The K_{Ic}, K_{Id}, and related ratio values develop a sharp rise to infinity conditions in the temperature interval of NDT to NDT + 100 to 120°F. The static plane strain transition is completed in the interval of NDT to NDT + 40 to 60°F. The temperature dependence of the ratios squared, which represents the true index of plane strain fracture toughness, is indicated by the scales at the top.

range. The infinity plane strain condition for static loading is conservatively estimated to be at 40°F lower temperature, i.e., NDT + 60°F. The basis for this estimate will be clarified in the following discussions. The infinity notation signifies that plane strain conditions cannot be attained. For purposes of numerical reference we shall indicate that the ratio 2.0 level is attained immediately before the plane strain limit is reached. This would signify that K_{Ic} specimens of 10- to 12-in. B thickness would be required to establish the temperature at which the ratio 2.0 is reached.

For purposes of correlation with the DT test energy transition, we now need to index the values of dynamic and static ratios to be expected at NDT temperatures, i.e., at the start of the DT transition. Previous calculations by Irwin (8) indicated a K_{Id}/σ_{yd} ratio of 0.78 at the NDT temperature — discussions in one of the following sections will indicate the bases for the authors' opinion that the dynamic ratio is in the range of 0.4 to 0.7. The experimental data which support this deduction are conclusive, as indicated by the fact that specimens of relatively small B thickness (1 in. or slightly less) are adequate for determining K_{Id} values to temperatures near or at the NDT temperature. Above the NDT temperature, specimens of large B dimensions are required, and no data are reported in the literature due to experimental difficulties in conducting such investigations (machine capacities). The determination of static K_{Ic} values at temperatures approaching the NDT has required the use of specimens in the order of 3-in. or greater B thickness. This requirement signifies that the K_{Ic}/σ_{ys} ratio at NDT is in excess of 1.0. Data for A302-B and A533-B steels have been reported (9-11), which show a temperature dependence of K_{Ic} from very low temperatures to those approaching NDT, as indicated in Fig. 20.

The "boxes" in Fig. 20 indicate the ratio features at very low temperatures and the NDT temperature. The static ratios fall in the 1.0 to 1.5 range at NDT, while the dynamic ratios are in the range of 0.4 to 0.7. The dashed parts of the curves indicate extrapolations of the K_{Ic} and K_{Id} temperature dependence in the remaining narrow band of temperature, i.e., NDT to NDT + 40 to 60°F for the static case and NDT to NDT + 100°F for the dynamic case. The full K_{Ic} projection has been confirmed recently by 12-in.-thick K_{Ic} tests of A533-B steel (11) conducted by Wessel — these data indicate a ratio value of 2.0 at approximately NDT + 40 to 50°F. These tests provide the only existing data which extend to the ratio value of 2.0.

The low value of dynamic fracture toughness at the NDT temperature is a well-recognized fact, confirmed by flaw sizes involved in service failures. The new information of major importance is the indexing of the dynamic ratio value at NDT and the rapid increase of this ratio in the temperature range which lies between NDT and the steeply rising portion of the DT curve. We consider the K_{Id} projection to be proven by the DT test results for specimens of large B thickness. New information is provided also by the observation that the static ratios are relatively high at the NDT temperature and only a narrow range of temperature remains for completion of the static plane strain transition to infinity value. In effect, it is deduced that the applicability of fracture mechanics for the case of static loading is limited to temperatures which are below the NDT + 40 to 60°F index point. We shall now discuss other questions which must be considered before decisions are made to design on static load conditions for temperatures below the subject index point.

Considerable concern has arisen in the field of fracture mechanics relative to the experimental determination of K_{Ic} values and with respect to whether the static value for fracture instability can be relied on for the case of loading-rate-sensitive steels of relatively low strength. The problem is that the experimental procedures for measurement of the static K_{Ic} value crucially depend on events involved with very small, initial, slow extension of the crack (creeping instability) prior to attaining a popin (fast fracture). Some steels appear to tolerate more of this gradual "creeping" extension of the crack of

microscopic dimensions than others. It appears that all steels become involved in this type of crack extension to a greater degree with increasing temperature, i.e., with the development of a sharp rise of K_{Ic} values with increased temperature. In brief, the K_{Ic} determination becomes controlled by complex events involved in creeping, slow extensions of the crack rather than by a clear-cut instability (popin). Thus, there is a question as to the reliability of using K_{Ic} values based on such events as the basic criteria for fracture-safe design. It is suspected that such events may be critically related to small differences in loading rate and as such would suggest placing increased emphasis on K_{Id} values rather than on K_{Ic} values for fracture-safe design — certainly additional studies are required.

Another crucial question is involved in the requirements for developing the fatigue cracks. Procedures for fatigue precracking of K_{Ic} specimens recommended by the ASTM E-24 Committee involve the use of low K values for low-strength steels. This requirement results in a very high number of cycles and high expense in the preparation of specimens, particularly if they are of large B thickness. The reason for this limitation is the known fact that fatigue cracks which are not prepared with such care result in artificially high (invalid) values of K_{Ic} due to a residual, crack tip stress field and overlarge, residual fatigue crack PZS. It is not clear how this practical limitation to K_{Ic} testing can be resolved. If it cannot be resolved, static K_{Ic} testing will be of interest only for research purposes. Attempts to bypass the expense of high-cycle fatigue cracking, by use of high K values in fatigue, will simply produce invalid data.

This review also serves the purpose of emphasizing that the static K_{Ic} temperature relationships presented in Fig. 20 represent lower bound values, for carefully prepared specimens and for steels which develop "creeping" extensions to the highest possible temperatures (close to the dynamic transition as shown in the figure). Evidence is beginning to evolve that some steels (for example, different heats of A533-B steel) will undergo rapid increase in K_{Ic} at temperatures far below the NDT temperature; i.e., the infinity limit may be attained below the NDT. For such steels, static plane strain fracture mechanics is not applicable at temperatures above NDT. In effect, the engineer is forced to design on the basis of dynamic fracture mechanics (above the NDT) or forego the use of this approach by restricting the lowest service temperature to NDT + 40 or 100°F (depending on B thickness) and thereby use the plastic fracture resistance potential of the metal.

Since these problems of K_{Ic} values may not be clarified in the near future, we have taken the course of using the temperature-dependence relationships indicated in Fig. 20 as the only conservative deductions which can be made. The subject K_{Ic} data are valid and must be recognized; there is a relatively close approach to the K_{Id} temperature-dependence curve; therefore, the K_{Ic} curve could not be moved to much higher temperature. Any movement to lower temperatures would quickly lead to infinity K_{Ic}/σ_{ys} ratios at and below NDT temperatures. Therefore, all further considerations of the question of K_{Ic} temperature dependence will be based on what appears to the best and self-consistent published data which indicate limited utility for static K_{Ic} testing above NDT temperatures. These data represent lower bound values of K_{Ic} temperature dependence and as such present as favorable a case as can be made presently for the use of fracture mechanics K_{Ic} data in this temperature range.

There should be no concern for the exactness of the K_{Ic} and K_{Id} values indicated by the extrapolations. The steepness of the temperature-dependence relationships is the crucial aspect. In fact, the indicated slopes, per se, do not provide a true index of the dramatic increase in fracture toughness in this narrow band of temperature. A translation to the true increase of fracture toughness (fracture energy) is provided by the $(K_{Ic}/\sigma_{ys})^2$ and $(K_{Id}/\sigma_{yd})^2$ ratios indexed to temperature by the two scales at the top of the figure. In the interval of NDT to NDT + 100°F, the dynamic ratio squared jumps

from 0.3 value (brittle) to 4.0 value, which represents a high level of plane strain fracture toughness. In fact the jump is actually to infinity ratio. In the 40 to 60°F interval above NDT the static ratio squared increases from 1.5 (or less) to 4.0 (infinity). In comparison, there is a very slow decrease of the ratios squared with decreasing temperature to 150 to 200°F below NDT. Thus, the plane strain fracture toughness shows the same sharp increase in temperature dependence as the DT test, at temperatures above the NDT. The infinity limits are reached in the regime 1, toe region of the DT test. These results are in complete accord with the predictions of metallurgical microfracture processes. The same processes operate to cause the increase in the DT energy curve in this regime — this is the enlarging plane strain plastic zones which is the basic parameter controlling fracture toughness, whether measured directly by energy or indirectly by the elevation of the elastic stress fields, i.e., the K index.

The consequences of the very steep temperature dependence of K_{Ic} and K_{Id} in the NDT to NDT + 40 to 100°F range may now be interpreted in engineering terms. For this purpose it is most enlightening to index the rise in fracture toughness to flaw size-stress relationships. Figure A3 (Appendix A) presents the relationships of critical flaw sizes to relative stress and to the ratio values. These relationships are general and simply present graphically the results of fracture mechanics flaw size-stress calculations for plane strain fracture initiation — these apply to any metal. The temperature dependence of the ratios is indicated by referencing the average ratio value at NDT and noting the Δt required to attain higher ratios, as deduced from Fig. 20. When used to index NDT + Δt ratio increases, the diagram is defined as the NDT Ratio Analysis Diagram (NAD). The static Δt temperature scale indexes the increase of K_{Ic}/σ_{ys} ratios. The dynamic scale indexes the increase of K_{Id}/σ_{yd} ratios. The parabolic shape of the flaw size curves are a consequence of the ratio-squared factor which enters into the calculations of the flaw sizes. The reason for the two limit flaw geometries, stubby and thin, is described in Appendix A. Briefly, the stubby flaws feature lower stress intensification and constraint for the same depth, compared to the long thin flaws. Thus, the stubby flaws require higher relative stress for instability, at the same ratio value of fracture toughness. Between these two extremes there is a spectrum of curves relating to flaws of intermediate severity and constraint features. However, all of the intermediate flaw curves will be between the limits indicated by the stubby and thin flaws.

It is apparent that increasing the temperature by 60 to 100°F above the NDT sweeps through the major part of the plane strain regime, which is most significant to engineering design. Only a very small corner of the diagrams remains for definition below NDT temperatures for the dynamic case. This small corner relates to tiny flaw sizes, if the stress levels are high. Many structural failures develop at or below NDT temperatures from dynamic instability of small flaws located in weld residual stress fields or at points of yield stress loading for geometric details (corners, etc.). For such conditions, temperatures below NDT hardly need K_{Id} determinations or even calculation — the flaw sizes are all in the few tenths-of-inch size range. Evidence has been presented repeatedly that fracture mechanics calculations provide exact definition of critical flaw sizes for such conditions. While such exactness is to be expected, this does not say that similar definitions can be made above the NDT range which involves a sharp rise of fracture toughness with temperature. The critical flaw sizes then change rapidly in 20°F steps and a strong stress dependence develops. In effect, the multiplicity of critical flaw size conditions and the large effect of temperature in 20°F steps makes the practical application of exact failure mechanics in the transition range impossible, for either the static or dynamic case.

This deduction does not say that rough generalizations of great engineering value cannot be made. Practical use of fracture mechanics for the transition range must be based on considerations that the structures will experience use over finite temperature ranges and the lower limit temperature should be estimated conservatively. If this

procedure is followed, lower bound (conservative) estimates of flaw sizes that should be inspected for and eliminated can be made for specific temperatures. However, if this is to be done using K_{Ic} and K_{Id} data, large specimens must be tested over a narrow range of temperatures to define the transition interval. Use of fracture mechanics tests for this purpose is prohibitively expensive. The only alternative is to rely on projections of temperature-dependence relationships for K_{Ic} and K_{Id} values as indicated by Fig. 20. By this procedure K_{Ic} or K_{Id} values need to be determined only at NDT or lower temperatures, based on specimens of reasonable size. Such procedures would represent K_{Ic} and K_{Id} Δt approaches and also makes these approaches feasible. Fracture mechanics cannot provide alternatives to transition temperature procedures; it can only provide improved definitions for these procedures.

INTERPRETATIONS TO NDT

The relationships presented in Fig. 20 clearly indicate that the K_{Ic} and K_{Id} values increase rapidly in a narrow temperature range above the NDT. The critical flaw sizes increase in the same manner. There does not appear to be a singular point of reference — this is the argument that is raised with respect to the DWT, which features the use of a flaw of singular dimensions, loaded to a singular level of stress (yielding). Since the DWT-NDT flaw size-stress combination is "one of many," how can it have a singular meaning? The answer is to be found squarely in fracture mechanics analyses, now that the sharp temperature dependence of K_{Id} has been established. The general fracture mechanics significance of the NDT and of the mechanical behavior of the DWT has been explained by Irwin (8) and Pellini (1). Now we are prepared to examine the physical significance of the NDT in terms of the temperature dependence of critical flaw sizes.

The DWT features a small flaw of low severity; i.e., its geometric constraint potential is low as well as its stress intensification aspect. The low severity features of the flaw restrict the test to indexing of K_{Id}/σ_{yd} ratios of low values. The rapid increase in the K_{Id} level of fracture toughness in the vicinity of the NDT temperature signifies that the ratios and, therefore, the critical flaw sizes for yield stress loading are increasing rapidly with small increases in temperature. The small DWT flaw, which is subjected to yield level dynamic loading, therefore develops a "break-no-break" transition representing a dynamic plane strain to plane stress transition, i.e., K_{Id} to K_c. Figure 21 illustrates a conventional DWT-NDT "break-no-break" series, also, a test series with open-stop, so that the K_c transition to higher fracture toughness becomes apparent. The DWT flaw severity is too low for the required level of plane strain constraint at NDT + 20 to 30°F — at NDT it provides barely the exact level of required severity, and fracture results. How much larger the flaw would have to be to provide for plane strain fracture at NDT + 20°, 40°, etc., will be clarified by fracture mechanics analyses to follow.

We shall use the data of the A533-B steel noted in Fig. 20 for these analyses, because the temperature dependence of K_{Id} through the NDT region and beyond must be known, at least approximately. K_{Id} values are scarce because of the practical difficulties of conducting K_{Id} tests and also for defining dynamic yield strength values required for the K_{Id}/σ_{yd} definition. At the NDT temperature the K_{Id} value for the A533-B steel is known to be approximately 50 ksi $\sqrt{\text{in.}}$ At NDT + 80 to 100°F it is of infinity value — an estimate of a K_{Id}/σ_{yd} ratio value of 2.0 at NDT + 80°F is highly conservative for purposes of this analysis.

The value of the dynamic ratio for the NDT temperature may be decuced from the flaw size, geometry, and loading conditions of the DWT. The flaw (brittle weld) geometry corresponds to a semielliptical configuration of "stubby," 1:3 to 1:4 (depth-to-width) aspect. The depth is approximately 0.2 in., and the width is approximately 0.6 to 0.8 in.

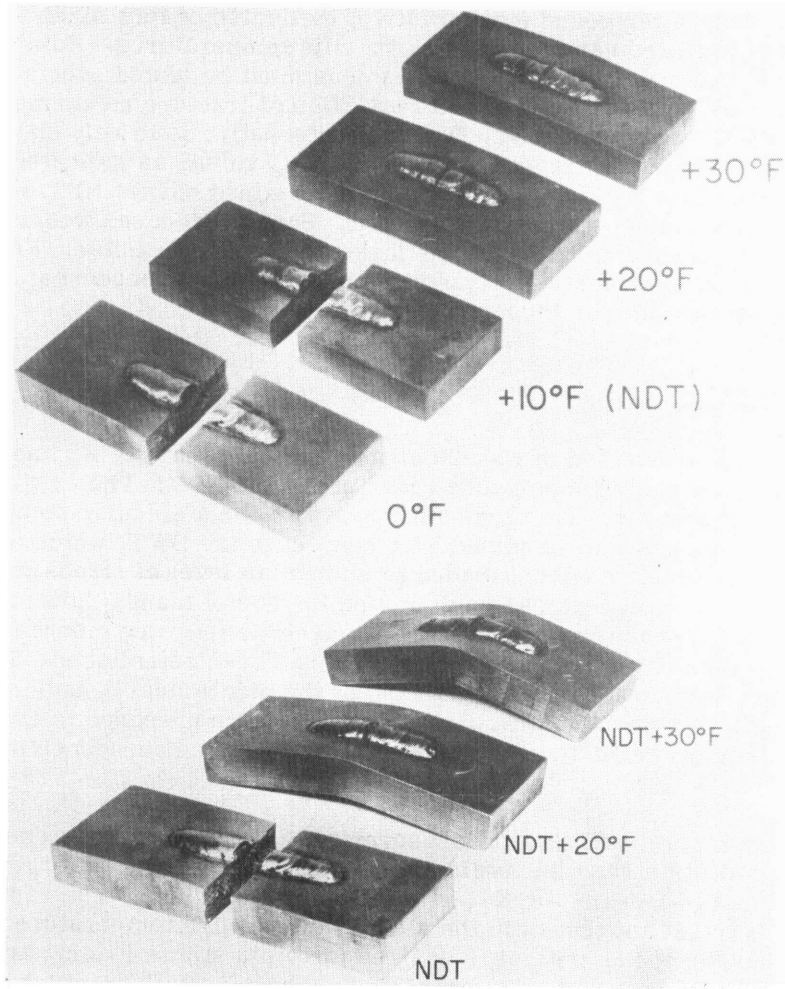

Fig. 21 - Typical drop-weight test series, illustrating NDT at 10°F (top). Open anvil test series illustrating ductility developed at temperatures above the NDT as compared to the flat breaks at and below the NDT (bottom).

An attempt to calculate the dynamic ratio has been made by Irwin (8). He assumed a 1:4 surface flaw and loading equal to the dynamic yield stress. The value of the dynamic yield stress was estimated by adding 30 ksi to the static yield stress, within the bound of low and intermediate strength steels. The calculation, using Irwin's K_{Ic} formula for a surface flaw in tension (Appendix A) indicates $K_{Id}/\sigma_{yd} = 0.78$. If the flaw geometry is assumed to be 1:3, the ratio is then indicated to be 0.71. The formula of Smith (12) for a surface flaw in bending is considered to give a better approximation to the actual conditions in the DWT. Use of this formula for 1:3 and 1:4 flaws gives ratios of approximately 0.5. Recent investigations by Shoemaker and Rolfe (13) based on K_{Id} studies for steels ranging from 35 to 135 ksi yield strength show a measured 0.5 to 0.6 ratio value as an upper bound.

In view of the expected variations in measured K_{Id} values, the specific size of the DWT flaw, and of the estimations required for the dynamic yield stress, it is not feasible

to define the ratio more exactly than to a ±0.1 ratio value. Sufficient evidence now exists to bracket the applicable ratio within the range of 0.4 to 0.6 and to assign a conservative value of 0.5 ± 0.1 for purposes of generalized reference. It is unlikely the more exact definition will be possible or warranted. The NDT represents the temperature at which the ratio value begins to increase rapidly — relatively small changes in temperature have a large effect on the ratio value.

Figure 22 indexes the NDT to NDT + 80°F temperature range to the dynamic ratios by following the course of the projected K_{Id} curve presented in Fig. 20. The ratio index at NDT is taken as 0.5, and at NDT + 80°F it is at least 2.0. A series of approximations of K_{Id}/σ_{yd} ratios in 20°F steps may now be made. Since the rise in K_{Id} values is very rapid, exactness in the ratio definitions is not required. The reality of this statement is evident by the sharp increase of critical flaw sizes in 20°F steps, as illustrated in Fig. 22.

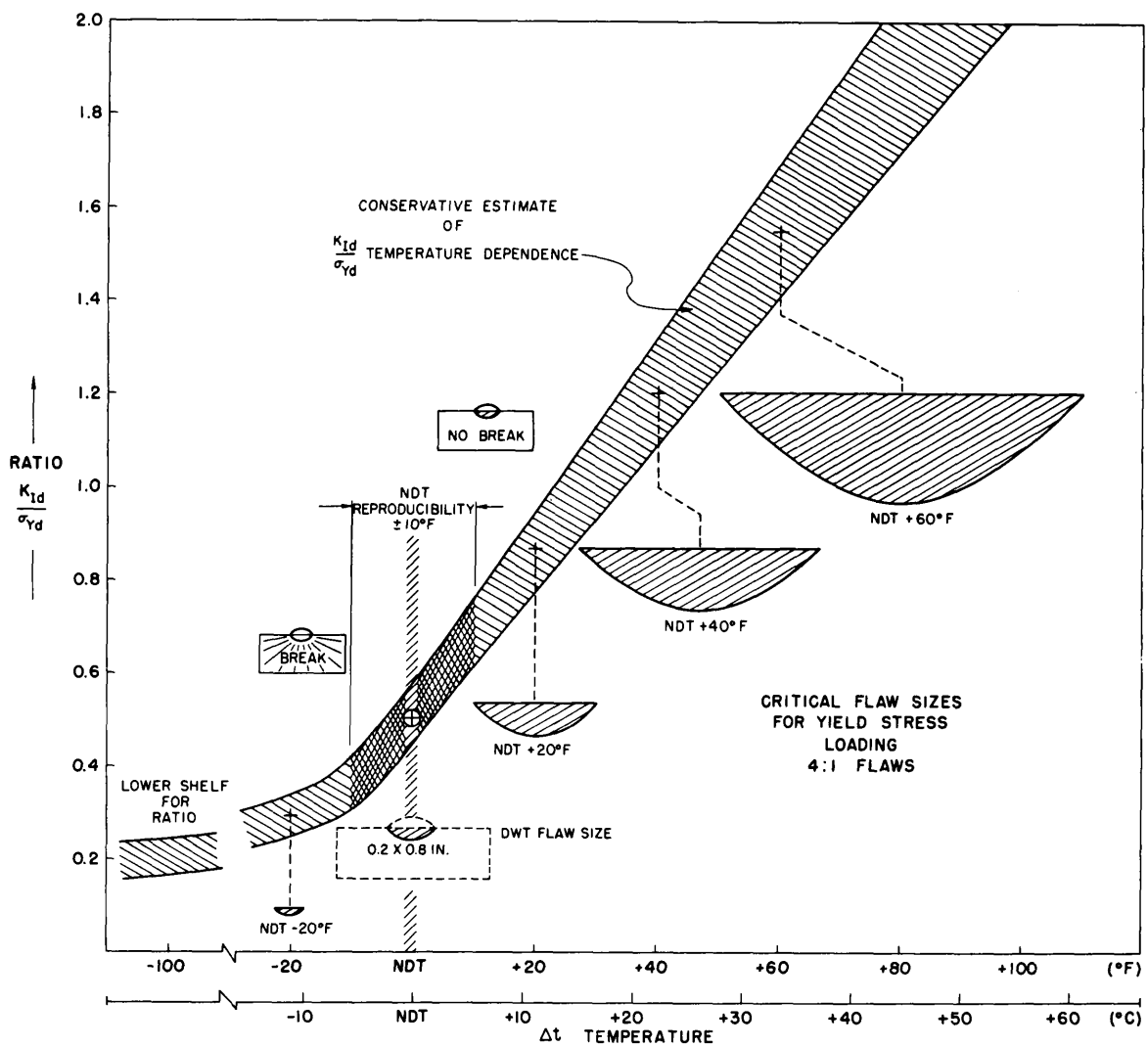

Fig. 22 - Basic significance of the DWT-NDT temperature. It marks the temperature of sharp change in the critical flaw size for dynamic fracture initiation at yield stress loading. Above the NDT temperature large flaw sizes are required for fracture initiation, while below the NDT tiny flaws are sufficient.

The translation of ratio values to the dimensions of critical flaw sizes is provided by the yield stress curve of Fig. A3. For example, at a ratio of 2.0 the required depth for a stubby flaw is approximately equal to 2.4 in. The DWT flaw size is used as a reference in Fig. 22 — the critical flaw sizes for temperatures below and above the NDT are proportioned by scaling to the DWT flaw size. Each of the illustrated flaw sizes should develop a sharp K_{Id} to K_c transition (break to no-break) as the indicated temperatures are exceeded by 20 to 30°F, similar to that illustrated for the DWT in Fig. 21. The reason for this is that the flaws are of exactly the critical size for reaching the required K_{Id} instability value (instability = break) at yield stress levels. As the temperature is raised by 20 to 30°F, the K_{Id} value has increased, and the flaws then become subcritical (stable) because the higher K_{Id} value will require a larger flaw for plane strain fracture. To "K_c" means that the flaw tip will relax its constraint, enlarge its PZS, and thereby increase its resistance to fracture by a large amount, while still primarily under the influence of elastic stress fields.

The significance of the NDT temperature should now be clear; as follows:

1. In accordance with its original definition, it represents the temperature of sharp change from tiny to large size flaw instabilities for yield stress loading. NDT ± 20°F clearly shifts the critical flaw size from tiny to large. The NDT ± 10°F range, which is within reproducibility limits of the DWT, clearly sits in the middle of this transition.

2. Equivalently, it may be recognized as representing a dynamic plane strain fracture toughness transition, relating specifically to the $K_{Id}/\sigma_{yd} = 0.5 \pm 0.1$ ratio value.

The reason for the selection of the specific size of weld bead crack for the DWT becomes apparent — it is a small, yet practical, size. The process by which this flaw size was arrived at, ca. 1952 in prefracture mechanics K_{Ic} - K_{Id} days, has its answer in the ship failure studies. It was noted that the break-no-break transition for DWT prepared with arc strikes (tiny flaw sizes 0.1 by 0.2 in.) showed a statistically significant difference in the correspondence to the DWT-NDT. Exact correspondence was obtained in some cases; however, 10 to 20°F lower temperatures were generally required for fracture of the arc strike specimens. The sharp temperature change in critical flaw sizes became clearly apparent. The arc strike and similar tiny weld defects were known to be the flaw sources for ship failures — not the large cracks. The presence of high residual stress fields around the arc strikes and the tiny weld cracks were also known. The fact that the instabilities of these tiny cracks were not arrested was all too well established by ship failures. In other words, all the information required to define the singular "tiny flaw" instability limit temperature for yield stress loading was available. Accordingly, the DWT was proposed and validated as a method for establishing the temperature limit for the instability of tiny flaws. The early literature cited that "small flaws will not become unstable above the NDT temperature."

As a matter of practicality, the DWT was designed to enforce a small degree of plastic strain rather than exactly yield stress loading when the specimen hits the stops without fracturing. It would be an impractical test if "exactly" yield stress level of loading was a requirement. This means that the weld crack placed on "DWT" test sections of 2-in., 3-in. or larger size may cause instability (fracture), if the degree of plastic overload is not controlled carefully; i.e., it will force a K_c fracture to NDT + 20 to 30°F temperatures. This fact was also known and led to attempts to normalize (control exactly) the crack size opening (COD) for the larger tests — this procedure was not practical. This was the reason for limiting the size of the DWT (5/8, 3/4, and 1 in.). The intent was to "build in" a protection device against variations in plastic overload without resort to normalizing crack opening displacement. Again, this is a matter which can now be explained more clearly by fracture mechanics — the thickness was kept small so that its low B constraint features would prevent K_c fractures. Two barriers exist to

total instability (break) of the DWT — the low flaw severity barrier and the small B constraint barrier. These work together to ensure that variations in plastic overload (small changes in stop, etc.) will not cause significant NDT deviations. Exceeding the true NDT by 20°F is made nearly impossible by the B limitation, which acts on both the downward and the outward fracture propagation resistance of the crack.

In summary, it is the flaw size severity conditions of the DWT that serve to index the temperature of sharp rise in dynamic plane strain fracture toughness. Repeated research attempts to shift the apparently "NDT" temperature by changing specimen size, weld bead size, plastic load levels, etc., should now be analyzed in terms of fracture mechanics parameters. What is being done to the flaw severity condition by such changes — is it being decreased, or increased? Since these are all questions of flaw severity and constraint, they should be investigated for this reason and not for reasons of questioning a simple test which depends on fixed flaw severity for its performance. All other questions involve the practicality of the test procedures — for general routine test laboratory use these should be made as close to foolproof as possible. The DWT-NDT test procedures were designed purposely to ensure that a fixed condition of flaw severity was imposed and to make significant deviations from this condition practically impossible. The reproducibility of the test between laboratories attests to achievement of these aims.

The sharpness of the NDT determination is a reflection of the sharpness of its metallurgical change. If it were not for this fact the rapid change in critical flaw sizes and related plastic constraint requirements would not evolve. It is worthy to note at this point that the sharp development of visible shear lips is itself a reliable index of the NDT temperature, for the same metallurgical reasons. Thus, DT tests of any size can be indexed accurately to the NDT temperature by noting the temperature at which shear lips become visible. Service fractures can also be indexed accurately to the NDT temperature by noting the size of the shear lips, if present. Many estimates of the NDT temperature, accurate to within ±15°F, have been made by the author and associates from preliminary observation of service fractures, prior to conducting DWT-NDT determinations.

The history of the evolution of NDT indexing procedures for the C_v test deserves mention. Correlations with ship failure steels evolved by 1952 indicated that the NDT was indexible to the toe of the C_v transition curve, at approximately 10-ft-lb levels. This correlation was in agreement with C_v correlations to ship failures; i.e., fracture "source" plates all featured C_v values below 10 ft-lb at the failure temperatures. However, it soon became evident that other steels developed different correlations; in general, the NDT index shifted to higher positions on the C_v curve. This NRL discovery by 1953 was catastrophic to the then general belief that the C_v curve provided a singular index for fracture-safe design for all types of mild steels. Confirmation of the validity for higher indexing on the C_v curve, as indicated by the DWT-NDT, was obtained from other service failures, notably those of A302-B steel (7). The lack of reliability of the C_v test for generalized definition of the LTTR is now an established fact. The apparent LTTR indicated by the "toe-to-shelf" transition of the C_v test may range from 20 to 150°F lower temperatures than the true LTTR transition. These erroneous inferences can be most serious, because they are always in the optimistic (lower-temperature) direction. Temperatures of brittle fracture can be indicated as temperatures of full ductility by the C_v test shelf index.

INTERPRETATIONS TO THE FRACTURE ANALYSIS DIAGRAM (FAD)

The FAD represents a practical procedure for the synthesis of fracture mechanics and transition temperature concepts. This will be illustrated by the following discussions,

which could only be made in terms of both concepts. Moreover, unless the basic aspects of fracture mechanics are understood (Appendix A), practical use of the FAD will be restricted to much less than its full potential.

The FAD defines the general level of stress that is required for developing instability of flaws covering a wide range of sizes. These are grouped in a series of size steps — small (less than 1 in.), medium (4 to 6 in.), large (6 to 12 in.), and very large (approximately 1 to 2 ft). It is not practical to attempt finer definitions because of various factors described previously. The flaw size-stress relationships are changing too rapidly in the transition range.

The FAD flaw sizes indicated for NDT and moderately lower temperatures were first defined (7) from experience based on a large number of structural failures, involving both small and large B thickness (0.75 in. to 16 in.). Later analysis of the correspondence of these flaw sizes to fracture mechanics predictions has been presented in Ref. 1. Interestingly, the FAD correspondence is with dynamic initiation conditions for the small flaw sizes which require near-yield stress levels for instability. For stresses below 0.5 yield levels, the large flaws corresponded more closely to static loading conditions for large sections and to K_c conditions for small sections.

The FAD therefore introduces experience factors into the analysis system by referencing the very small flaw sizes of the diagram to dynamic conditions of loading. The flaw sizes indicated for intermediate and low stress levels may be considered to apply for static conditions of loading and to be long with respect to depth, which is the necessary geometry for small B thickness. For thick sections, the flaw sizes again relate to conditions of static loading, and the length represents the long dimension flaws of stubby, elliptical geometry. These are the conditions defined for temperatures at or slightly below the NDT. The "flat" curves of the FAD below NDT are not meant to imply the absence of temperature effects but merely that this is the starting point for the diagram. For the dynamic case (the small flaws of the FAD), the effect of decreased temperature below the NDT is very small.

The important aspect of the FAD is its definition of the effects of increased temperature above the NDT on flaw size-stress relationships. It is the grouping of the flaw sizes into discrete ranges that makes such definitions feasible and also practical for ordinary engineering use. In principle, more detailed definitions of critical flaw sizes at NDT temperature may be deduced from the NAD of Fig. A3.

The relative stress index of the FAD has exactly the same significance as the load stress used for fracture mechanics calculations of critical flaw sizes. It is the load-over-area (P/A) stress acting in the region of the flaw; if the flaw resides in a flat plate, it is the P/A stress calculated directly. If the flaw resides in a nozzle, it is the geometrically intensified P/A stress of the nozzle, i.e., hoop stress times the appropriate geometric intensification factor which may range from 3X to over 5X. The P/A stress can be of yield stress levels for nominal hoop stresses of 0.3 yield. Reasonably correct engineering calculation (or estimate) of the stress acting over the general region of the flaw is assumed by the FAD, as for any fracture mechanics analysis. There are special situations which require "automatic" entry at yield stress levels, such as for weld residual stresses, which feature yield stress intensity. These are highly localized, yet large enough in expanse to contain tiny weld cracks. The tiny cracks will recognize the residual yield stress level as the effective P/A stress. Obviously, large cracks cannot reside in regions of localized weld residual stresses of high intensity.

A determination of the approximate stress level acting on the flaw must always be made prior to entry of the FAD. The stress acting on the flaw should not be confused with the elastic stress intensification due to the presence of the crack. The K value of

this highly localized stress field is a function of crack size and the P/A stress acting over the region containing the flaw.

The FAD predictions should be understood first in terms of a simple "flat-plate" configuration, loaded in axial tension. The special case of pressure vessels which feature flaws of sufficient length to cause bulging of the flaw area will be discussed in the subsequent section. This special case involves questions of geometric instabilities — appropriate stress analyses, similar to the case of a nozzle, are required.

Fracture mechanics cannot be applied for loads in excess of the yield stress level. The FAD diagram extrapolates into the plastic stress region. These extrapolations only serve the purpose of indicating that the level plastic stress should increase with increased temperature. The plastic stress levels are not indexed, because there are no procedures for calculations or failure experience which would indicate the specific relationships. The discussions to follow will emphasize the flaw size-stress relationships for elastic loading, since structures are not generally designed for plastic loading. The prime engineering interest is therefore the elastic stress region of the FAD.

Relationships between relative stress, flaw sizes, B thickness, and temperature are integrated to simplified presentation in the FAD in Fig. 23. These relationships provide adequate definition for most engineering uses. Figure 23 presents the original version of the FAD and the modification (expansion) which can now be made on the basis of the new information developed for thick sections. The following points should be noted:

1. The small-flaw curve (< 1 in.) for dynamic initiation is common to the original FAD and the expanded FAD below NDT. This is true, because a small section sufficiently constrains a small flaw to plane strain conditions below NDT. Therefore, an increase in section size can have no additional constraint influence. Above NDT the small-flaw curves for both FAD's should be qualitatively the same.

2. The increase in stress level with increased temperature for the larger flaws in thick sections is based on conditions of static initiation. The slopes above NDT + 60°F should be influenced by the development of K_c conditions, since the plane strain constraint limit is exceeded above this temperature for conditions of static loading.

3. Increasing the section size decreases the relative stress levels for instability of the large flaws, because a sufficient depth of metal is provided for approaching or reaching plane strain constraint conditions. This fact is noted by the ">B" arrow notation connecting the dashed curves relating to large flaws residing in thin sections with the same flaws (solid-line curves) residing in thick sections. Note that the decrease in stress requirement is progressive with increased B, to a maximum limit. The decrease relates to change from K_c to K_{Ic} (low limit) fracture toughness levels.

4. The shift in the instability temperature (flaw in small B as compared to large B thickness) must increase with increasing flaw sizes and increasing stress level. This relationship is noted from the temperature span between the dashed- and solid-line curves for the different flaw sizes.

We may now recognize that ordinary structures feature two general levels of stresses — (a) low stresses for regions of nominal loading and (b) yield or near-yield level stresses for regions of high geometric stress concentration. The latter are of the "concentrated" type and can only contain flaws which are smaller than the region of high stress.

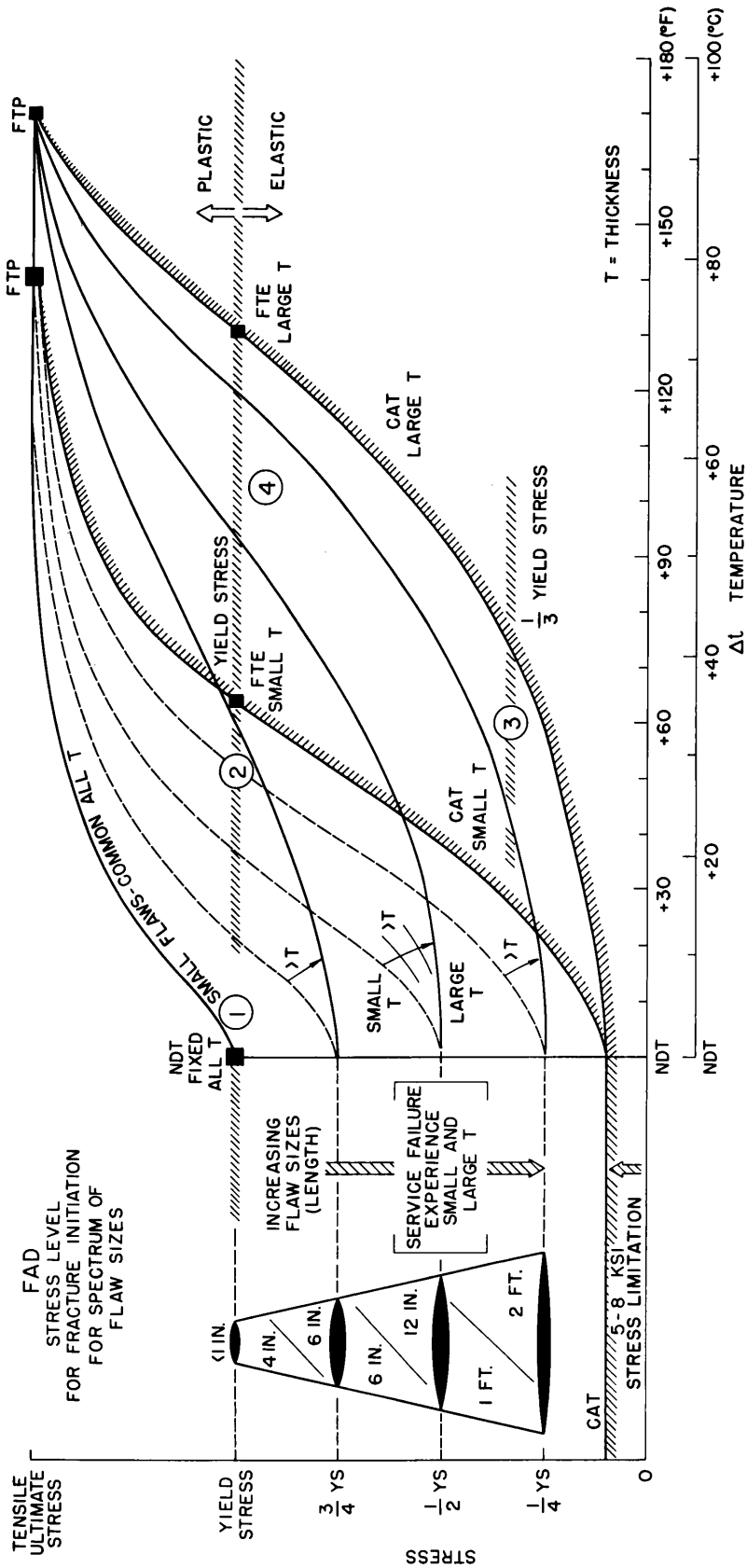

Fig. 23 – Fracture Analyses Diagram (FAD) for flaws residing in sections of small and large thickness

If the flaw size is small, say 1 in. or less, the flaw severity rather than the very large section size determines the failure stress. Thus, even for large section sizes, instabilities at points of geometric stress concentration (dynamic case) cannot develop at temperatures higher than NDT + 20 to 30°F as a conservative estimate. This is indicated by the structural analysis case 1 code in the diagram.

Elliptical flaws of approximately 6 in. length could be assumed to reside in nozzle regions of large pressure vessels which feature near-yield stress levels (as an example). The limiting temperature for static instability is approximately NDT + 60°F. This is indicated by the structural analysis case 2 code in the diagram. If the conditions are dynamic, the limiting temperature is shifted an additional 60°F, i.e., to near the CAT curve limit temperature.

Very large flaws are required for static instability at levels of stress in the order of 0.3 of yield, even at NDT temperatures. The shift in the static instability temperature for such large flaws (at this general level of stress) in very thick sections cannot be beyond the CAT curve. Thus, even for large increases of section size, the limiting temperature for instability is approximately NDT + 60 to 80°F. This is indicated by the structural analysis case 3 code in the diagram. Dynamic loading is not expected to increase the instability temperature significantly, due to the proximity of the CAT curve.

The unusual case of flaws of approximately 2 ft residing in yield stress regions must relate to extremely large structures or to plastic loading of large structures. This condition would provide for the highest limiting temperature of static instability in the order of NDT + 100°F. This is indicated by the structural analysis case 4 code of the diagram. Dynamic loading is not expected to increase the instability temperature significantly, due to the proximity of the CAT curve.

In consideration of these aspects it is apparent that the 60°F increase in the temperature range of unstable propagation (CAT) due to section size cannot be translated directly to similar shifts of all of the FAD flaw curves of the original diagram, for reasons which are fundamental to fracture mechanics concepts. The most common conditions for failure, very small flaws located in highly stressed regions of geometric transition, are not affected significantly by large increases in section size. Statically loaded, large flaws located in large sections may be expected to cause significant shifts related to section size. However, the shifts do not exceed 60°F as compared to the original FAD definition. Dynamic loading may be expected to increase the shift to temperature limits defined by the CAT curve.

These features, as indicated by the expanded FAD, provide sufficient guidance for the usual engineering assessments. Fracture mechanics considerations indicate that an increased span of Δt temperature with respect to the NDT is required to provide safety for flaws of intermediate and large sizes residing in thick sections. The Δt increase may range from 30 to 100°F depending on flaw size, stress level, and the possible development of dynamic conditions of loading. All known unstable (frangible) failures of heavy-section, low-strength steels have been at temperatures within the FTE limits of the original FAD (NDT + 60°F), for probability reasons. Unusual conditions involving relatively large flaw sizes, near yield level stresses, and dynamic loading (combined) are required to exceed this limit by an additional 60°F.

These analyses do not say that concern over the service characteristics of thick-section structures should not be intensified. The metallurgical properties are often degraded, and the NDT can be shifted to higher temperatures. Moreover, the introduction of new slack-quenched or spray-cooled heat treatments for heavy sections pose partly resolved metallurgical questions. In large measure the definition of the apparent transition temperature is based on the Charpy-V test, which is notoriously inadequate in its

predictive capabilities for such metallurgical microstructural conditions. Indeed, there should be serious concern over the properties of thick-section steels, for metallurgical reasons. The use of definitive fracture toughness tests is essential. Only if the LTTR can be established accurately and its inferences used, is it safe to conclude that failure rates of well designed, fabricated, and inspected structures would not be greatly different for the thick-section materials.

THE SPECIAL CASE OF PRESSURE VESSELS INVOLVING GEOMETRIC INSTABILITIES

Much concern has been expressed over the fact that fractures of pressure vessels may be initiated and propagated at nominal hoop stress levels above the CAT or the FTP temperatures, for the case of flaws which are very long with respect to wall thickness. This fact was first reported and explained in the original publication of the FAD (7). Such failures are due to geometric instabilities involving bulging of the flaw due to plastic overloads. Figure 24 presents these original data of burst pressure vessels of 1-in. thickness, featuring two sizes of flaws — 10 in. (10T) and 20 in. (20T). The failure stress plots indicate a low slope, which rises only gradually above the nominal hoop stress failure levels indicated for the NDT region. It was emphasized at the time that the nominal hoop stress cannot serve as the FAD index of stress "acting on the flaw," when bulging is developed. The flaw properly responds to the much higher levels of stress resulting from plastic bulging of the general area adjacent to the flaw. The fracturing process is then controlled by plastic overload stresses and is recognized as such by the flaw.

Plotting of the failure stress in terms of the hoop stress is informative in that it shows the relation to the flat plate condition, which actually determines the fracture process. The relationship of hoop stress to the flat plate condition for the 10T and 20T flaws is indicated by the notation GI (geometric instability) in Fig. 24. As long as these relationships are appreciated, such plotting provides practical interpretations; however, there is no basis for invalidation of the FAD definitions which relate specifically to the flat plate fracture conditions. Unfortunately, claims have been made that the plots of Fig. 24 indicate that the FAD is not valid. Such claims simultaneously challenge the validity of the CAT concept and fracture mechanics analyses. These claims are in error, as will be explained.

For use of the FAD or fracture mechanics one must know the stress acting on the flaw. There is no more justification for using nominal hoop stresses as reference for fracture conditions for the case of a long flaw which causes bulging than there is for using the hoop stress as direct reference for analyzing a nozzle region. The fact that principles of geometric instabilities are acting for a long flaw provides no reason to condemn the FAD or fracture mechanics. Both procedures require prior definition of the P/A stress levels acting in the region of the flaw.

It should be noted from Fig. 24 that there is no significant geometric instability effect indicated at NDT temperatures and that the effect increases with increasing temperature. This may be noted from the difference between the flat plate curve and the pressure vessel curve based on hoop stress indexing. The reason is perfectly obvious; bulging does not develop at the NDT because the metal is much too brittle to permit it. The degree of bulging increases greatly as the fracture toughness increases to FTE and FTP temperatures. The geometric instability has to "fight harder" to cause tearing fracture as the ductility of the metal increases with temperature. It does this by forcing the development of a larger bulge, thus gaining the required mechanical leverage with little increase in the general hoop stress level. The process is totally controlled by the geometric instability aspects of bulging. Figure 24 notes that arrests are obtained for hydraulic loading at temperatures immediately above the CAT — a short flaw extension

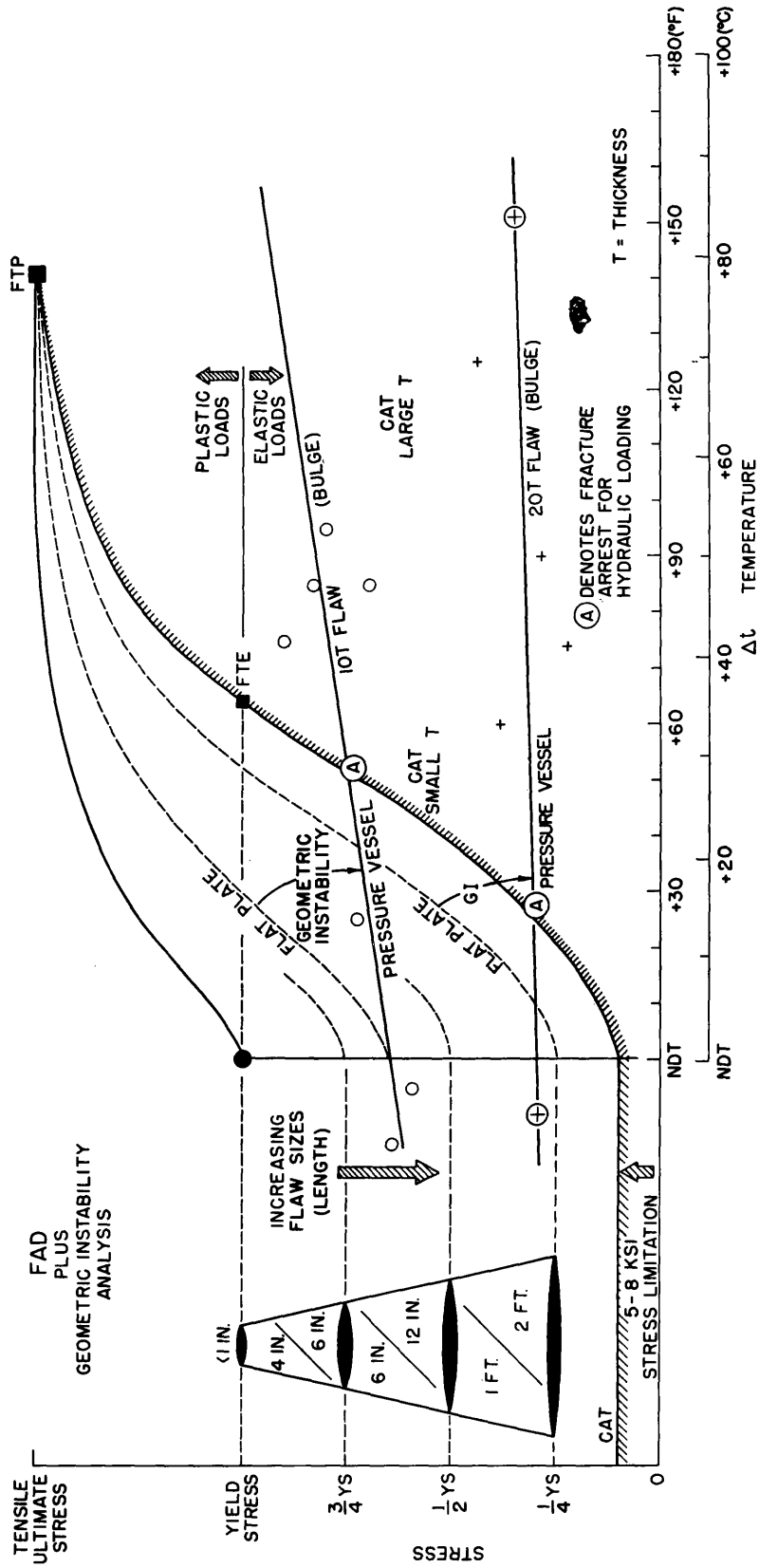

Fig. 24 - Extension of FAD to include conditions of geometric instability (bulging) for pressure vessels containing flaws over 5T length. These analyses are for 1-in. wall thickness. The same T relationship does not apply for thick walls (see text).

occurs and the pressurizing fluid is quickly lost. The flaws used for the burst tests were of 0.8T depth; i.e., a small bridge of metal retained the fluid until instability started. If the long cracks were open, there could not be a buildup of pressure to cause the burst. In these test series, pneumatic loading caused extensive bursts even at temperatures above FTP, involving fractures of full slant type.

Figure 25 illustrates representative burst conditions for the 1-in.-thick pressure vessels featuring 20T long (20-in.) flaws of 0.8-in. depth, prepared by slitting and final machining of a sharp notch at the base of the slit. The shattered flask represents a service failure at 10°F below the NDT temperature, from a 20-in.-long lamination. While this flask was pneumatically loaded, it does not matter because similar shattering was experienced at NDT temperatures for hydrostatic loading tests, as expected. The flaw regions for the service failure and for the burst tests at NDT temperature were flat without evidence of bulging. The arrested hydrostatic burst of the center flask at FTE + 20°F occurred after pronounced bulging was developed, as expected from the FAD analysis. The pneumatic burst at FTP clearly shows a large amount of bulging in the photograph; the slit flaw region is the shiny portion of the fracture. An interesting question may be asked for this failure which involved pushing out a flap. Is this a case of propagation of a tear or an arrest? Note that the flap represents a wiped-shearing-type fracture starting from the flaw tip. Obviously, the fracture toughness (enclave) was too high

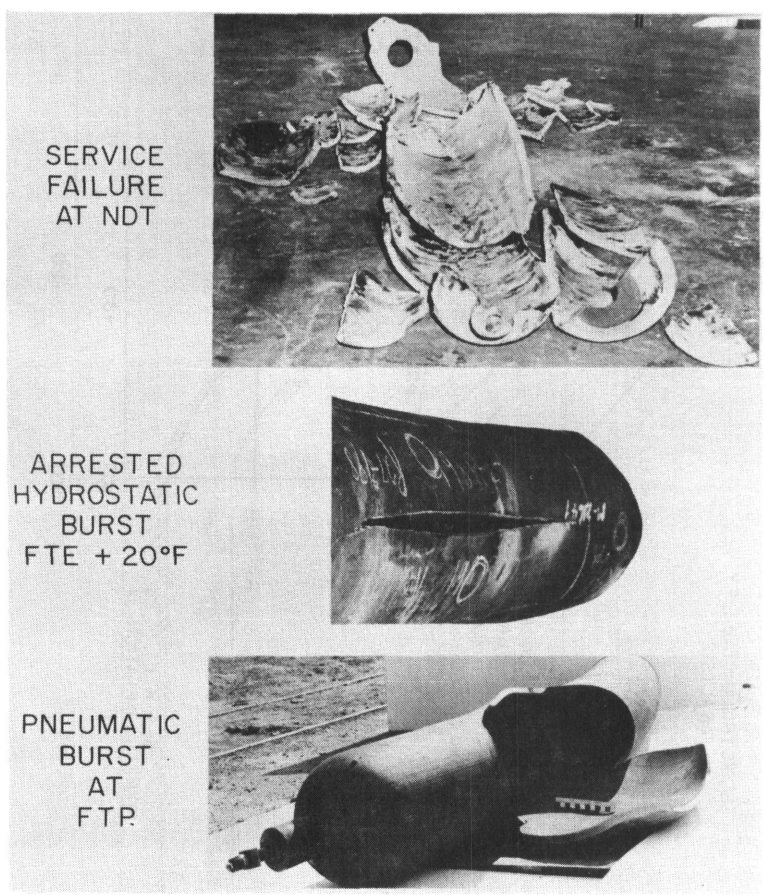

Fig. 25 - Effects of temperature, in the NDT to FTP range, on burst conditions for pressure vessels of 1-in. wall thickness, containing flaws of 20T length (7)

to permit tearing forward from the crack tip. It was easier energywise to push out the flap sideways. This is also an indication of geometric instability, in effect the flap is an extension of the bulge configuration. All of these failures are in conformance with FAD analyses, when the correct stress calculations are made.

The nominal hoop stresses for failure below the NDT and at NDT + 150°F for the shattered and flap failure flasks, respectively, are almost equal (circled points). Since the flaw lengths are the same (20 in.), equal K_c fracture toughness from the two failures would be indicated when their calculations are based on the hoop stress. This would be an obvious abuse of fracture mechanics, because K_c conditions are involved (due to the 1-in. thickness) for the near NDT failure case, and full enclave ductility applies for the flap failure temperature. The answer, of course, is that the stresses acting are of elastic and plastic levels, respectively, and not the same as indexing to nominal hoop stress would suggest. The arguments against the FAD that have evolved for the case of geometric instability arise from such calculations of pseudo-"K" values based on hoop stress. This is the procedure which is being applied to pressure vessel burst tests, which are now being conducted in relatively large numbers. These are not true K values but empirical definitions of failure levels for 10T, 20T, and even 30T flaw sizes — these would better be defined as X values. Having calculated pseudo-"K" values, the case is then made that fracture mechanics applies while the FAD does not — obviously, the case is not valid. Moreover, it would indicate an almost zero-slope temperature dependence of the "K" value, i.e., no change in fracture toughness.

Figure 24 may be used as an added FAD definition (Geometric Instability FAD) for failure conditions of thin-walled (1-in.) pressure vessels involving flaws in the 10- to 20-in. length range. Now we should consider the implications of these flat failure curves to the case of thick-walled pressure vessels. It should be obvious that the 10-in. or 20-in. flaws which are expected to cause plane strain instabilities for thick sections at NDT temperatures (documented in Ref. 7) should not follow the course of the flat curves for the thin-walled pressure vessels. Since bulging would not be possible for these flaws (assumed to be located in wall thicknesses of 6 in. or greater, i.e., less than 2T and 3T, respectively), the stress requirements for instability should follow the flat plate definitions of the FAD for thick sections. To develop geometric instability these flaws should be large with respect to thickness — flaw lengths in excess of 3T would be a conservative index of the lengths required.

We shall now consider the case of a 6-in.-thick vessel containing a 5T flaw of 30-in. length. Returning to the FAD we note that such a flaw size at NDT temperatures would be expected to fail at stress levels below 0.25 of yield stress. Should we now assume a flat-slope temperature dependence for the failure stress, as shown for the 10T and 20T flaws of the 1-in.-thick vessels? If so, the failure conditions in terms of T flaw length are completely out of line with the predictions for the thin section. The 5T flaw for the thick section would be located below the 20T curve for the thin section. What to expect is difficult to define exactly for a 5T flaw, because empirical "K" data of burst tests for thick pressure vessels are not available. In any event the T implications of the thin-walled vessels cannot be applied, as has been inferred in the literature.

We may now take a more exaggerated example for which a reasonable estimate can be made. Let us take the case of a 10T flaw for the 6-in.-thick pressure vessel. This would be a 60-in.-long flaw, and the failure stress at NDT would clearly be in the order of 0.1 yield stress or lower. Now we can reasonably assume a flat-slope dependence of the failure hoop stress with increasing temperature. The implications are clearly horrendous — flaw lengths which can cause geometric instabilities for thick-walled pressure vessels are insufferable. Once flaw sizes exceed the lengths that follow the flat-plate FAD definition of approximately 2-ft size (flaws less than 3T thickness), the decrease in load bearing characteristics of the pressure vessels at high temperature

(FTE and FTP) is dramatic. As the flaw size is increased from 1T to 5T and then to 10T, the failure hoop stress at FTE temperature can be expected to drop from yield stress levels to approximately 0.1 of yield stress levels. The drop would appear to be quite large for the 1T to 5T range.

There is little comfort to be gained from thinking in terms of the 10T and 20T relationships indicated by the thin-walled pressure vessels. It is such inferences that have beclouded analyses of potential failures for thick-walled pressure vessels when large flaws are assumed. There is no way to calculate the failure conditions of thick-walled pressure vessels featuring flaw lengths of approximately 5T at FTE to FTP temperatures because plastic fractures are involved — the only feasible route is to conduct empirical tests and establish empirical X parameters, as for the case of the 1-in.-thick pressure vessels. This is a very expensive operation which cannot be bypassed cheaply and indirectly by tests of vessels featuring small B thickness.

The FAD provides reasonable guidance for low and very high T lengths. It also serves to indicate the CAT limits of unstable fracture for thick-walled pressure vessels for intermediate, say 2T to 3T, values (expected to have a rising curve — not flat). The CAT curve for the thick plates is shown as the dashed curve of Fig. 24. For hydrostatic loading, the FAD prediction is that arrests would be developed above the thick-section CAT when geometric instabilities are sufficient to cause fracture initiation at hoop stress levels. In other words, the run of the fracture will be quite limited.

SUMMARY

The relationships between the micromechanical and macromechanical aspects of the brittle-to-ductile transition for cleavage fracture of steels are now evident. Clarification of these issues emerges from the integration of the product of three separate schools of effort — basic metallurgical studies of microfracture mechanisms, transition-temperature investigations, and fracture mechanics theory. It is unfortunate that splintering of research studies, reports in separate literature, separation of conferences, and neglect of other viewpoints have prevented earlier integration. The coalescence of microfracture mechanism studies with transition-temperature studies occurred most actively during the last 5 years. The coalescence of the integrated metallurgical concepts with fracture mechanics theory is the product of the past 2 years. In fact, conflict over predictions for the reliability of large pressure vessels for critical applications (nuclear pressure vessels) was required to stimulate cooperative research which led to the present state of integration.

It is now clear that none of these concepts could stand entirely on their own — they were all part of the full picture. The confusion created in engineering circles by discord between fracture specialists was instrumental to a stalemate in the evolution of practical, yet definitive fracture characterization tests. As the result, fracture-safe design practices for intermediate and low strength steels remained in question. The desirable oblivion of the Keyhole test has been delayed, and appreciation for the pitfalls of the Charpy-V test was obscured. These 1905 tests remain the industry standard, by default of agreement between fracture specialists.

This review has as its primary purpose the integration of concepts and the demonstration that there are no basic conflicts. In summary,

1. Microfracture theory properly defines the genesis of transition temperature effects.

2. The transition temperature approach is soundly based and in consonance with microfracture theory.

3. The macromechanical aspects of brittle fracture can be described adequately only by reference to fracture mechanics definitions of constraint and stress intensity.

4. The macromechanical aspects of ductile fracture are not analyzable by fracture mechanics in its present state of development. However, failures for the ductile state are precluded by other engineering practice safeguards.

5. Simple engineering tests which provide for interpretations to fracture mechanics parameters are now available.

6. Continued research in integrated fashion should provide additional information as to details — the major issues are clear.

7. It is time to translate all of this information to practical technological progress in standardization of tests, specifications, and codes.

Much of the confusion regarding apparently conflicting viewpoints is derived from popular misconceptions of the cleavage process. The appearance of cleavage does not necessarily indicate brittle fracture of low energy absorption. Extensive deformation may precede the development of cleavage — in fact, the transition temperature results from the increasing level of deformation required for the development of cleavage instability with increasing temperature. The appearance of full fibrous fracture simply marks the end point of the cleavage fracture transition — it is the result of rather than the cause of the transition. The development of shear lips at fracture surfaces (mixed mode fracture) certainly contributes to increased fracture toughness in the transition range; however, these features simply indicate that the cleavage ductility transition of surface regions precedes that of the central regions. The prefracture ductility of the central (flat) regions is increasing as the shear lip thickness increases.

Misconceptions that the increase in fracture toughness is related to the shear lip fraction lead to unwarranted predictions that increased mechanical constraint (thick sections) should eliminate the transition. This follows from equating ductility to fibrous fracture and brittleness to all types of cleavage fracture. On such an erroneous premise it is then inferred that if fibrous fracture of the central regions could be prevented, these regions would be retained in the state of "brittle" cleavage. Such is not the case, therefore, increased constraint cannot serve to suppress totally the increased fracture toughness resulting from the increased ductility of cleavage fracture processes with increased temperature. Increased constraint should serve only to delay the transition, i.e., shift it to moderately higher temperatures. These are the predictions of metallurgical microfracture theory.

Fracture mechanics theory correctly predicts that increased mechanical constraint (large cracks in large sections) should inhibit the development of crack-tip ductility with increasing temperature. However, mechanical constraint has finite limits, which can be effective only in the initial stages of increased microfracture ductility with increased temperature. Beyond a limiting temperature the microfracture ductility becomes too high, and mechanical constraint is lost.

Fracture mechanics defines the maximum condition of constraint as plane strain — this signifies a triaxial stress state of the utmost severity that can be imposed on the metal. For such condition, the level of stress intensity K that is required for developing instability is defined as K_{Ic} for static (slow) loading and K_{Id} for dynamic loading. Now we must recognize another popular misconception, that K_{Ic} and K_{Id} define fracture

toughness — this is not the case. The K parameters simply define a level of stress intensity and have no direct significance to fracture toughness unless related to the yield strength — static or dynamic. The true indices of fracture toughness are the $(K_{Ic}/\sigma_{ys})^2$ and $(K_{Id}/\sigma_{yd})^2$ ratio parameters. The higher the ratio, the larger the plastic zone size (PZS) that is developed at the crack tip prior to fracture, i.e., the higher the energy absorption prior to fracture initiation. In all cases for which plane strain applies, it is essential to "think ratio" — for simplicity of graphical presentations, this report uses the ratio definition of K_{Ic}/σ_{ys} and K_{Id}/σ_{yd}.

If we "think" of temperature effects as involving increased metallurgical ductility, we may also "think" of temperature effects as involving increased ratios. Higher-ratio plastic zone sizes will develop prior to instability with increased temperature. The next aspect that must be considered is that of the temperature dependence of the ratios in the transition temperature range. The popular misconception was that the rise of ratio value with temperature in the transition range involved a low slope. It is now demonstrated that the rise of the ratios has a very steep temperature dependence for both static and dynamic conditions of fracture initiation. In other words, the fracture mechanics ratio transition is "sharp," like any other fracture test transition.

Now we must "think" of section constraint effects in terms of the sharp ratio increase with temperature. The larger the ratio, the larger the section size and flaw size that must be used to retain plane strain constraint. Thus, small section sizes and small flaws lose constraint earlier in the transition range; i.e., the transition covers a narrower temperature range. Large section size and large flaws lose constraint at higher ratios; therefore, the transition covers a moderately broader temperature range.

The highest possible (limiting) transition temperature range (LTTR) is developed for the condition of dynamic fracture propagation. The LTTR evolves over a temperature range of 120 to 140°F for thin sections (1 to 2 in.) and over a moderately expanded temperature range of 160 to 180°F for very thick (semi-infinite) sections. The transition always starts at the same temperature — increased constraint simply expands the temperature range.

The LTTR is definable by dynamic fracture tests, as follows:

NDT (Nil Ductility Transition) — the temperature at which the dynamic transition is started.

FTE (Fracture Transition Elastic) — the temperature which separates unstable fracture propagation (fast) from stable fracture propagation (slow, forced fracture).

FTP (Fracture Transition Plastic) — the temperature at which full ductility is attained, i.e., the shelf condition.

While this terminology may be changed, the physical significance remains. These are critical points in the transition interval. Increased section size expands the NDT to FTE temperature interval. For thin sections (1 to 2 in.) the range is NDT to NDT + 40 to 60°F; for thick sections (6 in. plus) the range is NDT to NDT + 100 to 120°F. The static K_{Ic}/σ_{ys} and dynamic K_{Ic}/σ_{yd} ratio transitions are fully developed within these respective ranges for the thin and thick sections.

A simple translation may now be made as to the significance of fracture toughness tests which define the NDT, FTE, and FTP temperature index points of the dynamic fracture toughness transition. The NDT to FTE range covers the totality of fracture mechanics ratio transitions which are of practical interest. Unstable fracture can only be developed below the FTE temperature. The FTE to FTP range involves plastic fracture

processes which cannot be defined by fracture mechanics. Because of the narrowness of the transition temperature range, direct use of fracture mechanics is not practical; the flaw size-stress relationships are changing too rapidly for both the static and dynamic transitions. The large sizes of K_{Ic} or K_{Id} specimens required to follow the ratio transitions also make the use of such tests impractical. Thus, it is necessary to index fracture mechanics relationships by reference to fracture tests of relatively small size. These should serve three purposes — (a) define the transition range for small section size directly, (b) index the expansion of the transition range for thick sections, and (c) provide for indexing static and dynamic ratios to the appropriate temperature interval for small and large sections. If these desirable features are attained, indirect use of fracture mechanics becomes possible with the aid of simple graphical interpretations. The temperature range of fracture safety assured by plastic fracture processes is also defined for thin and thick sections.

The Charpy-V specimen has been demonstrated to have basic limitations which preclude reliable use for definition of the LTTR. In effect, it requires special calibrations for different types of steels. This leads to unacceptable complications for generalized use across large varieties of steels. The DWT-NDT test serves to index the NDT temperature and is acceptable for the generalized use described above. However, it does not provide an index of shelf-level fracture toughness, which becomes an important consideration for high strength steels of intermediate and low shelf values. The DWT-NDT test is specialized to the lower-strength-level, high-shelf-fracture-toughness steels. It should not be discounted, because these materials represent a very large fraction of the total tonnage produced.

The new Dynamic Tear (DT) test fulfills all of the stated requirements. A standardized version of 5/8-by-1-5/8-by-7-in. size may be tested in a simple pendulum machine. A deep, sharp notch may be substituted for the electron beam weld. It indexes the NDT, FTE, and FTP temperatures directly for the small thickness. The shift in the FTE and FTP temperatures for thick sections are easily deduced.

This information has provided the basis for the evolution of an advanced version of the Fracture Analysis Diagram (FAD). The diagram presents flaw size-stress relationships for fracture initiation of flaws residing in thin and thick sections. In this advanced form it should serve most engineering requirements. When finer distinctions of flaw size-stress relationships are required, recourse is provided to a ratio diagram indexed to the NDT temperature. This is defined as the NDT Analysis Diagram (NAD).

These various analytical procedures indicate that the major causes of failure can be controlled and eliminated by indexing a critical temperature span of approximately 30 to 60°F. Engineering judgment should be used to determine conditions for which a wider range has to be considered. However, the widest possible range (low probability cases) is less than 100°F.

These analyses immediately point to the importance of metallurgical quality — shifting of the critical transition intervals, which are only 30 to 60°F wide, to below service temperatures is the best approach to fracture-safe design. Steels are available which provide a wide range of transitions and therefore a wide range of economical choice to fit the purpose. There is no basic need for design based on highly brittle steels — a metallurgical improvement involving a decrease of the transition temperature by 30 to 60°F transforms a brittle steel to a ductile, fracture-safe material for most engineering purposes.

The case for the direct use of fracture mechanics for the cleavage fracture transition rested entirely on the expectations that thick sections would give a very low temperature dependence of plane strain fracture toughness. It is now demonstrated that this is

not the case — all temperature transitions are sharp. Thus, while fracture mechanics provides the rationale and basis for mechanical state interpretations of the sharp transition, it cannot provide test methods which can compete economically with simple engineering tests of low cost.

The 5/8-in. DT test also provides an index of shelf (FTP) fracture toughness levels. These levels will vary with rolling direction and steel quality (cleanliness). With increase in strength level, the shelf fracture toughness can fall to low values — in fact, to plane strain fracture toughness levels. For this condition (temperature insensitive), the DT test can be used to index K_{Ic} values indirectly. As such, it serves as an inexpensive substitute for fracture mechanics tests. Since the shelf transition is not involved in dynamic effects, the test is applicable to all metals. It has been used extensively for ultrahigh-strength steels, titanium, and aluminum alloys.

We propose that serious consideration be given to the potentialities of the DT test as the means for generalized (transition and nontransition) translation of fracture mechanics principles to technological use, for metals which are of the plane strain type. It clearly indicates whether a metal is of this type or the plastic fracture ductility type. As such it would eliminate much of the confusion that exists between tests. The separation of tests into categories of plane strain and nonplane strain types is artificial. Metals feature a spectrum of fracture toughness properties; it is not practical to shift from one test to another as the "thin edge" boundary which separates plane strain from nonplane strain fracture toughness is crossed. A practical test must be able to cross the boundary without losing definition. It should apply equally to temperature transition and temperature insensitive aspects of fracture.

REFERENCES

1. Pellini, W.S., "Advances in Fracture Toughness Characterization Procedures and in Quantitative Interpretations to Fracture-Safe Design for Structural Steels," NRL Report 6713, Apr. 3, 1968; Welding Res. Council Bull. Ser. 130 (1968)

2. Tetelman, A.S., and McEvily, A.J., Jr., "Fracture of Structural Materials," New York:Wiley, 1967

3. Averbach, B.L., Felbeck, D.K., Hahn, G.T., and Thomas, D.A., "Fracture," Proceedings of International Conference on the Atomic Mechanisms of Fracture, Swampscott, Mass., Apr. 12-16, 1959; New York:Wiley, 1959

4. Cohen, M., "Metallurgical Structure and the Brittle Behavior of Steel," Ships Structure Committee, SSC Report 183, National Academy of Sciences, Washington, D.C., May 1968

5. Goode, R.J., Judy, R.W., Jr., and Huber, R.W., "Procedures for Fracture Toughness Characterization and Interpretations to Failure-Safe Design for Structural Titanium Alloys," NRL Report 6779, Dec. 5, 1968; Welding Res. Council Bull. Ser. 134 (1968)

6. Judy, R.W., Jr., Goode, R.J., and Freed, C.N., "Fracture Toughness Characterization Procedures and Interpretations to Fracture-Safe Design for Structural Aluminum Alloys," NRL Report 6871, Mar. 1969; Welding Res. Council Bull. Ser. 140 (1969)

7. Pellini, W.S., and Puzak, P.P., "Fracture Analysis Diagram Procedures for the Fracture-Safe Engineering Design of Steel Structures," NRL Report 5920, Mar. 15, 1963; Welding Res. Council Bull. Ser. 88 (1963)

8. Irwin, G.R., Krafft, J.M., Paris, P.C., and Wells, A.A., "Basic Aspects of Crack Growth and Fracture," NRL Report 6598, Nov. 1967; Whitman, G.D., Robinson, G.C., Jr., and Savolainen, A.W., editors, "Technology of Steel Pressure Vessels for Water-Cooled Nuclear Reactors," ORNL-NSIC-21, Oak Ridge National Laboratory, Dec. 1967

9. Loss, F.J., and Pellini, W.S., "Dynamic Tear Test Definition of the Temperature Transition from Linear Elastic to Gross Strain Fracture Conditions," NRL Report 6787, Nov. 29, 1968; ASME Winter Annual Meeting, Dec. 1-5, 1968, Paper 68-WA/ER-1

10. Wessel, E.T., "State of the Art of the WOL Specimen for K_{I_c} Fracture Toughness Testing," Eng. Fracture Mech. 1:77-103 (1968)

11. Wessel, E.T., "Linear Elastic Fracture Mechanics for Welded Steel Pressure Vessels: Material Property Considerations," Symposium on Fracture Toughness Concepts for Weldable Structural Steels, Culcheth, England, Apr. 29-30, 1969

12. Smith, F.W., Emery, A.F., and Kobayashi, A.S., "Stress Intensity Factors for Semicircular Cracks, Part 2," J. Appl. Mech., Trans. ASME Ser. E, 34:953 (1967)

13. Shoemaker, A.K., and Rolfe, S.T., "The Static and Dynamic Low-Temperature Crack-Toughness Performance of Seven Structural Steels," Eng. Fracture Mech., pending publication

BIBLIOGRAPHY

"Tentative Method for Conducting Drop-Weight Test to Determine Nil-Ductility Transition Temperature of Ferritic Steels," ASTM E208-66T

Puzak, P.P., and Lange, E.A., "Standard Method for 1-Inch Dynamic Tear (DT) Test," NRL Report 6851, Feb. 13, 1969

Pellini, W.S., and Puzak, P.P., "Practical Considerations in Applying Laboratory Fracture Test Criteria to the Fracture-Safe Design of Pressure Vessels," NRL Report 6030, Nov. 5, 1963; Trans. ASME, Series A, J. Eng. Power 86:429-443 (1964)

Brubaker, E.H., and Dennison, J.D., "Use of Battelle Drop-Weight Tear Test for Determining Notch Toughness of Line Pipe Steel," J. Metals 17:985-989 (1965)

Pellini, W.S., Goode, R.J., Puzak, P.P., Lange, E.A., and Huber, R.W., "Review of Concepts and Status of Procedures for Fracture-Safe Design of Complex Welded Structures Involving Metals of Low to Ultra-High Strength Levels," NRL Report 6300, June 1965

Nibbering, J.J.W., Van Lint, J., and Van Leeuwen, R.T., "Brittle Fracture of Full Scale Structures Damaged by Fatigue," Netherlands Ship Research Center, Delft, Holland, Report 85S, May 1966

LaGasse, P.E., and Marquet, F., "Side Bend Test Procedure," Centre National de Recherches Metallurgiques, Liege, Belgium, RA 389-65, Jan. 1965

Irwin, G.R., "Fracture Mechanics," in "Structural Mechanics," Goodier, J.N., and Hoff, N.J., editors, New York:Pergamon, 1960

Irwin, G.R., "Fracture," in "Encyclopedia of Physics," Vol. VI, Berlin:Springer, pp. 551-590, 1958

Bluhm, J.I., "A Model for the Effect of Thickness on Fracture Toughness," Proc. ASTM 61:1324-1331 (1961)

Srawley, J.E., and Brown, W.F., "Fracture Toughness Testing," NASA Technical Note NASA TN-D-2599, Jan. 1965

Brown, W.F., and Srawley, J.E., "Plane Strain Crack Toughness Testing of High Strength Metallic Materials, ASTM Special Technical Publication (ASTM-STP-410), Philadelphia:American Society for Testing and Materials, p. 126, 1966

"Fracture Toughness Testing and Its Applications," ASTM STP 381, 1965

"Plane Strain Crack Toughness Testing of High Strength Metallic Materials," ASTM STP 410, 1966

Irwin, G.R., "Relation of Crack Toughness Measurements to Practical Applications," Welding J. Res. Suppl. 41 (No. 11):519s-528s (1962)

Krafft, J.M., "Correlation of Plane Strain Crack Toughness with Strain Hardening Characteristics of a Low, a Medium, and a High Strength Steel," Appl. Mater. Res. 3:88-101 (1964)

Appendix A

ELEMENTARY ASPECTS OF FRACTURE MECHANICS

This introduction is limited to the primary aspects which must be understood; otherwise, the coupling of concepts cannot be clarified. The basic concepts are relatively simple when considered in terms of their physical significance. We shall emphasize these aspects, a more extensive introductory coverage is provided in Ref. 1.

The first aspect which must be understood is the significance of the K parameter in relation to the plastic zone developed at the crack tip. The K parameter defines the elastic stress intensification in the region of the crack tip, Fig. A1; it is a function of the flaw geometry and the nominal stress acting in the region in which the flaw resides. Metals develop a plasticized region at the crack tip, which can be defined generally as a function of the ratio $(K_{Ic}/\sigma_{ys})^2$. Except for conditions of extreme brittleness, fracture is initiated within this plastic zone. The instability event is basically related to a plastic strain limit (ductility) of the metal crystals located in the plastic zone. Fracture mechanics avoids the complications involved in definitions of strain conditions by referencing the development of instabilities in the plastic zone to the elastic stress intensity K levels required to attain unstable crack movement. The critical K level for the condition of maximum mechanical constraint (maximum triaxially, i.e., plane strain) that

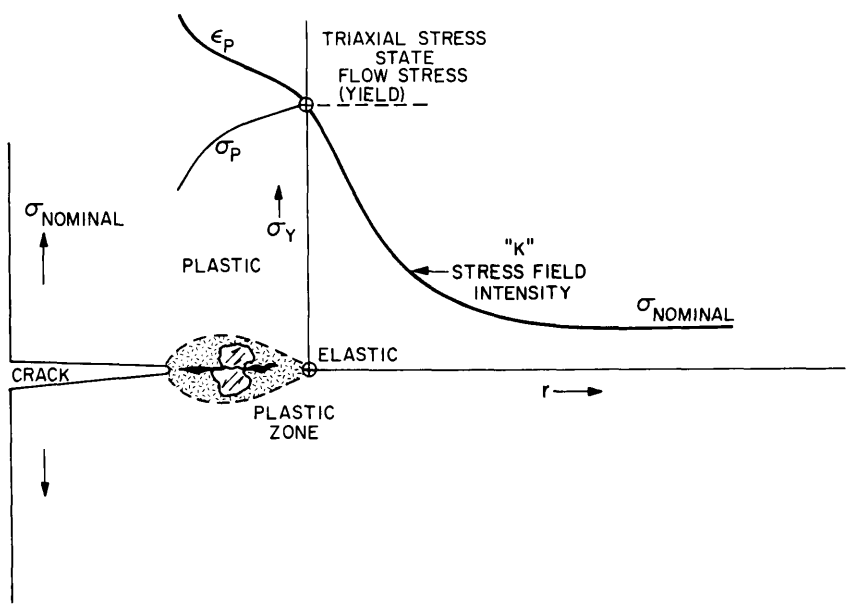

Fig. A1 - Relationships of elastic and plastic stress fields to the plastic zone at crack tips for the case of plane strain constraint. As plastic relaxation is developed (large plastic zone and crack tip blunting), the elastic stress fields are replaced by plastic strain fields. Elastic stress field K definitions are not possible for these conditions.

can be imposed on the region of the crack tip is defined as K_{Ic}. The connection between K_{Ic} and the corresponding plastic zone size (PZS) is crucial to ductility limits interpretations of fracture toughness in elastic stress field terms.

Unstable crack movement depends on the formation of a critical PZS; the larger the PZS at fracture, the tougher the material. Since the critical PZS is a function of $(K_{Ic}/\sigma_{ys})^2$, it is this ratio which properly defines fracture toughness and not K_{Ic} by itself. For example, a low ratio of $(K_{Ic}/\sigma_{ys})^2$, or simply K_{Ic}/σ_{ys}, means a small PZS. This, in turn means that little energy is expended to develop the unstable crack; consequently, the material is brittle. Just the opposite is true for a high ratio. It is impossible to evolve such a simple physical insight into the fracture conditions by sole consideration of K_{Ic} values. For instance, a K_{Ic} value of 60 ksi $\sqrt{\text{in.}}$ cannot be translated fracture toughness if the yield stress is not specified. If the yield stress is 30 ksi, a K_{Ic} of 60 ksi $\sqrt{\text{in.}}$ denotes a very high fracture toughness because the critical PZS is large. The value of $(K_{Ic}/\sigma_{ys})^2$ is then equal to 4.0. If the yield strength is 180 ksi, a K_{Ic} of 60 ksi $\sqrt{\text{in.}}$ denotes low toughness because the critical PZS is very small. The value of $(K_{Ic}/\sigma_{ys})^2$ is then 0.09, which represents a PZS approximately 1/40 of the previously cited case. Metals of different yield strength will have the same level of fracture toughness, if the ratio $(K_{Ic}/\sigma_{ys})^2$ is the same. The simple ratio K_{Ic}/σ_{ys} provides reference to this relationship and is the simplifying convention used in the text.

The physical significance of plane strain is that it indicates a condition of maximum degree of triaxial constraint to plastic flow that can be imposed (is allowed) by the metal. This means that the plane strain PZS developed at the point of fracture cannot be made smaller by increasing the depth or size of the crack (limit sharpness is always assumed and obtained by the use of fatigue cracks in K_{Ic} tests). If the PZS cannot be made smaller, the fracture toughness measured is the lowest possible value (singularity) for the metal. It is on this basis of singularity that K_{Ic} is considered a fundamental materials parameter.

The K definitions of elastic stress fields at crack tips appeal to designers and stress analysts in that all aspects of fracture (to their interest) may be described in terms of flaw size-stress parameters. To the metallurgist, the quality of a metal called fracture toughness relates to its ability to endure large strains at the crack tip before separation takes place. The limit strain that can be developed under maximum triaxial constraint is crucial to providing a connection between ductility concepts of fracture toughness, which guide the metallurgist in improvement of the metal, and the purely stress intensity definitions of K values, which are used to calculate flaw instabilities. The basic effects of the transition temperature and dynamic loading are expressible in terms of K values, but the physical interpretation of the metallurgical events can only be given in terms of mechanically constrained ductility.

The stress intensity at the crack tip is a function of the depth and shape of the crack and the P/A level of the engineering stress. A specific level of K_{Ic} stress intensity may be reached by combinations of large flaw sizes and low stresses, or small flaw sizes and high stresses. It is these relationships that provide the basis for linear elastic fracture mechanics calculations of instabilities. As the triaxially constrained plastic flow ductility of the metal increases (its fracture toughness), the P/A stress required to attain instability at the tip of a crack of specified dimensions will eventually exceed yielding. For a brittle metal (small critical PZS) small flaws are of sufficient severity to attain K_{Ic} stress intensity at levels of P/A stress below yielding. A more ductile metal (larger critical PZS) will require larger flaws of increased severity to cause failure at P/A stresses below yielding. Increased metal ductility requires both increased mechanical constraint for retention of the plane strain condition and increased flaw severity to develop instabilities at elastic levels of P/A stress.

The constraint to metal flow resulting from the presence of a flaw is of geometric origin — it is related to suppression of Poisson effects. The cracked area does not contract, because there are no longitudinal stresses acting on it. It tries to maintain its original dimensions, while the metal at the crack tip (plastic zone) is attempting to flow in the direction of the normal stress. To do so it must contract (Poisson effect) in the plane of the crack. The contracting along the crack front must be done while "tied" physically to the noncontracting cracked area. The effect of the crack is to limit lateral contraction and thus to limit extension in the normal direction. Increasing the size of the crack perimeter (flaw size) provides increased constraint because the noncontracting area is larger; therefore, the Poisson suppression effect is retained to larger plastic zone sizes.

There are three requirements for the development of instability with retention of the plane strain condition: (a) the volume of metal surrounding the crack must be large enough to contain the necessary triaxial elastic stress fields, (b) the crack must be large enough to feature adequate constraint (noncontracting crack area) for prevention of lateral contraction, and (c) the crack depth must be sufficient to attain the critical K level for instability at stress levels below P/A yielding.

The physical aspects of these relationships are evident in the features of K_{Ic} specimens, which are suggested as guidance by the ASTM E-24 Committee, based on K_{Ic} test experience:

$$B \geqq 2.5 \left(\frac{K_{Ic}}{\sigma_{ys}}\right)^2$$

where B = specimen thickness (in.). The crack depth is suggested as 0.5B for tension loaded specimens, as is the uncracked (ligament) depth. These conditions combined should generally provide for the necessary level of constraint and severity features required by the level of fracture toughness defined by the K_{Ic}/σ_{ys} ratio. Increasing the crack depth (with retention of the 0.5 ligament depth) merely results in decreasing the stress level at instability — the K_{Ic} value is not changed. Increasing B does not change the level of instability stress if the crack depth is held constant — the K_{Ic} value is not changed. If the ligament depth is less than the required size, there will not be sufficient volume of metal to contain the triaxial elastic stress fields — plane strain constraint will be lost, and K_c conditions then apply. This will be the case even if the crack depth and B value meet the requirements. The B requirements of the above relationship indicate $B \geqq 0.6$, 2.5, and 10.0 in. for K_{Ic}/σ_{ys} ratios of 0.5, 1.0, and 2.0, respectively.

With this introduction we may now provide a simplified physical interpretation of section thickness-flaw size relationships for surface cracks, as shown in Fig. A2, which places two edge-cracked K_{Ic} specimens in superposition to two surface cracks. The B thickness of the specimens is assumed to be the minimum value. For a low K_{Ic}/σ_{ys} ratio a small B is adequate, while for a high ratio a larger B value is required. Next we assume that the volume of metal below the K_{Ic} specimen and the surface cracks is sufficient to establish the necessary elastic stress fields. The size of surface cracks required for plane strain fracture instability will vary with the minimum B value. For near-yield stress loading (maximum permissible) the critical flaw size related to low K_{Ic}/σ_{ys} ratio metal will be much smaller in comparison to the high-ratio metal. For lower stress levels the flaw sizes indicated schematically will increase; however, for any relative stress the critical flaw size of the low-ratio metal will always be much smaller compared to the high-ratio metal.

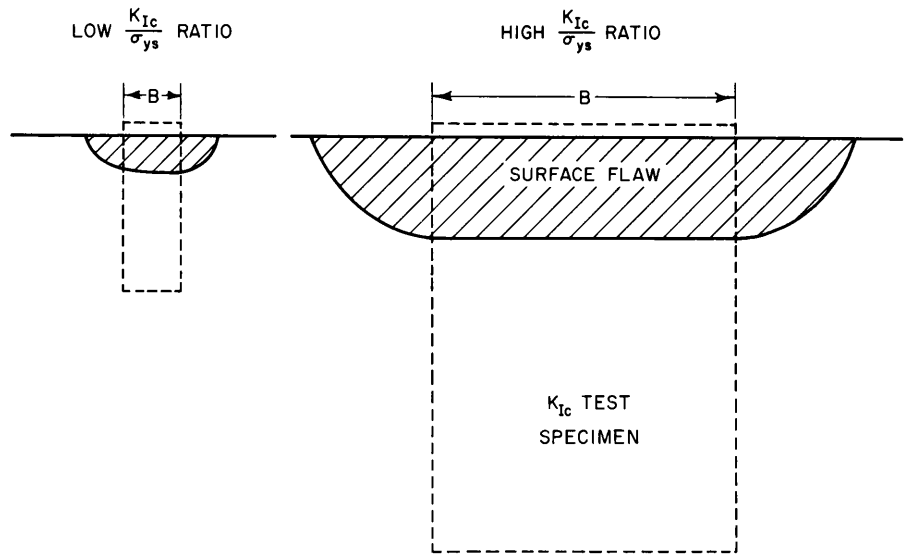

Fig. A2 - Relationships of plane strain constraint requirements expressed in terms of section thickness B and surface flaw sizes

Actually the difference in relative sizes will increase with decreasing stress level. This simply says that the spectrum of stress-related flaw sizes which are critical for low-ratio metals will be small flaw sizes. Similarly, the spectrum of flaw sizes which are critical for high-ratio metals will be large flaw sizes. Small minimum B and small flaw sizes go together; increasing B above the minimum limit does not change the size spectrum of critical surface cracks. Similarly, if large B thickness is required for constraint, only large flaws can cause instabilities — the small flaws lead to over yield levels of stress.

The geometry of the flaw has a bearing because of the constraint aspects — stubby flaws feature lower severity as compared to long thin flaws of equal depth. The reason is that the perimeter (constraint index) is wider for the long thin flaw. As an approximation the stubby flaw must be two to three times deeper than the long thin flaw for equivalent severity. While these complexities must be understood in principle, there is no need for requiring engineers to become fracture mechanicians to use the concepts. These may be presented graphically in simple form.

The basis for calculating the graphical plots for semielliptical surface flaws in tension is provided by the following flaw size-stress relationship:

$$K_{Ic} = \frac{1.1}{\sqrt{Q}} \sigma \sqrt{\pi a}$$

where

a = crack depth

σ = nominal stress (P/A)

Q = flaw geometry parameter obtained from tables.

All of these factors are simplified to the full graphical presentations of Fig. A3. The various plots relate critical crack depth to the K_{Ic}/σ_{ys} ratio for four levels of

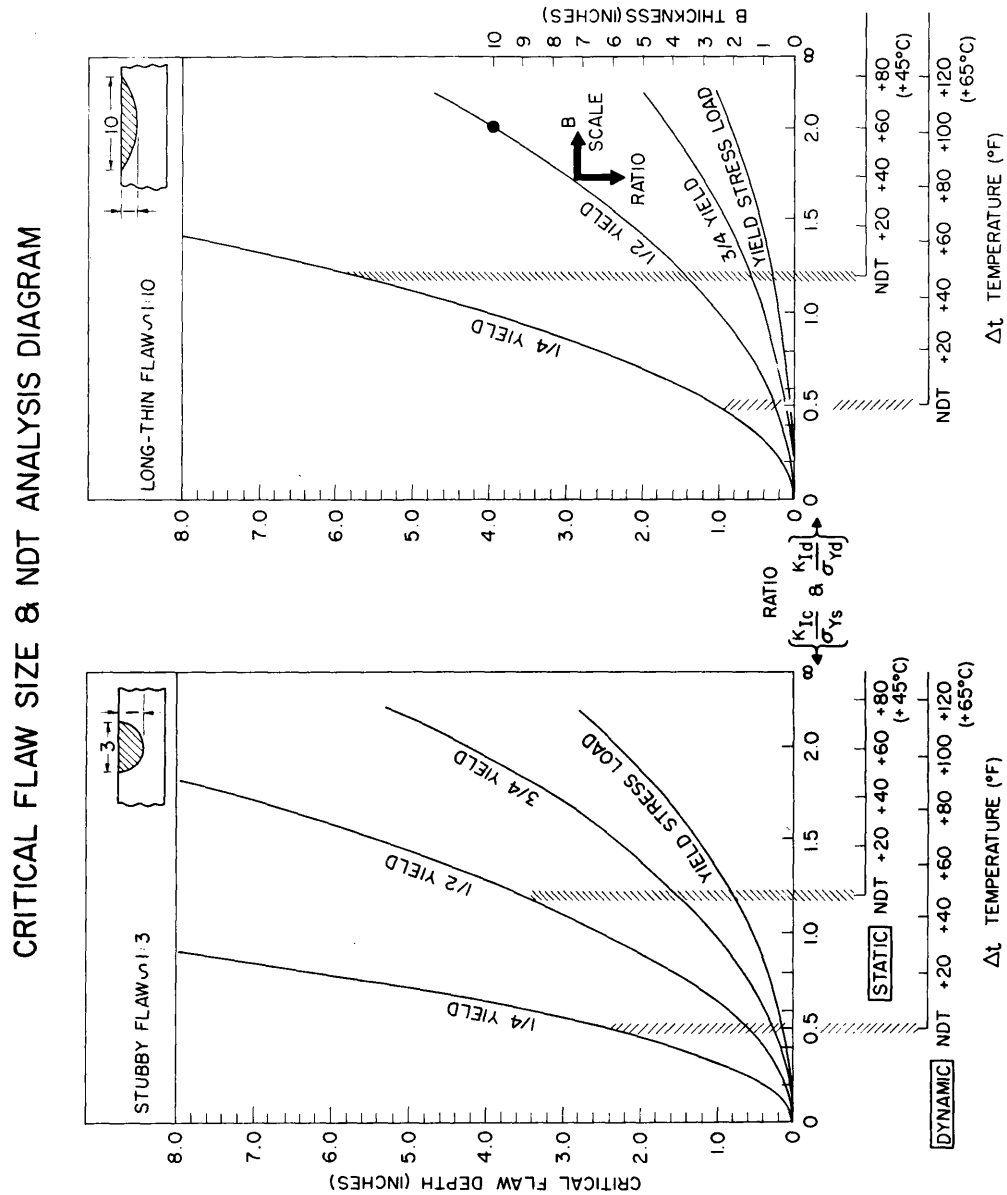

Fig. A3 – Relationship of flaw size–stress requirements for the initiation of plane strain fracture as a function of increasing ratios — these relationships are general. Specialized use for indexing the increase in static and dynamic ratios above the NDT temperature is noted by the Δt temperature scale. The Δt relationship scales are defined as the NDT Analysis Diagram (NAD).

relative nominal stress. The stubby and long thin flaw geometries represent the two extremes of flaw geometries. For most engineering purposes it is adequate to use one or the other of these extremes — all other Q aspects will lie between and may be interpolated if desired. The right-hand plot also relates the B thickness to the ratio by dual reference to one of the flaw size curves. The subject Flaw Size Index Diagram applies generally to all metals — the significance of the temperature notations are specific to transition temperature analyses for steels and will be described later. The diagram also indexes the B requirement for K_{Ic} tests and through-thickness cracks.

The K_{Ic} parameter relates to conditions of slow loading (static). Plane strain conditions for dynamic loading are defined as K_{Id}, and the applicable fracture toughness parameter is then the K_{Id}/σ_{yd} ratio. The diagram also relates to the dynamic ratios, and its use depends on determining K_{Id} and the dynamic yield strength.

The plane strain condition is tolerated only by relatively brittle metals — an index of the relative brittleness is provided by Table A1, which relates fracture mechanics calculations of PZS (used for plasticity corrections) to the K_{Ic}/σ_{ys} ratios. The B relationships for K_{Ic} test specimens indicate the constraint requirements.

Table A1
Comparison of Plane Strain Constraint Parameters

B (in.)	Ratio K_{Ic}/σ_{ys}	Plane Strain Instability PZS (in.)	Plane Stress K_c PZS
0.65	0.5	0.01	0.03
2.5	1.0	0.05	0.15
6.0	1.5	0.12	0.36
10.0	2.0	0.22	0.66

The increase in the K_{Ic} specimen section size required for retention of constrained (small) plastic zones is striking. This relationship provides the basis for many of the discussions to follow. The increase in PZS associated with transition to K_c (for the mere starting of constraint loss) is also striking. As constraint falls barely below the critical level, the PZS immediately jumps to three or more times that of the plane strain value, as indicated by the K_c column above.

If constraint is moderately inadequate, K_c instability may still be developed before reaching yield stress levels. If it is grossly inadequate, the increase in PZS causes crack tip yielding and blunting to develop as load is increased in attempts to reach K_c values. The stress levels will then rise to conditions of general yielding. This physical interpretation is of major importance in relation to the effects of the transition temperature. Once plane strain constraint is lost due to increasing metal ductility, the PZS begins to grow and causes crack tip blunting. The blunted crack accentuates the plasticizing process. The region in advance of the blunted crack tip may then be described as a small plastic enclave. This may be visualized as the "dimple" of reduced section noted in advance of tear fractures. The dimple region is similar to the neck region of a tensile specimen; it indicates that a relatively large volume of metal has suffered deformation. The energy required for fracture is then very high, and fracture instability cannot be developed.

Unstable fracture signifies that the elastic strain energy released at the instant of crack extension provides sufficient energy to produce the critical PZS required for crack

extension of the next increment of fracture. This is the reason for the propagation of brittle fractures at velocities the order of several thousand feet per second. Such instabilities can only be developed for dynamic plane strain fracture. As the K_c state is reached, the velocities decrease and quickly drop to zero — the crack is arrested, as for the Robertson test. Propagation of the fracture then requires step-by-step reapplication of load and strain at the crack tip — the sequence involves crack tip strain, crack extension, relaxation of local stress, repeated crack tip strain, etc.

In summary, the plane strain state for cleavage fracture involves nonarrestable instabilities. As the K_c state is entered, arrestable instabilities are developed as the crack tip is blunted microscopically — the physical size of the structure (small or large) can have an effect on the rate of strain energy release because of marginal conditions of energy balance. As the K_c state becomes more advanced (larger PZS), instabilities are no longer possible — forced propagation of fracture in progressive steps is required and nominal stresses exceed yield. As the enclave state is entered, loads must rise to plastic levels, as a parallel situation to a tensile specimen neck region.

In its present state of development fracture mechanics only applies to the plane strain state. However, the concepts may be extended qualitatively to describe the ductile, nonplane strain state.

Appendix B

FRACTURE MECHANICS TERMS AND EQUATIONS

1. Strain Energy Release Rate $\mathcal{G}$ — Elastic energy released, per unit crack surface area, as the crack extends. The strain energy $\mathcal{G}$ is a measure of the force driving the crack:

$$\mathcal{G} = \frac{\pi \sigma^2 a}{E}$$

where

a = one-half crack length for a through-thickness crack in a semi-infinite tension plate

σ = nominal applied prefracture stress

E = modulus.

2. Plastic Work Energy $\mathcal{G}_c$ — Index of resistance of the material to crack extension; it is related to elastic energy absorbed, per unit area of new crack surface, in crack extension. Plastic work energy at the crack tip opposes the elastic energy release $\mathcal{G}$. At the point of instability the elastic energy and the plastic work energy (resistance) are in balance:

$$\mathcal{G}_c = \frac{\pi \sigma_f^2 a}{E}$$

where

σ_f = nominal stress at crack extension for a through-thickness crack in a semi-infinite plate in tension

$\mathcal{G}_c$ = critical $\mathcal{G}$.

3. Stress Intensity Factor, K — Elevation of stress in advance of the crack tip plastic zone, which is related to the plastic work energy term as follows:

$$K = (E\mathcal{G})^{1/2} \qquad \text{(for plane stress)}$$

$$K = \left(\frac{E\mathcal{G}}{1 - \nu^2}\right)^{1/2} \qquad \text{(for plane strain)}$$

where ν = Poisson's ratio.

4. Stress Intensity Factor at Instability K_c — In the preceding equation, replace K with K_c and replace $\mathcal{G}$ with $\mathcal{G}_c$; therefore, use σ_f as nominal stress at crack instability. The subscript c means K is critical or at the point of instability.

5. Plastic Zone Correction — To correct for the presence of the plastic zone, apply an apparent increase in initial crack depth a_0 by adding r_p (plastic zone radius). The crack length then becomes $a = a_0 + r_p$,

$$r_p = \frac{1}{2\pi}\left(\frac{K_c}{\sigma_{ys}}\right)^2 \qquad \text{(plane stress)}$$

$$r_p = \frac{1}{6\pi}\left(\frac{K_{Ic}}{\sigma_{ys}}\right)^2 \qquad \text{(plane strain).}$$

6. Increase of Plastic Zone Size with Increase in K — The plastic zone is related to the plastic work energy described earlier. From above equations note that the plastic zone size increases as K^2 for a fixed level of yield stress. The increase is approximately three times larger for plane stress. For different yield strengths, the plastic zone size is a function of $(K_{Ic}/\sigma_{ys})^2$.

7. K_{Ic} Calculations for Plane Strain Condition Cracks — In a generalized form

$$K_{Ic} = \alpha\beta\sigma\sqrt{\pi a}$$

where

σ = nominal static stress applied under slow loading

a = crack depth or length

α = flaw geometry factor ranging from 1 to 3 (approximately)

β = function of crack tip sharpness, loading rate, crack tip metallurgical damage, etc. Ranges from 1/2 to 2 (approximately).

Thus, the critical flaw size for surface cracks may be influenced by combined α and β factors, which on the low side reduce the critical crack depth by a combined factor of 1/2 and on the high side increase the flaw depth by a factor of 6.

8. K_{Ic} Calculations for Plane Strain Surface Cracks — The formal equation for a surface crack in a tension-loaded plate is

$$K_{Ic} = \alpha\sigma\sqrt{\pi a} = \frac{1.1\sigma\sqrt{\pi a}}{\sqrt{Q}}$$

where

a = crack depth

σ = applied stress

$1.1/\sqrt{Q}$ = specimen and flaw-shape factor obtained from charts.

This equation assumes that K_{Ic} relates to either dynamic or static load-rate conditions. The calculated flaw depths are based on the same assumption.

9. K_{Ic} Calculations for Internal Cracks Which Become Unstable Under Plane Strain Conditions — Roughly generalized, for the same geometry, the internal crack depth (short dimension) requires a slightly higher stress for instability ($a = 1/\sqrt{Q}$) when the preceding equation is applied.

10. Calculation of Surface Crack Involving K_c (Plane Stress) — When the constraint necessary for plane strain is not present, an approximation may be made of the stress-intensity factor under plane stress conditions K_c. This approximation is based on a definition of K_{Ic}, σ_{ys}, and B for the material. The following equation may be used to estimate K_c:

$$K_c = K_{Ic} \left[1 + \frac{1.4}{B^2} \left(\frac{K_{Ic}}{\sigma_{ys}} \right)^4 \right]^{1/2}$$

From K_c, the critical flaw size for instability under plane stress conditions for the same level of nominal stress may be calculated:

$$\frac{K_c^2}{K_{Ic}^2} = \frac{a_{K_c}}{a_{K_{Ic}}}$$

where

a_{K_c} = critical flaw size under plane stress

$a_{K_{Ic}}$ = critical flaw size under plane strain.

Security Classification

DOCUMENT CONTROL DATA - R & D

(Security classification of title, body of abstract and indexing annotation must be entered when the overall report is classified)

1. ORIGINATING ACTIVITY (Corporate author) Naval Research Laboratory Washington, D.C. 20390	2a. REPORT SECURITY CLASSIFICATION Unclassified 2b. GROUP

3. REPORT TITLE

INTEGRATION OF METALLURGICAL AND FRACTURE MECHANICS CONCEPTS OF TRANSITION TEMPERATURE FACTORS RELATING TO FRACTURE-SAFE DESIGN FOR STRUCTURAL STEELS

4. DESCRIPTIVE NOTES (Type of report and inclusive dates)

Special summary and interpretative report

5. AUTHOR(S) (First name, middle initial, last name)

W.S. Pellini and F.J. Loss

6. REPORT DATE April 22, 1969	7a. TOTAL NO. OF PAGES 73	7b. NO. OF REFS 13
8a. CONTRACT OR GRANT NO. NRL Problems M01-25 and M01-14 b. PROJECT NO. RR 007-01-46-5432 c. RR 007-11-41-5409 d.	9a. ORIGINATOR'S REPORT NUMBER(S) NRL Report 6900 9b. OTHER REPORT NO(S) (Any other numbers that may be assigned this report)	

10. DISTRIBUTION STATEMENT

This document has been approved for public release and sale; its distribution is unlimited.

11. SUPPLEMENTARY NOTES	12. SPONSORING MILITARY ACTIVITY Department of the Navy (Office of Naval Research), Washington, D.C. 20360

13. ABSTRACT

The brittle-to-ductile transition for cleavage fracture of steels has been examined with integrated considerations of micromechanical and macromechanical features. The evolution of transition-temperature approaches to fracture-safe design has been based on concepts that metal ductility factors should override mechanical constraint factors, in the higher temperature range of the transition. The transition temperature range, determined by dynamic fracture tests, has provided the necessary guidance for the development of improved steels. Fracture mechanics concepts emphasize that macroscopic fracture toughness is controlled by mechanical constraint and flaw severity factors. While true, within limits, there has been an unwarranted extension of these principles to signify that the transition temperature does not have a basic significance to fracture processes. Contrary to popular beliefs, these concepts are not in opposition — metallurgical factors determine the intrinsic metal ductility, and mechanical parameters serve to describe the response of the metal to specific stress states. Recent investigations of the effects of large section size have demonstrated that increased mechanical constraint results in shifts of the transition temperature, as predicted by fracture mechanics theory. However, these shifts are of relatively small magnitude and, more importantly, do not eliminate transition temperature characteristics.

The rapid changes in fracture toughness which develop over a narrow temperature range indicate that practical engineering use of fracture mechanics must be based on transition temperature tests of simple types. Conventional fracture mechanics tests are not practical

(Over)

DD FORM 1 NOV 65 1473 (PAGE 1)

S/N 0101-807-6801

Security Classification

14 KEY WORDS	LINK A ROLE	LINK A WT	LINK B ROLE	LINK B WT	LINK C ROLE	LINK C WT
Engineering fracture mechanics						
Fracture toughness tests						
Fracture mechanics tests						
Fracture-safe design						
Structural steels						
Engineering fracture tests						
Interpretations of fracture tests						
Thick-section steels						
Design applications of fracture tests						
Interpretations of fracture mechanics theory to engineering design						
Steels for reactor technology						
Transition temperature for steels						
Micromechanics of cleavage fracture						

for transition temperature definitions because of large size, prohibitive expense and the very steep-slope temperature dependence of K_{Ic} and K_{Id} defined fracture toughness. In effect, the analytical capabilities of fracture mechanics are best used by contributions to improved definition of the significance of dynamic fracture toughness tests. For such use, the tests must be indexable to K_{Ic} and K_{Id} parameters. The Dynamic Tear (DT) test represents the most advanced engineering test which provides accurate indexing of the true transition temperature range and the specific interval in this range for which fracture mechanics applies. The temperature interval of high fracture toughness which is outside the range of fracture mechanics capabilities is also defined. Size effect can be interpreted and related to expected transition temperature shifts.

All of these factors have been integrated into simple reference diagrams which index flaw size-stress relationships for fracture initiation in the transition range. The Fracture Analysis Diagram (FAD) procedure is now extended to cover the full range of thickness. Its validity is confirmed by these additional studies and is no longer based entirely on experience factors. Conversely, the experience factors serve to validate the predictions of fracture mechanics theory and continue to provide engineering assurance that the analytical methods can be relied on.